UNIVERSITY OF LATVIA
FACULTY OF PHYSICS, MATHEMATICS AND OPTOMETRY

UNIVERSITY
OF LATVIA

ARTURS BUNDULIS

INQUIRY OF THE KERR EFFECT ORIGINS IN ORGANIC MATERIALS: EXPERIMENTAL ASSESSMENT BY Z-SCAN METHOD

DOCTORAL THESIS

FOR A DOCTORAL DEGREE IN PHYSICS AND ASTRONOMY
SUBSECTOR: SOLID STATE PHYSICS

Riga, 2020

The work presented in doctoral thesis was carried out in the Institute of Solid State Physics, University of Latvia from 2016 to 2020.

The thesis contains the introduction, three chapters, conclusions, thesis and reference list.

Form of the thesis: dissertation in Physics and Astronomy, Solid State Physics.

Supervisor: Dr. phys. **Martins Rutkis**, senior researcher at ISSP, University of Latvia.

Reviewers:

1) *Dr. habil. phys.* **Andris Ozols**, Professor, Riga Technical University;
2) *Dr. phys.* **Janis Alnis**, Institute of Atomic Physics and Spectroscopy, University of Latvia;
3) *Prof.* **Jean-Michel Nunzi**, Professor, Queen's University.

The thesis will be defended at the public session of Doctoral Committee of Physics, Astronomy and Mechanics, University of Latvia at 17:00 on December 17, 2020 in the conference hall of the Institute of Solid State Physics of University of Latvia.

The thesis is available at the Library of the University of Latvia, Riga, Kalpaka bulv. 4.

Chairman of the Doctoral Committee *Dr. habil. phys.* **Uldis Rogulis**

Secretary of the Doctoral Committee **Annija Sturmane**

Abstract

As the demand for higher bandwidth telecommunication systems grows, new technological approaches for information and communication technologies are necessary. Great attention is given to the possibility to implement an all-optical telecommunication system due to the existing electro-optical system is reaching its limits. For such a system to be implemented, one of the most essential aspects is the existence of nonlinear optical materials that can enable interaction between photons – mainly Kerr and Two-photon absorption effects. At this moment material selection is the main bottleneck for all-optical telecommunication system implementation.

Material selection can be either carried out by experimental work or by quantum chemical calculations. But both of these approaches have the same underlying problem – the credibility of results. This gives rise to the problems studied in this work:

- How to correctly measure the Kerr and the Two-photon effects of organic materials by separating them from other effects that induce similar responses in materials?
- How correct are Quantum Chemical calculations and how well they fit experimental measurements?

The first problem was studied by considering the Z-scan method for nonlinear optical properties characterization. For this chloroform and two organic compounds – DMABI and MeSBI dissolved in chloroform – were studied using a polarization-resolved Z-scan method with a picosecond laser, and nanosecond laser with variable pulse repetition rate. For chloroform, it was shown that while 30 ps laser pulse width was short enough to correctly evaluate the magnitude of the Kerr effect. At the same time, 8 ns pulse width was long enough to induce a thermo-optical response that was pulse repetition rate dependent. To extend Z-scan applicability, polarization-resolved measurements were carried out that showed: i) For 8 ns laser with pulse repetition rate under 1 kHz Kerr contribution could be separated from thermo-optical contribution; ii) Refractive index changes for chloroform induced by 30 ps laser is mainly due to molecular reorientation; iii) Kerr effect of organic chromophore could be separated into molecular reorientation and electronic contributions using 30 ps laser. This allowed pinpointing a specific measurement methodology to determine the magnitude of electronic contributions of organic compound that is dissolved in a solvent using 30 ps laser. On the other hand, Z-scan measurements of organic chromophores with 8 ns laser indicated that organic chromophore nonlinear optical response can be due to thermo-optical effect and this cannot be predicted by knowing linear or Two-photon absorption properties at incident wavelength. Lastly, the Z-scan method was also compared to the Mach-Zehnder interferometer and the advantages and disadvantages of both methods were identified.

To study Quantum Chemical calculation credibility Kerr and Two-photon absorption effects of 27 different organic compounds were studied and acquired results compared to quantum chemical calculation predictions by Gaussian 09. It was shown that linear polarizability values given by quantum chemical calculations can be used to predict experimental values of molecular reorientation contribution to the Kerr effect. Also, acquired Kerr values were compared to quantum chemical calculation results and two distinctive trends were observed.

For molecules that did not possess any significant two-photon absorption a linear relation between quantum chemical calculation results and experimental values for second-order hyperpolarizability was observed indicating that calculation results can be used to compare different molecules and predict which are more efficient. This conclusion was shown to be independent of the organic molecule type. On the other hand for materials that possessed an experimentally observable two-photon absorption effect, the ratio of experimental value to calculation results was linearly dependent on two-photon absorption cross-section, indicating that the implemented calculation method is not sufficient enough in predicting two-photon contribution to Kerr response.

Contents

List of symbols

E	Electric field
C	Speed of light in vacuum
ε_0	Vacuum permittivity
P	Polarization
ω	Electrical field frequency
ε	Relative electrical permittivity of media
n_0	Linear refractive index
α_0	Linear absorption
P_0	Initial polarization of the system
$\chi^{(n)}$	N-order dielectric susceptibility
I	Optical intensity
$D^{(3)}$	Degeneracy term
δ	Second-order hyperpolarizability
L	Local-field factor
N	Density of molecules as molecule number per cm^3
μ	Dipole moment
μ_{ij}	Electric dipole transition moment between levels i and j
$\Delta\mu_{ij}$	Difference between dipole moments of states i and j
E_{ij}	Energy difference between states I and j
e	Electron charge
m_e	Electron mass
N_e	Number of electrons in a molecule
n_2	Nonlinear refractive index
λ	Wavelength
$\hat{\sigma}_{\pm}$	Circular-polarization unit vectors
θ	Light polarisation angle
b	Nonlinear constant
Γ	Damping factor
$\rho_0 C$	Heat capacity per volume
κ	Thermal conductivity
w_0	Beam waist radius
v_s	Speed of sound in media
D_t	Thermal diffusivity
dn/dT	Thermo-optical coefficient
L	Length of media
η	Molar absorption coefficient
C	Molar concentration
σ	Absorption cross-section
α_2	Two-photon absorption coefficient
σ_{2PA}	Two-photon absorption cross-section
I_s	Saturation intensity

z_R	Rayleigh length
R	Beam size
f	Focal length of a lens
$\Delta\phi$	Induced phase change
τ	Laser pulls duration
ν	Laser pulls repetition rate
$d^{2\omega}$	Second-harmonic generation coefficient
N_{eff}	Oscillator strength
$\delta^{(n)}$	Miller's constant
P_C	Couchy principle value
L_C	Coherenc length
$\Delta\lambda$	spectral width of an optical signal
$S_{aperture}$	Aperture size
S_{beam}	Laser beam size
q	Two-photon absorption amplitude
I_0	Optical beam intensity at a focal point
T_p	Peak value of transmittance of closed aperture Z-scan measurement
T_v	Valley value of transmittance of closed aperture Z-scan measurement
ΔT_{pv}	Difference between peak and valley signals of Z-scan
F	Laser fluence
$\Delta\Psi$	Two-photon absorption induced transmittance changes
Δz_{pv}	Distance between peak and valley positions

List of abbreviations

NLO	Nonlinear optical
SHG	Second-harmonic generation
SOS	Sum-over-states
D term	Dipolar term
T term	Two-photon term
N term	Negative term
Re	Real part
Im	Imaginary part
CW	Continues wave
ns	Nanosecond
ps	Picosecond
2PA	Two-photon absorption
LA	Linear absorption
ESA	Excited state absorption
2PA-ESA	Two-photon absorption induced excited state absorption
ISC	Intersystem crossing
GB	Gaussian beam
BOA	Bond order alteration
BLA	Bond length alteration
DFWM	Degenerated four-wave mixing
QCC	Quantum Chemical calculations
HOMO	Highest Occupied Molecular Orbital
LUMO	Lowest Unoccupied Molecular Orbital
SM	Step motor
BD	Beam dump
BS	Beam splitter
OA	Open-aperture
CA	Closed-aperture
QWP	Quarter-wavelength plate
NLR	Nonlinear refractive

List of figures

List of Tables

Introduction

As the data amount transmitted through the telecommunication system grows[2], the necessity for a system with higher bandwidth becomes more relevant. Mainly two solutions to this problem are being considered – raising the bandwidth of the existing telecommunication system or moving towards a new system that would offer higher bandwidth. Considering the later solution, one approach to this problem could be moving from an electro-optical to an all-optical system. To do this necessary to have devices for optical information transfer, storage, and processing. While the former of these devices has partly been implemented in the form of optical fibers, the two later ones have only been demonstrated in a scientific laboratory scale. The main issue here is materials that could serve as media for interaction between optical signals. Here nonlinear optics start to play an essential role allowing for light interaction through optical dependent material properties. Although different nonlinear optical effects, such as the Kerr and Pockel effects, have been discussed and observe long before, the birth of nonlinear optics as a scientific field is assigned to 1961 when P. Franken and his group for the first time detected second-harmonic generation in quartz crystal[3]. This is widely considered to be the first nonlinear optical experiment and it didn't take long for nonlinear optical materials to become essential for many optical devices especially for information and communication technologies. Since then many works about nonlinear optical materials and experimental methods for measuring nonlinear optical effects has been published. Main focus has been given to mainly two nonlinear optical effects for all-optical devices – Kerr effect and Two-photon absorption effect[4].

Motivation

Through the years few numbers of experimental methods for third-order nonlinear optical characterization have established them self's as the base for material characterization. The main two methods have been the Degenerated four-wave mixing[5] and Z-scan[6]. Although the Degenerated four-wave mixing method was the main approach for a long time for Kerr effect characterization, nowadays the Z-scan method is the most popular mainly due to the simple experimental setup and possibility to measure the Kerr and the Two-photon absorption effects simultaneously. Even though this method has been around since 1990 new publication regarding the Z-scan measurement methodology is being published in 2020 trying to establish a unified method for interpretation of the Z-scan measurements[7]. The main issue here is that the Kerr effect is measured through refractive index changes. At the same time, it is not the only effect that can induce refractive index changes of materials and the Kerr effect needs to be correctly separated from others, mainly from thermo-optical contribution. The problem with the thermo-optical effect is that it can lead to refractive index changes through single laser pulse contribution or accumulative effects, even further complicating the separation. Also, the Kerr effect response can be separated into multiple contributions of which only electronic is of interest for high-bandwidth all-optical applications. All these aspects have different responses to laser pulse repetition rate, laser pulse width, and optical polarization of the light beam (characterized by the ratio of induced refractive index changes at linear

polarization and circular polarisation) that are compiled in Table A. In literature NLO properties are measured using CW lasers as well as ns, ps and fs lasers with pulse repetition rates from 1 – 40 000 Hz complicating correct comparison between materials studied by different scientific groups. Another approach to this problem could be finding some other experimental approach to Kerr effect measurements. One such alternative could be Mach-Zehnder interferometer that has been widely used for electro-optical effect measurements[8]. As there are only a few publications regarding the Mach-Zehnder interferometer for Kerr effect measurements, more research is necessary to conclude if this method could be an alternative.

Table A: *Thermo-optical and Kerr effect dependence on laser parameters. "Yes" means that effect is specific parameter dependent while "No" – effect is independent of specific parameter*

Effect	Contributions	Pulse repetition rate	Pulse width	Lights polarization
Thermo-optical	Single-pulse	No	10^{-9} - 10^{-8}	No
	Accumulative	Both are connected (40 kHz for 150 fs; 500 Hz for 15 ns)		No
Kerr	Electronic	No	10^{-15}	Yes – Ratio 3/2
	Libration	No	10^{-13}	Yes – Ratio 4
	Collision	No	10^{-13}	Yes – Ratio 3/2
	Reorientation	No	10^{-12} – 10^{-11}	Yes – Ratio 4

Another essential problem for finding efficient nonlinear optical materials is finding a fast way for material screening for applicability. Although many papers regarding organic materials nonlinear optical properties have already been published, the studies of nonlinear optical active organic materials is still a very active scientific field. But finding novel nonlinear optical organic materials by systematic experimental measurements is too time-consuming. To reduce the amount of experimental work for material selection, scientists have long worked to derive theoretical guidelines to structure-property relations of organic molecules. This includes generalized Miller's rule for extension of second-order susceptibility over spectral range[9], further continuation, and experimental verification of this rule for third-order susceptibility[10–12], Ducuings observation of π-conjugated materials as promising for nonlinear optical applications[13–15] and others. While there are numerous papers regarding different structural-property relation studies[16–20], over-all knowledge is still insufficient for theoretical designing of nonlinear optical chromophores. Another solution could be Quantum Chemical calculations to predict hypothetical molecules NLO properties. This could allow shifting most of the material development from experimental to theoretical work by simpler structure screening. Although different Quantum Chemical calculations methods have already been employed for calculations of molecular linear optical as well as for NLO properties, there still

isn't a widely accepted approach to calculations of the third-order nonlinear optical properties of organic materials.

The main goal of this work is to establish a correct methodology for the third-order nonlinear optical effect studies using the Z-scan method and see how well values of refractive index changes acquired with Quantum Chemical calculation corresponds to experimental values. This will be done by carrying out the following tasks:

- Study how the Z-scan measurements are influenced by laser pulse width, pulse repetition rate, and polarisation,
- Compare the Z-scan method to the Mach-Zehnder interferometer to establish in which situations each of the methods are more applicable,
- Carry out the Z-scan measurements for 27 organic compounds to study structure-property relation of these molecules,
- Compare acquired experimental results to the Quantum Chemical calculations results.

Structure of the thesis

The main text of the thesis is divided into five parts – Theory, Literature review, Experimental section, Results and Discussion, and Conclusions and defendable thesis.

In the Theory section, an overview of the nonlinear optical effects will be given with the main focus on the third-order nonlinear optical effects, such as the Kerr and the two-photon absorption effects. This will include a general description of how the electrical field interacts with media, mathematical description of the nonlinear optical effects as nonlinear changes of molecules polarisation with the main focus on third-order effects. More in-depth attention will be given to induced refractive index and absorption changes and various effects that can lead to such property variations. This description will be given with the main focus on how to correctly separate Kerr and two-photon absorption effects from other contributions when measuring the refractive index and the absorption changes. Lastly, a short insight will be given to the general relation between linear and nonlinear optical properties of materials as well as the relation between real and imaginary parts of linear and nonlinear optical properties.

In the Literature review, a brief overview of different material groups studied for the nonlinear optical applications will be given. This includes inorganic materials, metamaterials, graphene-like 2D materials, inorganic/organic hybrid materials, and lastly organic materials. As the organic materials are the main focus of this work, a more detailed look on the nonlinear optical organic materials will be given. This part will consist of main experimental conclusions, that are specific for either non-centrosymmetric or centrosymmetric molecules, concluded with a list of guidelines for nonlinear optical material selection. Switching from nonlinear optical materials to methods how to study these materials, descriptions of the nonlinear optical measurement methods used in this work – the Z-scan and the Mach-Zehnder interferometer – will be given alongside one of the most classical methods for more general knowledge on this topic – the Degenerated Four-wave mixing method. Lastly, a very superficial look on the Quantum Chemical calculations will be presented, as it is used in this work but is not the main focus.

The Experimental section will be compiled of sample preparation routines, sample characterization methods, and the Z-scan and the Mach-Zehnder interferometer experimental setup descriptions. Also, more details about what type of settings was used for the Quantum Chemical calculations will be given.

Results and Discussion will consist of three main parts. First will be the characterization of the Z-scan and the Mach-Zehnder interferometer methods through various types of experiments. The second part will be a summary of all nonlinear optical values of various organic materials studied in this work. And lastly, a comparison of the experimental results to the Quantum Chemical calculations will be presented for these molecules.

Finally, all results from this work will be summarized in Conclusions and Thesis.

Author's contribution

The experimental setups presented in this work were mainly constructed by the author of this work, excluding custom-built electronic parts that were made by a colleague Janis Busenbergs. The author prepared all of the samples studied in this work and carried out optical absorption measurements for sample characterization. All of the nonlinear optical measurements with both the Mach-Zehnder interferometer and the Z-scan methods were done by the author. The Quantum Chemical calculations were carried out by colleague Igors Mihailovs.

All of the data processing, including writing MatLab or Python codes for data fitting, and result interpretation were done by the author.

Scientific novelty

This work presents an outline for a correct approach for correct interpretation of refractive index changes induced by optical irradiation. This includes separation of thermo-optical effects and Kerr effect separation and decomposition of the Kerr effect into electronic and molecular contributions when using the Z-scan method by employing polarization-resolved measurements.

A nonlinear optical property characterization of multiple novel organic materials is presented in this work that has not been previously studied, with some exhibiting large two-photon absorption values that could be used for optical limiting applications.

A correlation between the two-photon absorption effect in organic materials and how much the experimental values for the Kerr effect differs from the Quantum Chemical calculations carried out by Gaussian 09 has been presented. This correlation is shown to be independent of the organic material group.

1. Theory

1.1. Electrical field in media

Electromagnetism is the base for the description of optical wave propagation and interaction with specific media. In this section, a brief introduction to the electrical wave equation will be given that is based on O. Students' "Optika" book[21]. Using Maxwell's equations, the electrical field can be described using the wave equation:

$$\nabla^2 E - \frac{1}{c^2}\frac{\partial^2 E}{\partial t^2} = 0, \tag{1.1}$$

where *E* is the electrical field and *c* is the speed of light in vacuum. If light propagates through some dielectric media, it is essential to take into account the polarization of media, defined as dipole moment per unit volume. To do this equation (1.1) needs to be rewritten as:

$$\nabla^2 E - \frac{1}{c^2}\frac{\partial^2 E}{\partial t^2} = \frac{1}{\varepsilon_0 \cdot c^2}\frac{\partial^2 P}{\partial t^2}, \tag{1.2}$$

where ε_0 is the vacuum permittivity and *P* is the polarization of the material. This equation describes the propagation of light in media that are electrically neutral, non-conducting, and non-magnetic. If the assumption is made that polarization is linearly dependent on the electrical field and that electrical field is a monochromatic wave, equation (1.2) can be further rewritten in Helmholtz equations form:

$$\left(\nabla^2 - \varepsilon \cdot \frac{\omega^2}{c^2}\right) E(r, \omega) = 0, \tag{1.3}$$

where ω is the electrical field frequency and ε is the relative electrical permittivity of media (ratio of the absolute electrical permittivity of media to that of the vacuum). When deriving the form of the electrical field for isotropic media, where the electrical permittivity is a scalar quantity, the following approximation of relative electrical permittivity can be used for calculations:

$$\sqrt{\varepsilon} = n_0 + i \cdot \frac{c}{2\omega} \cdot \alpha_0, \tag{1.4}$$

where n_0 and α_0 is the linear refractive index and the linear absorption, respectively. By inserting equation (1.4) into equation (1.3) and solving, an equation describing monochromatic light propagation in specific media can be obtained:

$$E(z,t) = E_0 \cdot e^{-\frac{1}{2}\cdot\alpha\cdot z} e^{-i\left(n_0 \cdot \frac{\omega}{c} z - \omega \cdot t\right)} + c.c., \tag{1.5}$$

where c.c. denotes the complex conjugate. When an electrical field is applied to a material, its polarization will change. As polarization is connected to various properties of the material – refractive index, optical absorption, and others – the external field can induce changes in these properties. When the magnitude of the electrical field is relatively small (less than 10^6 V/m)[4], these changes can be described as linear relation from the electrical field. But for the case of a strong external field, a linear approximation is not precise enough. In general case material polarization can be expressed as a polynomial of the form:

$$P(\omega) = P_0 + \chi^{(1)} \cdot E(\omega) + \chi^{(2)} \cdot E^2(\omega) + \chi^{(3)} \cdot E^3(\omega) + \cdots \quad (1.6)$$

where P_0 is the initial polarization of the system when no external field is applied, $\chi^{(n)}$ is the n-order dielectric susceptibility, $E(\omega)$ is the complex electrical field, and ω is the frequency of the electrical field.

1.2. Nonlinear optical effects

The polynomial nature of polarization gives rise to multiple nonlinear optical (NLO) effects. The most popular and widely accepted approach to grouping these effects is by the order of dielectric susceptibility that corresponds to the specific effect. Linear optical effects are characterized by the first-order susceptibility and correspond to the linear optical absorption and refractive index. If all other polynomial elements of polarization are equal to zero, the refractive index and the optical absorption is independent of the electrical field or optical intensity. The second-order NLO is characterized by $\chi^{(2)}$. The most notable effects in this group are the second-harmonic generation (SHG) and the electro-optical effect or also called as a Pockels effect. In this section, a superficial overview of these effects will be presented based on W. Boyds' book "Nonlinear optics"[4].

Second-harmonic generation. In second-order NLO media two photons of the same frequency can interact to create a single photon with double frequency through a virtual level. The created photon is coherent in-phase and space with the original photons but has double frequency compared to the original photons (see Figure 1.1A).

Pockels effect. If the external electrical field is applied to material that possesses second-order NLO properties, the refractive index of specific media will change linearly from the applied electrical field. These changes will differ in spatial directions inducing birefringence. This is characterized as the Pockels or the electro-optical effect and can be used to modify the phase or the polarization of the optical beam (See Figure 1.1B). It is widely used in electro-optical

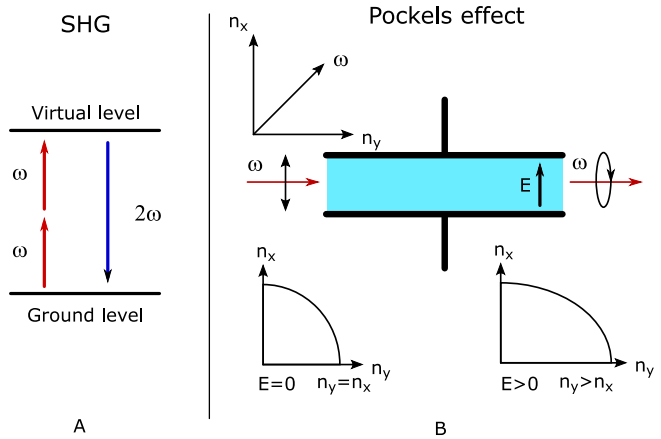

Figure 1.1: *A – Second-harmonic generation effect. Two incoming photons are combined through a virtual level into a single photon with double frequency. B – Pockels effect. By applying the electrical field to material, its refractive index starts to change by inducing birefringence. If an incoming optical beam is linearly polarised so that it is in 45^0 angle to the optical axis, polarization will be changed from linear to circular.*

modulators and is an essential part of the modern information and communications technology (ICT) sector.

The third-order NLO effects are characterized by $\chi^{(3)}$ and, respectively, any nth-order NLO effects – by $\chi^{(n)}$. As this work is mainly focused on the third-order NLO effects, they will be described more in detail in the following sections with no more in-depth look at higher-order effects.

1.3. Third-order susceptibility

Next, let's consider the third-order dielectric susceptibilities contribution to systems polarization. Two main approaches can be used to describe third-order effects – photon and wave approach. For the photon approach, third-order effects are based on various ways of how three photons can interact simultaneously with the material. This can be described using Feynman diagrams[4] (see Figure 1.2) and can be divided into two categories – three photons interact to create a new photon of different frequency (third-harmonic generation, three-wave mixing) and two photons change the properties of media that are probed by a third photon (Optical Kerr effect, DC Kerr effect).

For a more classical approach, the wave model can be applied and will be used to acquire most of the expressions for third-order susceptibility. Extending the third-order term in equation (1.6)[4] the result is:

$$P^{(3)}(t) = \chi^{(3)} \cdot E^3(t) = \chi^{(3)} \cdot (E \cdot \cos(\omega \cdot t))^3 = \frac{\chi^{(3)} \cdot E^3 \cdot \cos(3\omega \cdot t)}{4} + \frac{3 \cdot \chi^{(3)} \cdot E^3 \cdot \cos(\omega \cdot t)}{4} \qquad (1.7)$$

From this equation two different ways the material can interact with light can be derived: i) material response with the frequency of 3ω due to an electrical field with the frequency ω, ii)

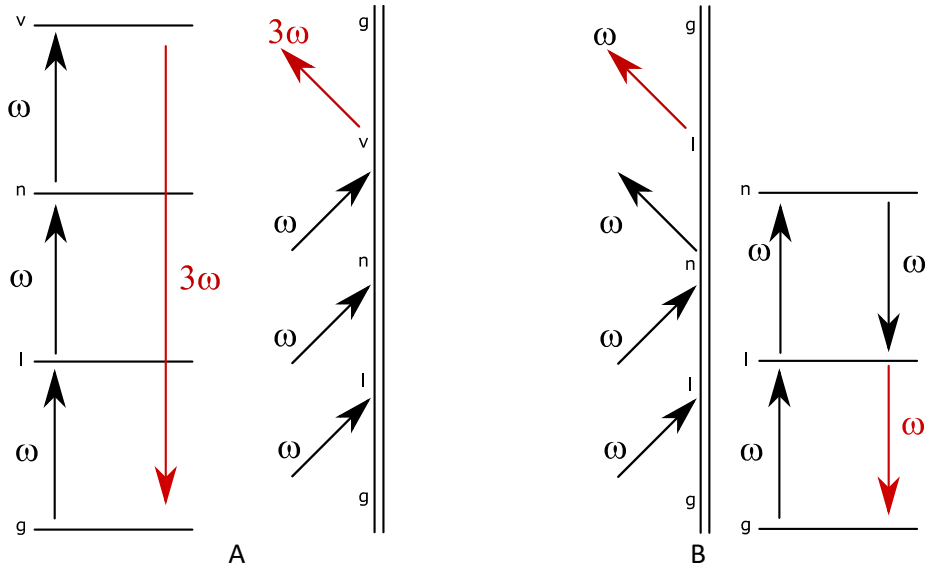

Figure 1.2: The *Feynman diagrams for three-photon interactions with respective energy level schemes. A – one of the permutations of how third-harmonic generation can, B – one of the permutations how third-order reaction can happen at the same frequency as incident photon.*

nonlinear response with the frequency ω of the incident electric field. In case when frequencies of interacting waves (photons) differ, the mathematical model becomes more complicated and will only be studied superficially in this work. In this work, a mixture of both approaches will be used with the wave approach for mathematical description while the photon approach will be used for more contextual description. Next, let's study in more detail both terms of equation (1.7).

The first term of equation (1.7) and Figure 1.2A describes the third-harmonic generation. In this case, the system starts to generate third-harmonic of the incident electric field. This can be viewed as three-photon of the frequency *ω* conversion into one photon with the frequency *3ω* through virtual levels. Similarly, as for SHG, the produced photon is coherent in-phase and space with the original photons. If third-order interaction is happening between three photons of different frequencies, the transmitted signal will consist of the fundamental frequencies as well as different sums of fundamental frequencies.

The second term of equation (1.7) and Figure 1.2B describes how material interaction with the incident frequency depending on its intensity. For this term, polarization can be expressed as:

$$P(t) = \chi^{(1)} \cdot E \cdot \cos(\omega \cdot t) + \frac{3}{4}\chi^{(3)} \cdot E^3 \cdot \cos(\omega \cdot t) = \chi_0 \cdot E \cdot \cos(\omega \cdot t), \ where\ \chi_0 = \chi^{(1)} + \frac{3}{4}\chi^{(3)} \cdot E^2 = \chi^{(1)} + \chi^{(3)}_{eff} \cdot I \quad (1.8)$$

where *I* is the optical intensity. Further influence of intensity contribution to susceptibility and its effects on material properties will be discussed in the section "Intensity Effects". In the general case the third-order susceptibility is written as forth-rank tensor:

$$\chi^{(3)}_{ijkl}(\omega_\sigma; \omega_1, \omega_2, \omega_3) \quad (1.9)$$

where *I,j,k,l* indicates the tensor element, ω_1, ω_2, and ω_3 are the incident photon frequencies and ω_σ characterizes the interaction between incident photons. When discussing NLO effects, usually Fourier transformation of polarization is used, converting *P(t)* to *P(ω)*. This leads to third-order polarization having the form of 1x3 matrix with elements:

$$P^{(3)}_i(\omega_\sigma) = \sum_{jkl} \chi^{(3)}_{ijkl}(\omega_\sigma; \omega_1, \omega_2, \omega_3) \cdot E_j(\omega_1) \cdot E_k(\omega_2) \cdot E_l(\omega_3), \quad (1.10)$$

Equation (1.10) does not denote the only way how the third-order susceptibility can be defined. Mainly five different conventions are used to define third-order susceptibility[22] whith different definations for polariziaton, electrical field and relation between their Fourier transformations.

Convention I[23,24]:

$$P^{(3)}_i(\omega_\sigma) = \sum_{jkl} \chi^{(3)}_{ijkl}(\omega_\sigma; \omega_1, \omega_2, \omega_3) \cdot E_j(\omega_1) \cdot E_k(\omega_2) \cdot E_l(\omega_3)$$
$$with\ P(t)\ and\ E(t)\ defined\ as\ A(t) = \frac{1}{2}\sum_{\omega \geq 0}\left[A^{(\omega)} \cdot e^{-i\omega t} + A^{(-\omega)} \cdot e^{i\omega t}\right]' \quad (1.11)$$

This approach is wildly used for experimental result description. The advantage of this convention is that no extra numerical factors need to be taken into account. The disadvantage is that one cannot assume that different third-order effects will have the same value in the

zero-frequency limit. This convention has been used in this work to describe experimental results. In this case, all unique frequency combinations need to be taken in account when calculating $\chi(\omega_\sigma; \omega_1, \omega_2, \omega_3)$ - $\chi(\omega_\sigma; \omega_1, \omega_2, \omega_3)$, $\chi(\omega_\sigma; \omega_2, \omega_1, \omega_3)$, $\chi(\omega_\sigma; \omega_3, \omega_2, \omega_1)$ and so on. This is not an intrinsic property of the third-order susceptibility and can be eliminated by implementing specific multipliers, which is the case for other Conventions. The coefficient ½ for *P* and *E* definition is introduced so that for cases when *E(t)* or *P(t)* is real, the definition could be simplified to:

$$A(t) = \sum_{\omega \geq 0}\left[A^{(\omega)} \cdot \cos(\omega t)\right], \tag{1.12}$$

Convention II[25,26]**:**

$$\begin{gathered} P_i^{(3)}(\omega_\sigma) = \frac{D^{(3)}}{2^{q-p}} \sum_{jkl} \chi_{ijkl}^{(3)}(\omega_\sigma; \omega_1, \omega_2, \omega_3) \cdot E_j(\omega_1) \cdot E_k(\omega_2) \cdot E_l(\omega_3) \\ with\ P(t)\ and\ E(t)\ defined\ as\ A(t) = \frac{1}{2}\sum_{\omega \geq 0}\left[A^{(\omega)} \cdot e^{-i\omega t} + A^{(-\omega)} \cdot e^{i\omega t}\right], \end{gathered} \tag{1.13}$$

where q is the number of the nonzero input frequencies, p is the number of nonzero output frequencies and $D^{(3)}$ is the degeneracy term. $D^{(3)}$ is equal to 1 in the case when all of the input frequencies are indistinguishable, 3 if two frequencies are indistinguishable and 6 if none of the frequencies are indistinguishable[27]. This term is due to distinguishable ways the optical frequencies can be arranged. The advantages are that different third-order effects will have the same value at the zero-frequency limit.

Convention III[28,29]**:**

$$\begin{gathered} P_i^{(3)}(\omega_\sigma) = \sum_{jkl} \chi_{ijkl}^{(3)}(\omega_\sigma; \omega_1, \omega_2, \omega_3) \cdot E_j(\omega_1) \cdot E_k(\omega_2) \cdot E_l(\omega_3) \\ with\ P(t)\ and\ E(t)\ defined\ as\ A(t) = \sum_{\omega \geq 0}\left[A^{(\omega)} \cdot e^{-i\omega t} + A^{(-\omega)} \cdot e^{i\omega t}\right], \end{gathered} \tag{1.14}$$

While this convention appears similar to Convention I they differ in aspect, how P(t) and E(t) are defined.

Convention IV[30,31]**:**

$$\chi_{ijk\ldots m}^{(n)}(-\omega_{n+1}; \omega_1, \omega_2, \ldots, \omega_n) = \frac{\partial^n P_i^{\omega_{n+1}}}{\partial E_j^{\omega_1} \partial E_k^{\omega_2} \ldots \partial E_m^{\omega_n}} \tag{1.15}$$

This approach is usually used in the finite field calculations and the Quantum Chemical calculations (QCC). This approach is widely used to calculate the static limits of the third-order susceptibility.

Convention V[4]**:**

$$\begin{gathered} P_i^{(3)}(\omega_\sigma) = D^{(3)} \sum_{jkl} \chi_{ijkl}^{(3)}(\omega_\sigma; \omega_1, \omega_2, \omega_3) \cdot E_j(\omega_1) \cdot E_k(\omega_2) \cdot E_l(\omega_3) \\ with\ P(t)\ and\ E(t)\ defined\ as\ A(t) = \sum_{\omega \geq 0}\left[A^{(\omega)} \cdot e^{-i\omega t} + A^{(-\omega)} \cdot e^{i\omega t}\right], \end{gathered} \tag{1.16}$$

Similarly, as for Convention III, Convention V is similar to Convention II but differs in the way that P(t) and E(t) are defined for this convention. Although the multiplier for the definition is different than for Convention II the advantage that different third-order effects will have the same value at zero-frequency limit is still valid.

These Conventions are related by specific equations. Most essential for this work is how Convention IV relates to Convention I. For the Kerr effect and static limit this can be expressed by equations:

$$\begin{cases} \chi_{ijkl}^{I(3)}(\omega_\sigma;\omega_1,\omega_2,\omega_3) = \frac{1}{8}\cdot\chi_{ijkl}^{IV(3)}(\omega_\sigma;\omega_1,\omega_2,\omega_3) \\ \chi_{ijkl}^{I(3)}(0;0,0,0) = \frac{1}{6}\cdot\chi_{ijkl}^{IV(3)}(0;0,0,0) \end{cases} \quad (1.17)$$

In many cases, the third-order susceptibility can be simplified from a fourth-rank tensor to a more straightforward expression. For example, in an isotropic media one can show that this tensor consists of only three independent elements and can be written as[4]:

$$\chi_{ijkl}^{(3)} = \chi_{1122}^{(3)}\cdot\delta_{ij}\cdot\delta_{kl} + \chi_{1212}^{(3)}\cdot\delta_{ik}\cdot\delta_{jl} + \chi_{1221}^{(3)}\cdot\delta_{il}\cdot\delta_{jk} \quad (1.18)$$

where δ is the Kronecker's delta symbol. Each of the possible three-photon interactions is defined by specific third-order susceptibility with some examples shown in Table 1.1. Also, as a different system of units can be used to describe the third-order susceptibility it is essential to know how to convert values from one to another. In this work mainly two systems of units will be used – SI and the Gaussian (esu) systems. Conversion between both systems can be done by relation[32]:

$$\chi^{(3)}\left[\frac{m^2}{V^2}\right] = \left(\frac{4\cdot\pi}{3}\cdot 10^{-4}\right)^2\cdot\chi^{(3)}[esu], \quad (1.19)$$

This is especially important when comparing experimental results to theoretical calculations, as experimental results are usually given in the SI system while theoretical calculations are given in the Gaussian system.

Table 1.1: *Third-order susceptibility notation for different effects*

Effect	Third-order susceptibility notation
Three wave mixing	$\chi^{(3)}(\omega_1+\omega_2+\omega_3;\omega_1,\omega_2,\omega_3)$
Third-Harmonic generation	$\chi^{(3)}(3\omega;\omega,\omega,\omega)$
Optical Kerr effect	$\chi^{(3)}(\omega;\omega,\omega,-\omega)$
DC Kerr effect	$\chi^{(3)}(\omega;\omega,0,0)$

Third-order susceptibility characterizes materials macroscopic reaction to the electrical field and does not give us any information about this interaction on a molecular or atomic scale. For this, we introduce hyper-polarizability. For third-order interaction, we use the second-order hyper-polarizability. When transitioning from microscopic parameters to macroscopic parameters, usually some type of averaged value is used. For example, in the case of solutions, one can use the isotropic average of the second-order hyperpolarizability[27,33]:

$$\begin{cases} \langle\gamma_{xxxx}\rangle = \frac{1}{15}\sum_{k,l}^{x,y,z}(\gamma_{kkll}+\gamma_{klkl}+\gamma_{kllk}) \\ \langle\gamma_{xxyy}\rangle = \frac{1}{30}\sum_{k,l}^{x,y,z}(4\gamma_{kkll}-\gamma_{klkl}-\gamma_{kllk}) \\ \langle\gamma_{xyxy}\rangle = \frac{1}{30}\sum_{k,l}^{x,y,z}(4\gamma_{klkl}-\gamma_{kkll}-\gamma_{kllk}) \\ \langle\gamma_{xyyx}\rangle = \frac{1}{30}\sum_{k,l}^{x,y,z}(4\gamma_{kllk}-\gamma_{kkll}-\gamma_{klkl}) \end{cases} \quad (1.20)$$

Here *k* and *l* denote the molecular coordinate system while *x* and *y* denote the macroscopic coordinate system. Usually, this transition between molecular system to macroscopic system is done with the second-order hyper-polarizability and not with the third-order susceptibility as it represents the properties of media and is in its core defined by macroscopic coordinates. Another conclusion that can be made from equation (1.20) is that any symmetry rules that can lead to additional tensor elements being equal at the molecular level lead to the same symmetry at the macroscopic level. This parameter is then connected to third-order susceptibility through relation[34]:

$$\chi^{(3)}(\omega_\sigma;\omega_i,\omega_j,\omega_k) = \sum_p \sum_{i,j,k,\sigma} L^{(p)}_{i,j,k,\sigma}(\omega_\sigma;\omega_i,\omega_j,\omega_k)\cdot\langle\gamma^{(p)}_{i,j,k,\sigma}\rangle \tag{1.21}$$

where $\gamma_{i,j,k,\sigma}$ is the second-order hyper-polarizability and $L_{i,j,k,\sigma}$ is the local-field factor. The first sum in equation (1.21) is overall the microscopic elements of the system (atoms, molecules, molecular bonds, etc.). The second sum is over all frequencies present in the material. In the general case, third-order susceptibility is a complex term, with real and imaginary parts characterizing different changes in material (described more in section "Intensity effects"). Depending on the type of system being measured, equation (1.21) can be simplified in different forms. For instance, for solutions equation (1.21) can be rewritten as[35]:

$$\langle\gamma\rangle = \frac{\chi^{(3)}}{L^4\cdot N}, \tag{1.22}$$

where *N* is the density of molecules expressed as molecule number per cm^3. For one compound solution we can also use the Lorentz approximation for the local-field factor[36]:

$$L = \frac{({n_0}^2+2)}{3}, \tag{1.23}$$

When considering a system where one compound in a minority is dissolved in a solvent, a different approach has to be used, where the difference of refractive indexes of both materials is taken into account. This type of system can be modeled as a dye molecule placed in a smooth dielectric media. In this case local, the local field factor can be expressed as[36]:

$$L = \left(\frac{3\cdot {n_{0;1}}^2}{2\cdot {n_{0;1}}^2+{n_{0;2}}^2}\right)\frac{({n_{0;2}}^2+2)}{3}, \tag{1.24}$$

To theoretically characterize NLO properties one of the most popular approaches is Sum over States (SOS) quantum theory. The description given further will be based on these works of literture[36,37]. In general, this theory uses the perturbation method to derive nonlinear susceptibility from the dipole operator matrix and the energy eigenvalues of the Hamiltonian. Due to the complexity of the molecular state structure of real organic molecules (multi-level systems are needed to correctly represent organic molecules energetic structure), usually a more simplified approaches are used – most commonly two-level or three-level systems. In specific cases, the three-level system is extended to a five-level system differencing between singlet and triplet states for specific excited levels. A two-level system is usually used as a first assessment of NLO properties for molecules that possess a permanent dipole moment. In this model the third-order susceptibility consists of two terms – the first term characterizing a single transition between the ground state and the excited state proceeded by a change in the permanent dipole moments (one-photon term) while the second term involves two successive

one-photon transitions from the ground state to the excited state and back (two-photon term; full equation can be viewed in Appendix A). For a two-level system to possess any two-photon contribution, it needs to have a permanent dipole moment. Both of these terms also differ by their dependence on frequency. While both real and imaginary parts of the one-photon term are always negative, two-photon term changes its sign depending on frequency:

- The real part changes the sign from negative to positive when crossing the two-photon resonance,
- The imaginary part is negative before the two-photon resonance, changes to positive at half-frequency of two-photon resonance, and changes back to negative after two-photon resonance.

This means that positive sign for the real part of third-order susceptibility can be acquired only at a frequency above two-photon resonance and for systems that have a permanent dipole moment. This is not a fundamental aspect for all materials as a two-level system has very limited practical application especially for symmetrical molecules that possess no permanent dipole moment. For such cases, three-level systems are most widely used. Such a system consists of an even-symmetry ground state, an odd symmetry excited state, which is strongly coupled to the ground state, and a lowest-lying even-symmetry excited state that is strongly coupled to odd symmetry excited state via a large transition dipole moment. Similarly, as for the two-level system, the terms in the full expression for third-order susceptibility can be separated into two terms – one-photon and two-photon (full equation can be viewed in Appendix A). This equation also shows that the sign of the nonlinearity is determined by the ratio[37]

$$\frac{|\bar{\mu}_{21}|^2 \cdot \bar{\omega}_{10}}{|\bar{\mu}_{10}|^2 \cdot \bar{\omega}_{20}}, \tag{1.25}$$

where μ_{10} and μ_{21} are the electric dipole transition moments between the ground state and the first odd symmetry excited state, and the first odd symmetry excited state and the dominant even symmetry excited state, respectively. When this ratio is greater than unity, the net nonlinearity is positive.

In reality, a combined system of both two-level and three-level systems are used to characterize materials. The most widely applied model in organic material studies is a simplified three-term equation[1]:

$$\gamma_{xxxx} \propto \frac{\mu_{ge}^2 \cdot \Delta\mu_{eg}^2}{E_{ge}^3} - \frac{\mu_{ge}^4}{E_{ge}^3} + \sum_{e'} \frac{\mu_{ge}^2 \cdot \mu_{ee'}^2}{E_{ge}^2 \cdot E_{ge'}}, \tag{1.26}$$

where the first term is called the D term (dipolar term, which is zero for centrosymmetric systems), the second is the N term (negative term due to sign) and the third – the T term (two-photon term) (see Figure 1.3). This model can be used for molecular systems, where assumption can be made that only one excited state is strongly coupled with the ground state and the primary components of the excited state and transition dipole moments are aligned along one molecular axis (in this case denoted as x).

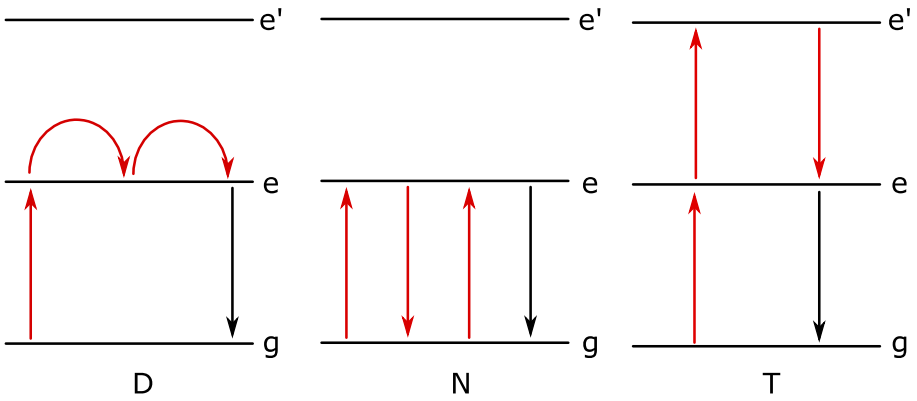

Figure 1.3: *Illustration of second-order hyperpolarizability terms – D (Dipolar term), N (Negative term), and T (Two-photon term). Red arrows indicate photons that influence material while black lines indicate the observed photon and g is ground state while e and e' – excited states.*

1.4. Second-order hyper-polarizability fundamental limits

In NLO material studies the essential question is – how to increase NLO coefficient values of materials? The trend of discovering new more efficient materials have gone on for some decades, but one can wonder are there any limits to these coefficients. M. G Kuzyk calculated fundamental limits of second-order hyper-polarizability in 2000 using a three-level model[38]:

$$-\frac{e^4\cdot\hbar^4}{{m_e}^2}\cdot\left(\frac{{N_e}^2}{E_{10}^5}\right)\leq\gamma\leq 4\cdot\frac{e^4\cdot\hbar^4}{{m_e}^2}\cdot\left(\frac{{N_e}^2}{E_{10}^5}\right), \tag{1.27}$$

where e is the electron charge, m_e is the electron mass and N_e is the number of electrons in the molecule. Although this result has been known for many years there are still many unknown and unproven aspects of it, such as: i) What molecular design could approach fundamental limits of NLO effects and cross the Kuzyk quantum gap; ii) Is the three-level approximation completely correct model for the derivation of fundamental limits[39].

1.5. Intensity effects

Now the focus of this work will shift from fundamental aspects of third-order susceptibility to specific macroscopic effects in materials that arise du to it. In this section, we will look closer at the intensity effects of third-order susceptibility. The description given in this section is based on W. Boyd's' book "Nonlinear optics"[4]. First, let's consider how the refractive index related to the third-order susceptibility:

$$n=\sqrt{1+\chi_0}=\sqrt{1+\chi^{(1)}+3\chi^{(3)}\cdot|E(\omega)|^2}=\left[n_0=\sqrt{1+\chi^{(1)}}\right]=n_0\cdot\sqrt{1+3\frac{\chi^{(3)}\cdot|E(\omega)|^2}{{n_0}^2}}\cong n_0+\frac{3}{2}\frac{\chi^{(3)}\cdot|E(\omega)|^2}{n_0}=n_0+\frac{3}{4}\frac{\chi^{(3)}\cdot I}{{n_0}^2\cdot\varepsilon_0\cdot c}=n_0+n_2\cdot I \tag{1.28}$$

where c is the speed of light, ε_0 is the dielectric constant of vacuum, n_0 is the materials linear refractive index and n_2 is the nonlinear refractive index. This shows that third-order effects can induce refractive index changes proportional to the intensity of the electrical field, also known as the Kerr effect. In general case refractive index and dielectric susceptibility is defined as complex parameters:

$$\begin{cases} n_k = n_{k;Re} + i \cdot n_{k;Im} \\ \chi^{(k+1)} = \chi_{Re}^{(k+1)} + i \cdot \chi_{Im}^{(k+1)} \end{cases} \quad (1.29)$$

where *Re* denotes the real part and *Im* – the imaginary part. The imaginary part of the refractive index characterizes optical absorption of material[40]:

$$n_k = n_{k;Re} + i \cdot \frac{\alpha_k \cdot \lambda}{4\pi} \quad (1.30)$$

where λ is the wavelength. Thereby refractive index changes due to the electrical field are also characterized by two parts – real and imaginary parts describing the refractive index changes and the optical absorption changes, respectfully. Combining equations (1.29) and (1.30) we can formulate relations between third-order susceptibility and the nonlinear refractive index and absorption[41]:

$$\begin{cases} n_2 = n_{2;Re} + i \cdot \frac{\alpha_2 \cdot \lambda}{4\pi} \\ \chi^{(3)} = \chi_{Re}^{(3)} + i \cdot \chi_{Im}^{(3)} \end{cases} \rightarrow \left[n_2 = \frac{3}{4} \frac{\chi^{(3)}}{{n_0}^2 \cdot \varepsilon_0 \cdot c} \right] \rightarrow \begin{cases} \chi_{Re}^{(3)} = \frac{4 \cdot {n_0}^2 \cdot \varepsilon_0 \cdot c}{3} \cdot n_2 \\ \chi_{Im}^{(3)} = \frac{{n_0}^2 \cdot \varepsilon_0 \cdot c \cdot \lambda}{3 \cdot \lambda} \cdot \alpha_2 \end{cases} \quad (1.31)$$

To better compare the nonlinear refractive index properties on a molecular scale, the nonlinear refractive cross-section can be used, defined as[42]:

$$\delta_{\mathrm{NLR}} = \frac{\hbar \cdot \omega \cdot \mathrm{k} \cdot \mathrm{n}_2}{\mathrm{N}} \cdot 10^{58}, \quad (1.32)$$

Here the acquired value's unit of measure is the refractive Göppert-Mayer (RGM).

Till this moment we looked at effective values of the third-order susceptibility and neglected the tensor nature of this variable. In the case of the Kerr effect in isotropic media when all of the incident frequencies are equal media possesses only two independent tensor elements χ_{1122} and χ_{1221} and can be written as:

$$\chi_{ijkl}^{(3)} = \chi_{1122}^{(3)} \cdot \left(\delta_{ij} \cdot \delta_{kl} + \delta_{ik} \cdot \delta_{jl} \right) + \chi_{1221}^{(3)} \cdot \delta_{il} \cdot \delta_{jk} \quad (1.33)$$

This allows rewriting the nonlinear polarization term as:

$$P^{(3)} = 6\chi_{1122}^{(3)} \cdot (E \cdot E^*)E + 3 \cdot \chi_{1221}^{(3)} \cdot (E \cdot E)E^* = A \cdot (E \cdot E^*)E + \frac{B}{2} \cdot (E \cdot E)E^* \quad (1.34)$$

The difference between two elements that contributes to nonlinear polarization can be better understood through energy level diagrams, similar to ones shown in Figure 1.2, with A characterizing both one- and two- photon contributions and B characterizing only two-photon contributions. Another essential aspect of these elements is that the ratio between both tensor elements can allow understanding what effects induce the polarization changes (will be further discussed in section "Nonlinear refractive index").

Let's now consider a laser beam of arbitrary polarization propagation through nonlinear media in the positive *z*-direction. An electrical field can be decomposed into a linear combination of two circular-polarization components:

$$E = E_+ \cdot \hat{\sigma}_+ + E_- \cdot \hat{\sigma}_- \tag{1.35}$$

where circular-polarization unit vectors and electric field amplitudes are defined as:

$$\hat{\sigma}_\pm = \frac{\hat{x} \pm i \cdot \hat{y}}{\sqrt{2}} \; and \; E_\pm = E_0 \cdot \frac{\cos\theta \pm i \cdot \sin\theta}{\sqrt{2}} \tag{1.36}$$

where E_0 is the amplitude of the electrical field and θ is the polarization angle. Similarly, we can define polarization changes as a sum of two circular-polarization components and rewrite equation (1.34) in the form:

$$P^{(3)} = P_+^{(3)} \cdot \hat{\sigma}_+ + P_-^{(3)} \cdot \hat{\sigma}_- \;\rightarrow\; P_\pm^{(3)} = A \cdot \left|E_\pm\right|^2 \cdot E_\pm + (A+B) \cdot |E_\mp|^2 \cdot E_\pm \tag{1.37}$$

In a similar way we can express both the third-order susceptibility and the refractive index:

$$\begin{cases} \chi_\pm^{(3)} = A \cdot \left|E_\pm\right|^2 + (A+B) \cdot |E_\mp|^2 \\ n_\pm = n_0 + \frac{2\pi}{n_0} \cdot \left[A \cdot \left|E_\pm\right|^2 + (A+B) \cdot |E_\mp|^2\right] \end{cases} \tag{1.38}$$

From equation (1.38) we can see that in general cases both circular-polarized components travel with different phase velocities. The difference between both refractive indices is:

$$\Delta n = \frac{2\pi \cdot B}{n_0} \cdot (|E_-|^2 - |E_+|^2) \tag{1.39}$$

This can lead to a rotation of polarization ellipsoid. As indicated by equation (1.38) rotation angle will only depend on coefficient B and can be expressed as:

$$\varphi = \frac{\Delta n}{2} \cdot \frac{\omega}{c} \cdot z, \tag{1.40}$$

Measurements of this angle provide a very sensitive method to determine the value of coefficient *B*. There are two cases in which both phase velocities are equal – linearly and circularly polarized light. For these cases the nonlinear refractive index can be written as:

$$\begin{cases} n_{2;linear} = \frac{2\pi}{n_0} \cdot \left(A + \frac{B}{2}\right) \cdot |E|^2 \\ n_{2;circular} = \frac{2\pi}{n_0} \cdot A \cdot |E|^2 \end{cases} \tag{1.41}$$

By knowing refractive index changes in both of these cases, we can calculate coefficients *A* and *B* and know the values to third-order susceptibilities tensor elements. This is essential a, previously stated, the ratio of coefficients *A* and *B* can allow determining the mechanism involved in inducing refractive index changes (see Table 1.2).

1.6. Nonlinear refractive index

Kerr effect is not the only effect that can induce refractive index changes. To better understand how to measure the Kerr effect, we need to understand how to correctly separate the Kerr effect contribution from other effects that can induce the refractive index changes. In general, all materials possess a nonlinear refractive index that can vary from an order of 10^-

^{20} m^2/W for water till 10^{-4} m^2/W for complex organic thin films. While for water this coefficient is small and negligible for practical applications more complex structures reaching the order of 10^{-4} m^2/W for n_2 could be applicable for different NLO devices. But the magnitude of the effect is not the only variable important for NLO applications. Modern technologies are heading towards higher and higher bandwidth, meaning that switching time for NLO effects starts to play a role in material selection. Here it is important to specify what effect is inducing refractive index changes as they vary by response time - the major four mechanisms being electronic, molecular reorientation, electrostrictive and thermal processes. Response time, as well as the ratio of constants B and A (see Section Intensity Effects), are arranged in Table 1.2.[4]

Table 1.2: *Parameters B/A ratios and corresponding mechanisms inducing refractive index changes*

Ratio B/A	Inducing effect	Response time, s
6	Molecular reorientation	10^{-12}
1	Non-resonant electronic response	10^{-15}
0	Electrostriction, thermo-optical	10^{-9}

Kerr effect. Kerr effect itself consists of multiple types of responses from molecules to external optical irradiation. In the first approximation, these contributions can be divided into two groups – electronic and nuclear. This nomenclature comes from inorganic material studies of simpler atomic structures, but in the case of complex organic materials, nuclear effects should be renamed as molecular effects to emphasize that for organic materials these contributions describe the combined response of all atoms of organic molecules. Due to this in this work, a variation from the classical approach will be used by substituting nuclear contributions with molecular contributions. A more detailed description of both contributions will be given in the following passages.

Electronic contribution. This mechanism is based on a bound electron response on the applied optical field. Compared to other mechanisms electronic contribution is relatively small but it is present in all dielectric materials and has the fastest response time. It has been shown that π electron delocalization can greatly increase the magnitude of electronic contribution. Its contribution can also be greatly enhanced by using the electrical field close to the materials resonance frequency, although this also leads to an increase in absorption effects that in many cases can be unwanted. To calculate third-order susceptibility of electronic contribution, one can use the anharmonic oscillator model to show that:

$$\chi^{(3)}_{ijkl}(\omega;\omega,\omega,-\omega) = \frac{N\cdot b\cdot e^4\cdot\left[\delta_{ij}\delta_{kl}+\delta_{ik}\delta_{jl}+\delta_{il}\delta_{jk}\right]}{3\cdot m^3\cdot D^3(\omega)\cdot D(-\omega)}, \tag{1.42}$$

where b is the nonlinear constant of the order ω_0^2/d^2 (d is the atomic dimension and ω_0 is the optical absorption frequency) and $D(\omega)$ is:

$$D(\omega) = \omega_0^2 - \omega^2 - 2\cdot i\cdot\omega\cdot\Gamma, \tag{1.43}$$

where Γ characterizes the damping force. For the non-resonant case, this equation can be simplified to:

$$\chi^{(3)} \cong \frac{N \cdot e^4}{m^3 \cdot \omega_0^6 \cdot d^2}, \tag{1.44}$$

where N is the molecule concentration per volume unit. Third-order susceptibility can also be described using the quantum-mechanical model. This gives a complicated result showing that the electronic contribution is governed by two terms – two-photon resonant term and one-photon resonant term (SOS model). But this model can also give a way to evaluate the order of magnitude for the non-resonant cases:

$$\chi^{(3)} \cong \frac{8 \cdot N \cdot \mu^4}{\hbar^3 \cdot \omega_0^3}, \tag{1.45}$$

where μ is the typical value of the dipole matrix element. For these cases, both models give similar order for third-order susceptibility.

Molecular effects. Another effect group that can influence refractive index is the molecular contribution that usually is characterized by a non-instantaneous response with a time constant between 0.15-1.5 ps.[43–45] This range of time constants arises due to multiple molecular processes that can influence the refractive index. Molecular effects play the most significant role when studying NLO properties of solutions and will be further discussed for such cases. First, let's consider noble gases and highly symmetrical molecules. Experimental measurements of liquid Xe and CCl_4 have shown that most of the refractive index changes are due to electronic contribution but around or less than 10% of refractive index changes have time-delayed response with a time constant of 450 fs. For symmetrical molecules, it is accepted that a dipole induced dipole interaction creates a molecular response[45,46]. But this process is not simply explained as molecules dipole changes due to neighboring molecules dipole changes. In solution, molecules are packed relatively close and electronic overlap starts to play a significant role. In literature, regarding NLO effects this effect usually is denoted as collision contribution. Similarly, as for electronic response, this effect has isotropic symmetry leading to similar polarization dependence as an electronic response. Theory becomes more complicated for asymmetrical molecules with permanent polarization anisotropy. For such cases, molecular effects are usually divided into three groups of effects – libration, collision-induced variations, and diffusive reorientation. The libration process can be explained as small molecules vibrations due to external optical irradiations in the potential well of neighboring molecules[44,45,47]. In literature, this motion is often described as molecule "rocking" in a potential well. The essential condition for this is that excitation pulse is shorter than molecules lifetime in this potential well and usually has a time constant of around 150 fs. The slowest of these three effects is called diffusive reorientation. This can be viewed as the next step of the libration process when a molecule is excited from one potential well to another[47] and has a time constant around 1.5 ps. As this process is studied in this work, a more in-depth review of it will be given below. Experimental studies of molecular symmetry's influence on molecular contributions have been carried out by studying CCl_4, $CHCl_3$, and CH_2Cl_2 showing that by going from anisotropic structures to more symmetrical ones, libration and reorientation contributions start to diminish[44].

Molecular reorientation. If media is composed of anisotropic molecules, in the presence of the electric field, molecules will try to reorient their dipole moment parallel to the applied electrical field. This will lead to media becoming partially anisotropic. As this effect possesses electrical-dipole interaction as well as thermal aspects due to molecule reorientation, it is important to distinguish in which cases nonlinear refractive index can be used to describe this process. In general molecular reorientation model can be applied in cases when thermal energy is large compared to electric-dipole interaction energy. By considering a molecule with polarizability α_1 in *x* and *y* direction and α_2 in *z* direction and $\alpha_2 > \alpha_1$ irradiated by an optical wave, molecules will try to align with electrical field direction. It is important to emphasize that this response is proportional to E^2. This gives rise to two types of responses – near zero frequency response through induced dipole moment interaction with the applied optical field and two times the optical frequency. The molecule motion is not able to respond to 2ω frequency and reacts to near zero frequency. Resulting nonlinear refractive index changes can be written as:

$$n_2 = \frac{4 \cdot \pi \cdot N}{45 \cdot n_0} \cdot \left(\frac{n_0^2+2}{3}\right)^4 \frac{(\alpha_2-\alpha_1)^2}{k_B \cdot T}, \tag{1.46}$$

From this equation, it is evident that for molecular reorientation nonlinear refractive index depends on the difference of molecular polarizations as well as temperature. A general equation for materials with different polarizabilities in each of directions has been presented by D. H. Close and his group in their 1966 paper[48]. This equation is of the form:

$$n_2 = \frac{\pi \cdot N}{45 \cdot n_0} \cdot \left(\frac{n_0^2+2}{3}\right)^4 \frac{\left((\alpha_2-\alpha_1)^2+(\alpha_3-\alpha_1)^2+(\alpha_3-\alpha_2)^2\right)}{k_B \cdot T}, \tag{1.47}$$

In most cases, the optical Kerr effect is associated with the molecular and the electronic contributions (as it is always present in media to some level).

While in general many literature sources would use this type of description for molecules NLO response as a base, there is still one aspect where a discrepancy between specific literature sources arises – that is regarding reorientation and vibration contributions. Works referenced up till now mainly view that only these three types of contributions correspond to molecular effects, but there can be found a significant amount of works that also mentions vibrational contribution as another component. M. G. Kuzyk in his overview of third-order NLO properties of organic molecules states that both vibrational and reorientation contributions affect molecular response to the electrical field with vibrational effects having a faster time constant that corresponds to vibrational frequencies of molecules (see Figure 1.4 A)[36]. Experimental works are showing that the vibrational aspect of both CS_2 and CO_2 gases influence second-order hyperpolarizability proving the existence of this effect in general[49,50]. On the other hand, there are works in literature that explain the pulse-width dependence of Kerr response of molecules, excluding the vibrational aspect but using just a single time-dependent function (see figure 1.4 B)[45]. A unified approach to this question has still not been established.

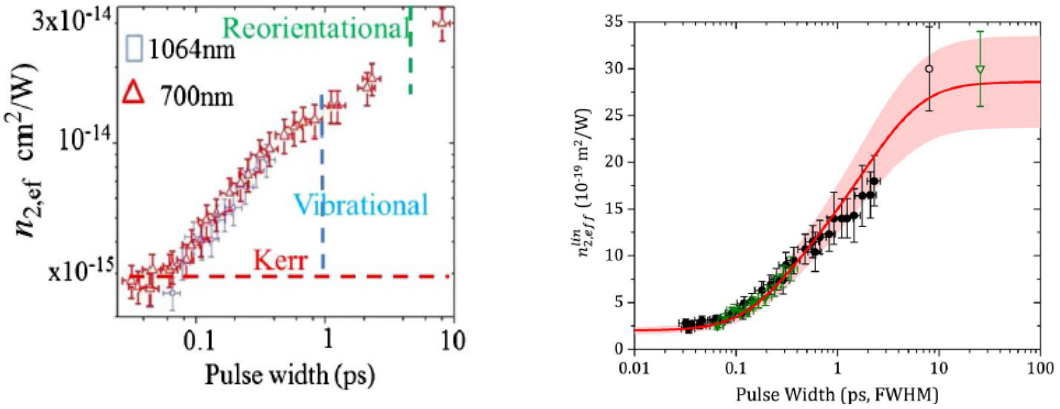

A B

Figure 1.4: *Different interpretations of same experimental results for CS_2. A – M.G. Kuzyks approach in Ref [33]. B – M. Reichert approach in reference [43]. Both graphs has been taken from the original papers. Approach A seperates results into thress different levels indicating atleast two step-functions, while B use a single step-function to approximate all data.*

Vibrational contribution. While in general vibrational and reorientation contributions differ from each other, an argument can be made that it is not always essential. In general, for third-order NLO effects, vibrational contributions are divided into four parts denoted as [μ^4], [α^2], [$\alpha\mu^2$], and [$\mu\beta$] where μ denotes dipole contribution, α denotes polarizabilities contribution, and β – first-order hyperpolarizabilities contribution[51]. These elements indicate what types of electronic properties interact for enhancement of third-order response. At the same time, similar contributions can be identified for reorientation processes. The previously mentioned molecular reorientation process corresponds to [α^2] element. In specific cases, second-order susceptibility also contributes to the third-order properties due to molecules orientation parallel to applied field[52]. This contribution can be expressed as the connection between second- and first- order hyperpolarizabilites[23]:

$$\gamma = \frac{\mu \cdot \beta}{5 \cdot k_B \cdot T} \tag{1.48}$$

where μ is the molecule's dipole moment. But not all vibrational contributions influence all types of third-order NLO responses. For the Kerr effect only the [α^2] term is significant, similarly as for reorientation. It is important to emphasize that polarization-resolved measurements used in this work cannot separate libration, vibration, or reorientation contributions. Due to this in the further text, all these three contributions will be denoted as reorientation effects as this is a widely used denomination for Kerr contributions with the ratio B/A=6. Literature sources are indicating that for specific organic solvents equation (1.47) can predict molecular contribution to the Kerr effect from experimental values of linear polarizability quiet well indicating that this approach is not so incorrect when predicting Kerr response for pulses longer than 1 ps[53].

Electrostrictive contribution. This mechanism is based on molecular displacement due to inhomogeneous optical intensity in the material. If some intensity pattern with bright and dark fringes is formed in the media, a force will be applied on dipoles moving them into regions with higher optical intensity.

Thermal effects. Another mechanism behind the nonlinear refractive index is through thermal effects. High-intensity optical irradiations can heat media leading to density changes thus inducing refractive index changes. This process is described by heat-transport equation[4]:

$$\left(\rho_0 \cdot C\right) \cdot \frac{\partial T}{\partial t} - \kappa \cdot \nabla^2 T = \alpha \cdot I(r), \tag{1.49}$$

where $\rho_0 C$ is the heat capacity per volume unit and κ is the thermal conductivity. Mainly two thermal effect types are considered – single pulse and accumulative effects. When optical light pulse length is longer than the time in which media can dissipate heat, a single laser pulse can induce thermos-optical effects. This is characterized by a time constant:

$$\tau_S = \frac{w_0}{v_s} \tag{1.50}$$

where w_0 is beam waist radius and v_s is the speed of sound in media. In most cases this time constant is of an order of few to tens of nanoseconds. On the other hand, if the time between two consecutive laser pulses is short enough, absorbed energy will accumulate and lead to thermal effects. This effect is characterized by a time constant:

$$\tau_D = \frac{{w_0}^2}{4 \cdot D_t}, \tag{1.51}$$

where D_t is the thermal diffusivity. At a certain pulse duration time, we can assume that media reaches thermal equilibrium and any laser with a longer pulse duration can be treated as a CW laser for specific media. This time constant can be acquired by solving the heat-transport equation, giving result:

$$\tau_E = \frac{\rho \cdot C \cdot {w_0}^2}{k}, \tag{1.52}$$

For the CW laser case the nonlinear refractive index can be expressed as:

$$n_2 = \left(\frac{dn}{dT}\right) \frac{\alpha \cdot {w_0}^2}{k}, \tag{1.53}$$

where dn/dT is the thermo-optical coefficient.

1.7. Two-photon absorption

If the light is traveling through a media, it can lose part of its optical power to media through absorption. This process is characterized by absorbance:

$$A = \log_{10} \frac{I_{out}}{I_{in}} \tag{1.54}$$

where I_{in} is the optical intensity of light before the media and I_{out} is the optical power on the exit surface of the media. While absorbance is a property of a specific media, in many cases we are more interested in parameters that characterize material or molecules of media. In

these cases either absorption coefficient α or molar absorption coefficient η is used defined as:

$$\alpha = \frac{A}{l} \; and \; \eta = \frac{A}{l \cdot C} \tag{1.55}$$

where *l* is the length of media and *C* is the molar concentration. Linear absorption can be used to calculate ground-state absorption cross-section by the equation:

$$\sigma_{ground} = \frac{\alpha}{N} \tag{1.56}$$

where *N* is the molecule concentration per cm^3. But similarly, as for the refractive index, optical absorption also can change due to optical irradiation. In the further text, we will discuss few of the mechanisms that can induce these changes.

Two-photon absorption. In previous chapters, we concluded that as refractive index is a complex number with an imaginary part characterizing optical absorption. Similarly, as for the nonlinear refractive index, it can be shown that absorption also changes linearly from the optical intensity in case of third-order NLO effects:

$$\alpha = \alpha_0 + \alpha_2 \cdot I \tag{1.57}$$

where α_0 is the linear absorption and α_2 is the nonlinear absorption, also known as two-photon absorption (2PA) coefficient. A simple way to understand this process is to view it as absorption of two photons at the same time. This leads to absorption changes proportional to the intensity at optical irradiation. It is also important to state that 2PA induced luminescence is un-coherent compared to SHG that is characterized by coherent irradiation. This is because 2PA involves a real molecular level to which electrons are excited through photon absorption. Due to this emitted photon is not coherent in-phase and space with original photons. While the 2PA coefficient characterizes media properties, often we need to describe a single molecule contribution to over-all absorption changes. In this 2PA cross-section is used, defined as:

$$\sigma_{2PA} = \frac{\hbar \cdot \omega}{N} \cdot \alpha_2 \tag{1.58}$$

where $\hbar \cdot \omega$ is the photon energy and *N* is the molecule concentration per cm^3. 2PA absorption depends not only on molecular properties but also on macroscopic sample properties. Scientific research groups have shown that 2PA depends on sample concentration[54]. In most cases, it is due to aggregation effects. At the same time, it has been shown that for low concentrations (*C*<1 mM) 2PA possesses threshold power at which absorption starts to change[54]. This is mainly an experimental issue as low concentration samples usually demand high laser intensities and can lead to higher-order effects contributing to absorption changes. 2PA is not the only nonlinear absorption effect that can influence absorption and distinguishing between different effects is essential. Saturable absorption, reverse saturable absorption and excited-state absorption can also significantly influence absorption[55–59].

Saturable absorption. To study NLO properties, it is necessary to implement high power lasers – often with intensity <10 GW/cm^2. In some cases this can lead to saturation of specific excited

molecular states, therefore, making the media transparent to appropriate wavelength. This process is called saturable absorption and is described by the following equation:

$$\alpha = \frac{\alpha_0}{1+\frac{I}{I_S}} \tag{1.59}$$

where I_s is saturation intensity. On the other hand, for cases when excited state absorption cross-section is much larger than ground-state absorption the reverse saturation absorption can occur leading to an increase in absorption. Both of the effects can be measured in the same material at different laser powers leading to unique absorption dependence on optical irradiance power[58,59]. One way to explain this transition is to use an extra level compared to two- or three- level schemes discussed before[60]. Both cases are shown in Figure 1.5. At low laser powers optical absorption is mainly influenced by the first two levels. In case, when $\sigma_0>\sigma_1$ saturable absorption effect occurs, as the ground state is depleted of electrons much faster than the first excited state. When optical intensity is increased, other transitions can start to deplete ground state by transition $S_0->S_2$. In cases when $\sigma_{2PA}>\sigma_0$ this effect can lead to the Reverse saturable absorption. This transition can include two-photon absorption that is intensity-dependent effect.

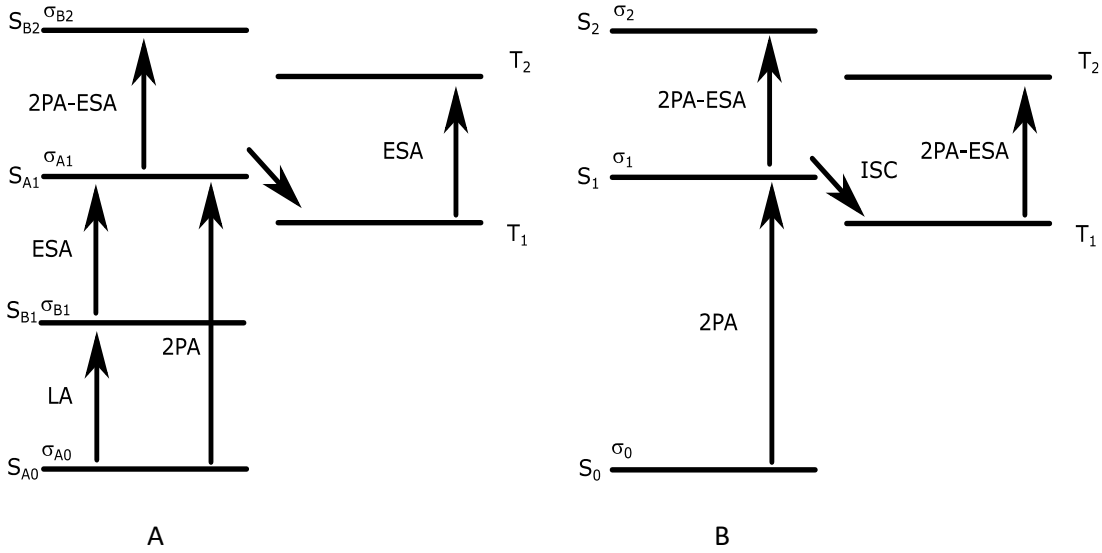

Figure 1.5. *Schematic description of absorption effects. LA – linear absorption; 2PA – two-photon absorption, ESA – excited-state absorption, 2PA-ESA – two-photon absorption induced excited-state absorption, ISC – intersystem crossing, S – singlet levels, T – triplet levels. A) Three-level diagram extended to the four-level system, to include 2PA-ESA and ESA effects. B and A denotes different symmetry level. One-photon transitions can occur only between levels with different symmetry while two-photon transitions need levels with the same symmetry. If $\sigma_{A0}>\sigma_{B1}$ then the saturation absorption can be observed. If $\sigma_{A1}>\sigma_{A0}$ then at higher optical intensities nonlinear processes will start to dominate and the reverse saturation absorption will occur. The intersystem crossing can increase the 2PA-ESA effect if electrons transit from singlet state to triplet. B) The two-level system extended to a three-level system to incorporate excited state absorption effects.*

Excited-state absorption. Process, when electrons from the excited level transits to an even higher level through optical absorption, is called the excited-state absorption. There are

various ways how this effect can occur but in this work, only 2PA induced excited-state absorption will be considered. When an electron is excited from ground level to the excited-state through 2PA, this electron can be excited to an even higher level through excited-state absorption (See Figure 1.5). This effect can be enhanced if the molecule can undergo intersystem crossing from singlet to triplet state.

1.8. Gaussian profile beam

Most of NLO studies are carried out using lasers as they are monochromatic sources with large optical intensity. One way to categorize laser beams is by their intensity profile. While various kinds of lasers have been implemented for NLO studies, Gaussian beam (GB) lasers are still the most widely used ones. Radial distribution of intensity for GB can be characterized by Gaussian distribution, hence the name of the beam. Electrical field amplitude for GB can be written as:

$$E(r,z) = E_0 \cdot \frac{w_0}{w(z)} \cdot e^{-\frac{r^2}{w(z)^2}} \cdot e^{-i\cdot\left(k\cdot z - atg\left(\frac{z}{z_R}\right) + \frac{k\cdot r^2}{2\cdot R(z)}\right)} \tag{1.60}$$

where E_0 is the electric field amplitude at focus, w_0 is beam waist radius at the focal point, k is wave number, z_R is Rayleigh length, and the rest of parameters are expressed as:

$$\begin{cases} z_R = \frac{\pi\cdot {w_0}^2}{\lambda} \\ w(z)^2 = {w_0}^2 \cdot \left(1 + \left(\frac{z}{z_R}\right)^2\right) \\ R(z) = z \cdot \left(1 + \left(\frac{z_R}{z}\right)^2\right) \end{cases} \tag{1.61}$$

where λ is the wavelength. The Schematic depicting focusing of GB is shown in Figure 1.6. For the far-field case ($z>>z_R$) changes of laser beam waist radius can be characterized by asymptote that intersects the z-axis at an angle:

$$tg(\theta) = \frac{\lambda}{\pi\cdot w_0} \tag{1.62}$$

Using this expression, we can derive a beam waist radius using the beam size on lens R and the focal length of lens f:

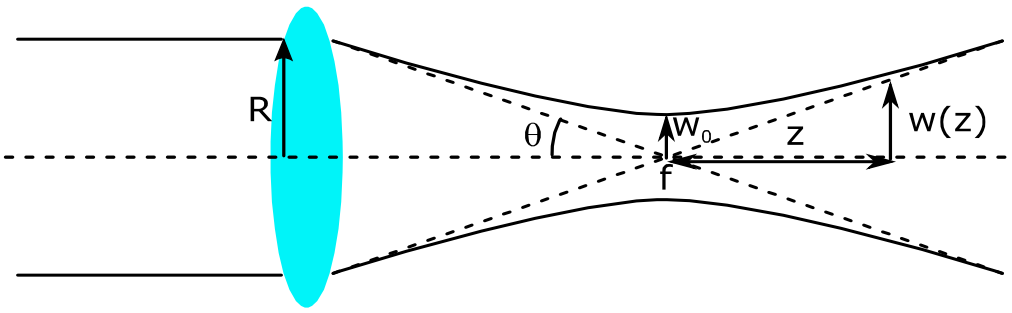

Figure 1.6. *Focusing of Gaussian Beam.*

$$w_0 = \frac{\lambda}{\pi} \cdot \frac{f}{R} \tag{1.63}$$

If GB has traveled through a media with unknown properties, it will experience arbitrary phase changes as well as a decrease in power due to absorption. Electrical intensity at the exit surface of this media can be written as:

$$E(r, z, \Delta\varphi) = E(r, z) \cdot e^{\frac{\alpha \cdot L}{2}} \cdot e^{-i \cdot \Delta\Phi} \tag{1.64}$$

where L is the length of media, α is it's the absorption and $\Delta\Phi$ is the induced phase change. To calculate the far-field profile of such beam we use the "Gaussian decomposition method" first introduced by D. Weaire and his group[61]. In this method GB is decomposed into a sum of various GB through expanding the nonlinear phase term through a Taylor series:

$$e^{-i \cdot \Delta\Phi(r,z)} = \sum_{m=0}^{\infty} \frac{(-i \cdot \Delta\Phi(r,z))^m}{m!} = \sum_{m=0}^{\infty} \frac{1}{m!} \cdot \frac{(-i \cdot \Delta\Phi)^m}{\left(1+\left(\frac{z}{z_R}\right)^2\right)^m} \cdot e^{-\frac{2m \cdot r^2}{w^2(z)}} \rightarrow E(r, z, \Delta\Phi) = E(r, z) \cdot e^{\frac{\alpha \cdot L}{2}} \cdot$$

$$\sum_{m=0}^{\infty} \frac{1}{m!} \cdot \frac{(-i \cdot \Delta\Phi)^m}{\left(1+\left(\frac{z}{z_R}\right)^2\right)^m} \cdot e^{-\frac{2m \cdot r^2}{w^2(z)}} \tag{1.65}$$

After all of the decomposed components are propagated along the z-axis and resumed to reconstruct the beam.

While using GB laser in experimental measurements it is essential to know the intensity of the laser beam. By knowing the electrical field amplitude of laser, intensity can be calculated as:

$$I = 2 \cdot \varepsilon_0 \cdot n \cdot c \cdot |E(r, t)|^2, \tag{1.66}$$

In most cases, it is easier to experimentally measure the power of laser beam defined for GB as:

$$P = \int_A I \cdot dA = \frac{\pi \cdot {w_0}^2}{2} \cdot I = \begin{cases} \frac{\pi \cdot {w_0}^2}{2} \cdot I_0 & CW\ laser \\ \frac{\pi \cdot {w_0}^2}{2} \cdot I_0 \cdot \tau \cdot \nu_{rep} & Pullsed\ laser \end{cases}, \tag{1.67}$$

where τ is the impulse duration and ν_{rep} is the pulls repetition rate.

1.9. Material selection rules

Material selection for NLO applications is mainly based on two principles – analytical models that connect different optical properties of material allowing to calculate spectral dispersion of one parameter by knowing others and correlations observed between molecular structure and NLO properties. First, let's examine the analytical model approach. One of the most fundamental ways to look at electrons under illumination is as a collection of harmonic oscillators while NLO effects correspond to deviations from harmonic behavior. On this basis, the first principles for NLO material selection rules were derived by R. C. Miller for second-order susceptibility. During his research[9], he showed that the SHG coefficient is proportional first-order susceptibility and an element of third rank tensor:

$$d_{ijk}^{2\omega} = \chi_{ii}^{2\omega} \cdot \chi_{jj}^{\omega} \cdot \chi_{kk}^{\omega} \cdot \delta_{ijk}^{2\omega}, \tag{1.68}$$

where χ elements are respective the first-order susceptibilities and δ correspond to the third rank tensor. The most important aspect of his work was showing that for multiple materials (KH_2PO4, ZnO, CdS, etc) coefficient δ was approximately equal for materials of the same symmetry class, making the SHG coefficient only dependent on linear optical parameters. This principle was been further extended by various scientists[10–12] that showed similar correlations for third-order susceptibility:

$$\begin{cases} |\chi^{(3)}| \sim [\chi^{(1)}]^a \; where \; 4 \leq a \leq 5 \; (Wynee \; work) \\ \chi^{(3)}_{ijkl}(\omega_\sigma; \omega_1, \omega_2, \omega_3) \propto \chi^{(1)}(\omega_\sigma) \cdot \chi^{(1)}(\omega_1) \cdot \chi^{(1)}(\omega_2) \cdot \chi^{(1)}(\omega_3) \cdot C_{ijkl} \; (Mizrahi \; work) \end{cases}, \quad (1.69)$$

Around 1970 C. C. Wang proposed a more universal rule that described the third-order susceptibility for quasi-static limit[62]:

$$\chi^{(3)}(\omega \to 0) = \frac{g}{N_{eff} \cdot \hbar \cdot \omega_0} \cdot (\chi^{(1)})^2, \quad (1.70)$$

where g is dimensionless quantity involving properties of the ground and the excited states, N_{eff} is the oscillator strength and ω_0 is the mean absorption frequency. Wang showed that this rule can be applied to low ionic crystals as well as low-pressure gases for which Miller's rule was not applicable. An essential aspect of Miller's rule was Bassani extension of this rule to any order of susceptibility by equation[63]:

$$\begin{cases} \chi^{(n)}(\omega, \dots, \omega) \approx \delta^{(n)} \cdot \chi^{(1)}(n \cdot \omega) \cdot \left(\chi^{(1)}(\omega)\right)^n \\ \delta^{(n)} = -\frac{1}{n!} \cdot \frac{m}{e^{n+1} \cdot N^n} \cdot \left[\frac{\partial^{n+1} V(x)}{\partial x^{n+1}}\right]_0 \end{cases}, \quad (1.71)$$

where $\delta^{(n)}$ is Miller's constant. From this, we can see that it is necessary to find Miller's constant for specific material or group of materials and NLO properties of those materials can be acquired from linear optical properties.

Another approach for characterization of NLO property spectral dispersion is by the Kramers-Kronig relations, that gives a relation between complex functions real and imaginary parts. As the name suggests, these relations were studied by two scientists, H. Kramers and R. Kroning, in 1926 and 1927. Although they did not give a complete description of these relations, they are still regarded as the original composers. The Kramers-Kronig relations have been studied by numerous scientists, each of them giving their own contribution. B. Hu showed how to derive these relations in 'two lines'[64] while M. Sharnoff proved in which cases these relations are valid[65]. The Kramers-Kronig relations can be expressed as:

$$\begin{cases} \chi_{Re}(\omega) = \frac{1}{\pi} \cdot P_C \cdot \int_{-\infty}^{\infty} \frac{\chi_{Im}(\omega')}{\omega' - \omega} d\omega' \\ \chi_{IM}(\omega) = -\frac{1}{\pi} \cdot P_C \cdot \int_{-\infty}^{\infty} \frac{\chi_{Re}(\omega')}{\omega' - \omega} d\omega' \end{cases}, \quad (1.72)$$

where P_C is the Couchy principal value. The Kramers-Kroning relations can be used to acquire spectral dispersion of refractive index or optical absorption by knowing the spectral dispersion of the other parameter. It important to emphasize that to get correct numerical values for spectral dispersion from the Kramers-Kronig relations, it is essential to know the value of the specified parameter at one point of spectral dispersion. It is important to emphasize that the Kramers-Kroning relation can be extended to higher-order susceptibilities[66,67]. For third-order

susceptibility this relation between refractive index changes and 2PA coefficient can be expressed as:

$$n_2(\omega,\Omega) = \frac{c}{\pi} \cdot P_C \cdot \int_{-\infty}^{\infty} \frac{\alpha_2(\omega',\Omega)}{\omega'^2-\Omega^2}\, d\omega' \tag{1.73}$$

where Ω identifies the cause of refractive index changes. If refractive index changes are induced and probed with the same frequency $\Omega=\omega$.

When discussing structure-property relations, in the first approximation, NLO properties can be based on donor/acceptor strength and parameters of π-conjugated chains. Both of these parameters interact in molecules leading to changes in bond order alternation (BOA) and bond length alternation (BLA) in π-conjugated chains. BOA is defined as the average alteration of adjacent carbon-carbon bond order in a polymethine chain and BLA is defined as the average difference in the length between adjacent carbon-carbon bonds. The neutral polymethine chain has BOA=-1 and BLA=0.11 Å. By adding donor and acceptor groups to this chain, additional electrons are pushed into this chain from donor to acceptor, changing both BOA and BLA parameters. Various specific values of BOA are defined with specific chemical limits:

- BOA=-1 is denoted as the polyene limit,
- BOA=0 is denoted as the cyanine limit,
- BOA=1 is denoted as the zwitterionic limit.

These names come from specific molecular groups that possess mentioned BOA values. By using the second-order hyperpolarizability terms introduced with equation (1.26) – Dipolar, Negative and Two-photon – specific relations for each term from BOA can be established. This has been widely studied in literature[1] and graphic relation based on the SOS model is given in Figure 1.7. Three extreme points for second-order hyperpolarizability can be seen in this graphic – two positive and one negative. Two positive peaks come from the D term and are between polyene and cyanine limits as well as cyanine and zwitterionic limit. The N term and

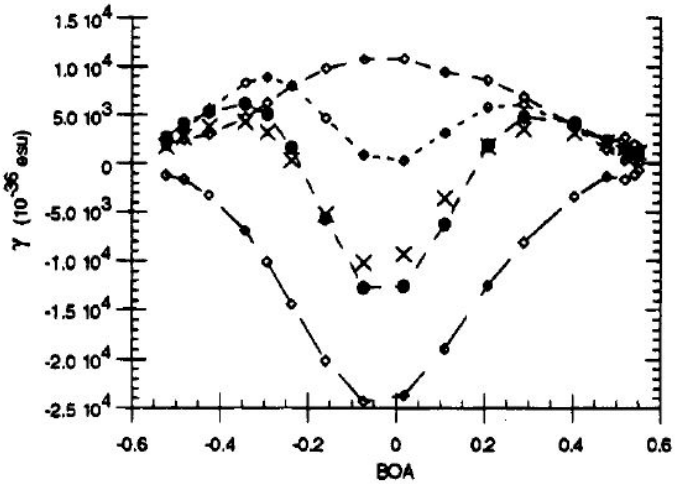

Figure 1.7: *The original graph is taken from reference[1]. Here diamonds with short dash line indicates D term, diamonds with medium dashed line indicates T term, diamonds with short dashed lines indicate N term, full circles give a sum of all terms and crosses are Sum-over-States model results.*

the T term have maximums at the cyanine limit giving overall a negative extreme. Taking into account that for centrosymmetric molecules the D term vanishes, we can conclude, that second-order hyperpolarizability will be negative for these molecules

2. Literature review

2.1. NLO Materials

The field of NLO studies has been active for five decades and various types of materials have been studied for use in NLO applications during this time. Most of the relevant NLO materials can be separated in the following groups – inorganic materials, metamaterials, graphene-like 2D materials, inorganic/organic hybrid materials, and organic materials. In the following chapter a short overview of each material group will be given, as well as a more detailed overview of the organic material group.

Historically first NLO studies were carried out for inorganic materials starting with P. Franken's observation of SHG from quartz[3]. The next essential leap in the field of NLO studies was through $LiNbO_3$. The earliest studies of $LiNbO_3$ NLO properties were regarding SHG[68,69] and electro-optical effect[70]. Even in those early years, it was speculated that $LiNbO_3$ is promising for phase-matched SHG as it possessed large negative birefringence and was the first material to display SHG coefficient more than 10 times larger than other materials studied at that time[71]. Although these values were known for a long time, it took a few decades till it was shown how to produce quasi-phase-matched $LiNbO_3$ waveguide for SHG generation[72]. Around the same time, $LiNbO_3$ become the state-of-the-art material for waveguide-based optical devices[73]. Regarding inorganic material third-order NLO effects, one of the most notable work is regarding semiconductor nonlinear refractive index dispersion and band-gap scaling[74]. In this work refractive index changes were measured for multiple inorganic semiconductors and compiled to show how third-order NLO properties depend on band-gap energy. It was shown that bond-electron contribution to refractive index changes is strongly influenced by the 2PA effect. Since then various inorganic materials have been studied and this material group still is the most commonly used in commercial devices employing NLO effects.

Another material group for NLO applications that have just recently attracted scientist's attention is graphene-like 2D materials. Graphene is an allotrope of carbon – a single layer of carbon atoms forming a two-dimensional hexogen layer. Third-order NLO studies of graphene started in the 2010s by measuring third-order susceptibility by four-wave mixing[75] as well as Z-scan[76]. These experiments showed that graphene possesses a very large nonlinear refractive index ($n_2 \approx 10^{-7}$ cm^2/W) and strong saturation absorption. This sparked a huge interest in graphene for mode-locked ultrafast lasers[77], electro-optical switching[78], and opto-optical switching[79]. As graphene proved that 2D materials should be considered for NLO applications, scientific groups turned their attention towards other graphene-like 2D materials. Since then the NLO properties of various materials, such as WS_2, WSe_2, MoS_2, and $Mo_{0.5}W_{0.5}S_2$, have been widely studied[80–84] as well as their applications for mode-locking lasers[85]. While these materials alone did not reach the commercial application level, the latest researchers in this field are headed towards graphene-like 2D material/polymer hybrid structures[86].

The previously mentioned approach to combine inorganic 2D materials and the organic polymer is not the only example of inorganic/organic hybrid structures. Some of the most popular inorganic/organic material types are metal-organic hybrids, organic materials with

metallic nanoparticles, and perovskite materials. Metal particles in organic material can lead to enhanced NLO properties as well as give a new platform for spectral tuning of NLO properties[87,88]. This can be due to various processes: i) new charge-transfer states can lead to an increased density of states, ii) d-orbital electrons in transition metals are more polarizable giving an additional contribution to NLO effects, iii) Coulombic interaction between organic/inorganic materials can lead to stronger local field factor. Research groups have shown that the SHG signal is increased due to columbic interaction[89] as well as that the SHG efficiency can be modified by functionalizing or extending ligand groups in this type of hybrid structures[90]. Regarding third-order NLO properties, it has been reported that for chalcogenide hybrid inorganic/organic polymers TPA can reach up to β=0.11 cm/GW and Kerr coefficient up to n_2=3.06 cm^2/GW in the infra-red region with high transparency in this region[91]. While these values do not seem too large, an interesting observation for these types of materials is that the experimental results fit quite well with semiempirical Miller's rule between the correlation of third-order and first-order optical properties for inorganic materials[92]:

$$n_2 = \frac{\delta \cdot 0.0395}{n_0^2} \cdot \left(\frac{n_0^2 - 1}{4\pi}\right) \tag{2.1}$$

where δ is Miller's constant for a specific material group. This shows that this rule extends beyond simple inorganic materials and could allow a simpler material screening through studying only the linear properties of specific inorganic/organic polymers. Another widely studied inorganic/organic material system for NLO applications is organic molecules mixed with metallic nanoparticles – most often gold, silver, or copper. It has been reported that different types of nanoparticles and nanoclusters can enhance Raman scattering[93], SHG[94] as well as third-order NLO response[95]. Regarding specific third-order effects, it has been shown that gold nanoparticles can enhance 2PA of organic materials[96]. Here the main enhancement effect comes from local field enhancement near nanoparticles through interference between incident and backscattered light. This means that for NLO enhancement, organic molecules need to be located in such distance from nanoparticle that corresponds to constructive interference between both light waves. Lastly, let's consider Perovskite materials that have been widely studied as active media for solar-cells, but recently scientific groups have started to also study their NLO properties. First publications showed that perovskites possess high 2PA coefficients (up to 8.6 cm/GW)[97] and broadband SHG[98]. Due to this most perovskite researches are focused on SHG and optical limiting[97–101]. Recent studies have shown that perovskite materials could also be used for optical switching due to their high nonlinear absorption coefficient[100]. In general, most of the studies regarding inorganic/organic materials hybrid structures are focused on SHG, 2PA, or saturable absorption and device applications such as optical limiters, mode-locking lasers, and optical switching based on 2PA**.**

While previously viewed material groups are based on atomic-structure materials, an alternative approach to the creation of NLO media is through meta-atomic structures built from artificial units. This type of material is widely known as metamaterials. The greatest advantage of metamaterials is that their structure can be tuned to possess positive, zero, or even negative refractive index, dielectric permeability, or magnetic permeability, creating media with unique effects[102]. This can include phase mismatch-free material by having zero refractive index[103], NLO energy exchange between ordinary and backward waves through

negative refractive index media[104], decrease in switching time through creating a non-uniform electron temperature in maetastructure[105], and numerous other unique effects. Metamaterials are mainly used in two ways for NLO applications – locally enhance the electrical field in an area containing NLO media and creation of artificial "atoms" with unique properties[106]. While the first type of metamaterials has a lot of common with metal/organic structures and metallic plasmonic structures, the second type of metamaterials are the ones that can lead to essential advances in the field of NLO devices. Also compared to natural atomic structure materials, metamaterials do not follow similar selection rules and correlations between linear and nonlinear optical properties[107]. This also raises the question if metamaterials follow similar fundamental limitations to NLO properties as natural materials or metamaterials could be a key to exceed these limitations.

Lastly, a more in-deep overview of organic NLO materials will be given in the next section. Compared to other material groups organic NLO materials are promising for NLO applications due to an immense number of molecular structures as well as structural adjusting, compatibility with other commonly used inorganic and organic materials, ability to form flexible photonic devices, and low price.

2.2. Nonlinear optical organic materials

In this section, an extended overview of experimental work and related conclusions regarding structure-property relations for organic materials will be presented. One of the essential experimental conclusions that allowed organic materials to compete with inorganic alternatives was around the 1970s when J. Ducuings and J. P. Hermann groups identified π-conjugated materials as promising for NLO applications[13–15]. They showed that by increasing π-conjugated bond length the higher-order hyper-polarizability increased very fast (polyene with 11 double bonds had a third-order polarizability three orders of magnitude larger than that of other small conjugated molecules). This was a significant increase, compared to σ contribution that could be described as a sum of independent bond polarizations. Although large second-order hyper-polarizability is an important prerequisite for material applicability it is not the only one. For all-optical applications, materials must have insignificant 2PA in communication wavelengths as well as it must be possible to create optical waveguides from these materials, which is an issue for many π-conjugated polymers[108].

For further enhancement of NLO properties, greater attention has been given to donor and acceptor influence on NLO properties. The most basic molecules for such studies are donor-acceptor substituted polymethine molecule, denoted as D-π-A type molecule. In the case of weak donor and acceptor groups, molecules ground level is mainly dominated by neutral resonance state and has large BLA values. By adding stronger donor and acceptor groups, charge-separated resonance state dominance to ground state increase and BLA value decrease and eventually changes its sign. It is important to emphasize that the ground-state of this type of molecules is strongly influenced by the polarity of the solvent. The more polar solvent will increase ground-state polarization, making charge-separation resonance more dominant[16]. For short polymer chain molecules (polymethyn-like molecules) donor/acceptor properties are more pronounced while for longer polymer chain molecules (polyene-like molecules) π-conjugated chain starts to strongly influence molecular properties. Regarding

spectral dispersion of 2PA for non-centrosymmetric molecules, it is widely accepted that it correlates well with molecules one-photon absorption. Study of D-π-A cyanines has shown that it is not that straightforward and that for molecules with large angles between transition dipole moment and difference in the ground and the excited state dipole moments (around 70^0) can have very weak 2PA absorption to one-photon resonance level[109]. In these cases, the vibration arm of linear absorption can have much stronger 2PA absorption. It has been experimentally observed that polyene-like molecules are more influenced by solvent polarization[20]. Next, let's consider the simplest symmetrical molecules of form D-π-D or A-π-A. Experimental evidence shows that symmetrical polymethyn molecules are more robust to solvent polarization influence compared to their unsymmetrical counterparts[110]. 2PA of symmetrical polymethyn molecules increase by adding stronger donor/acceptor groups or lengthening polymethyn chain[18]. Here we already start to notice a new focus for NLO studies – centrosymmetric molecules. As in many aspects, they are better than their non-centrosymmetric counterparts and greater attention was directed towards them, especially for 2PA applications.

To better understand specific centrosymmetric molecules NLO properties, let's consider one of the most popular centrosymmetric molecular groups for - squaraine molecules of form D-π-A-π-D. Experimental work has shown that squaraine molecules have larger 2PA values than counterpart symmetrical polymethene molecules[20]. Also, an observation has been made regarding the positions of one-photon resonance and two-photon resonance. When comparing doubled energy of one photon resonance and two-photon resonance energies, it has been observed that for most squaraine molecules, two-photon resonance has larger energy. Also in many cases, two-photon resonance is located on the vibronic shoulder of absorption band[111]. This is an important aspect as it gives an insight into the mechanism of how centrosymmetric molecules can have 2PA to a level near their one-photon absorption resonance. Similar aspects have also been reported for polymethines and fluorenes[112,113].

Through various researches, an overview of fundamental differences between centrosymmetric and non-centrosymmetric molecules can be formed. By studying allowed transitions for both types of molecules, we can conclude that NLO properties of non-centrosymmetric molecules can be described using a two-level system. In the case of

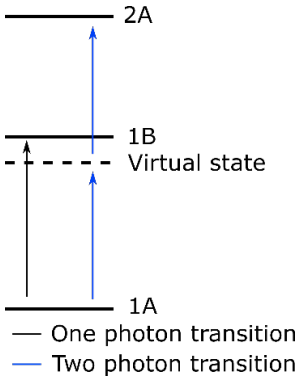

Figure 2.1: *Optical excitations in centrosymmetric molecules. States A and B has different molecular symmetries.*

centrosymmetric molecules, it is necessary to use at least a three-level system, as discussed in section "Third-order susceptibility". Also, it is important to emphasize that for a three-level system of centrosymmetric molecules one-photon transition is only allowed from 1A state to 1B state and is forbidden from 1A to 2A due to change of state symmetry (see Figure 2.1). At the same time, the two-photon transition is allowed from 1A to 2A. Although in some works a two-photon transition to a vibronic shoulder of one-photon resonance has been observed. For 2PA applications it is widely accepted that centrosymmetric molecules will be more effective than their non-centrosymmetric counterparts[114]. By comparing a molecule of structure D-π-A-π-D and its counterpart D-π-A, the following aspects need to be addressed:

I. For centrosymmetric molecules, the possibility of resonance with intermediate level greatly increases 2PA cross-section,
II. The transition moment will be larger for centrosymmetric molecules as they will be effectively polarized by both parts of the optical field while non-centrosymmetric molecules will respond only in one direction.

General guidelines can be defined for molecules regarding how to maximize the Kerr and the 2PA effects. For 2PA a general overview has been given by M. Pawlicki et. al. in their overview of 2PA molecules[114]. Their main points were:

1. Long π-conjugated chains that ensure large conjugation length,
2. Donor and acceptor group preferably placed in the center and ends of the molecule,
3. For centrosymmetric chromophores, molecules should possess a strong one-photon transition close to the two-photon transitions virtual state,
4. One-photon and two-photon absorption bands should be as narrow as possible.

For the Kerr effect, the guidelines must be constructed differently, because NLO properties follow different rules depending on how close the wavelength is to either one- or two- photon resonances. Again a separation will be made for non-centrosymmetric molecules (two-level approach) and centrosymmetric molecules (three-level approach). This overview will be based on M. G. Kuzyks work[36].

I. Non-centrosymmetric molecules:
    a. Close to one-photon resonance Kerr effect becomes proportional to transition dipole moment $\chi^{(3)} \sim \mu_{10}^4$,
    b. Close to two-photon resonance both transition dipole moment and the difference between ground state and excited state dipole moment start to influence Kerr effect, leading to $\chi^{(3)} \sim \mu_{10}^2 \Delta\mu_{10}^2$,
    c. In non-resonant case (ω->0) all terms contribute equally and $\chi^{(3)} \sim \mu_{10}^2(\Delta\mu_{10}^2 - \mu_{10}^2)$.

In overview, it can be said that for non-centrosymmetric molecules, the third-order susceptibility is defined by:

$$\chi^{(3)} \propto \frac{\mu_{ge}^2 \cdot \Delta\mu_{eg}^2}{E_{ge}^3} - \frac{\mu_{ge}^4}{E_{ge}^3} \tag{2.2}$$

where the first term characterizes the two-photon resonance, the second term characterizes the one-photon resonance and both terms contribute equally to the non-resonant case. Depending on what combination of absorption and Kerr effect properties are desirable, a different approach to molecules dipole moments needs to be taken. In most cases molecules with a strong Kerr effect with insignificant one- and two- photon absorption is desirable.

II. Centrosymmetric molecules:
    a. For one-photon resonance, it is difficult to give a simplified relation for third-order susceptibility,
    b. For two-photon resonance, the third-order susceptibility is proportional to $\chi^{(3)} \sim \mu_{10}^2 \, \mu_{12}^2$,
    c. In non-resonant case $\chi^{(3)} \sim \left(\frac{{\mu_{21}}^2}{\omega_{20}} - \frac{{\mu_{10}}^2}{\omega_{10}}\right)$.

For centrosymmetric molecules, the non-resonant case can be either positive or negative depending on which element dominates – two-photon or one-photon. The main guidelines for symmetrical molecules in the non-resonant case to increase one of these contributions while minimalizing the other.

2.3. Third-order NLO measurement methods

In this section, a brief overview of different methods used in literature for NLO studies will be given – Z-scan, Mach-Zehnder interferometer (MZI), and Degenerated four-wave mixing. In this work, the main focus will be on Z-scan as the central method for NLO measurements. MZI will be studied as an alternative to the Z-scan and a comparison of both methods will be presented. Although some papers regarding the MZI for third-order NLO studies[115,116] as well as comparison to Z-scan have already been published[117], they are not thorough enough. Regarding Degenerated four-wave mixing only a brief theoretical description will be given as it is one of the most popular approaches to third-order NLO studies, but will not be studied at the experimental level in this work as there are plenty of works regarding comparison to Z-scan.

2.3.1. Z-scan

The Z-scan method was first proposed by Sheik-Bahae in 1990[6]. Consisting of a very simple experimental setup of an optical lens, movable sample holder, beam splitter, and aperture (Figure 2.2) it becomes one of the most popular methods for third-order NLO studies. Since then scientific groups have introduced many alterations to the original setup – eclipsing Z-scan[118], pump-probe Z-scan[119], two-color Z-scan[120], and other. To better understand all of the pros and cons of this method, we will in detail study the experimental setup of Z-scan. Experimental measurements are carried out by focusing a laser beam on to sample and moving it along the optical axis while measuring the transmitted light. When describing light propagation, the optical axis is often denoted as a z-axis. During the measurement, the sample is scanned along the z-axis giving the method its name – Z-scan.

First of all, let's consider a sample possessing the Kerr effect. A laser beam with a Gaussian profile will induce a spatial refractive index change in the sample (see Figure 2.3), causing it to act as a thin lens that focuses or defocuses the laser beam. At each sample position laser beam profile differs due to focusing, leading to variations of induced thin lens focal length. Measuring transmitted light at far-field ($d>>z_R$) we will observe changes in beams size from sample position. This can also be characterized as changes in laser beam intensity. To measure intensity, a small aperture ($S_{aperture}<<S_{beam}$) is placed before the detector that measures laser

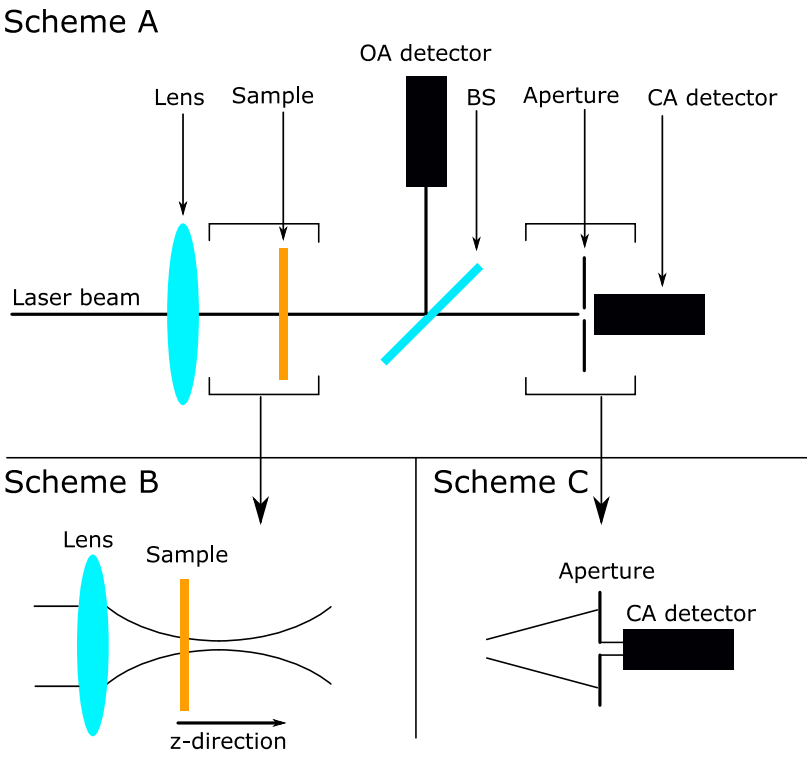

Figure 2.2. *Z-scan setup. Scheme A – Basic Z-scan system consisting of a lens, sample, a beam splitter (BS), and two detectors – open-aperture (OA) and closed- aperture (CA). Scheme B – to measure sample optical property dependence on laser intensity it is moved through the focal point. The transmittance signal is measured with both detectors as a function from the sample position. Scheme C – aperture is placed in front of the CA detector. This separates a small central part of the beam and allows detecting any changes in beam size.*

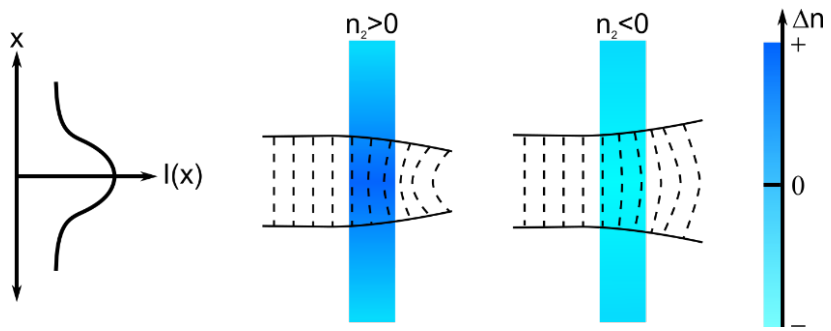

Figure 2.3. *Self -focusing and -defocusing of Gaussian Beam induced by the Kerr effect.*

power. In further text, experimental data gathered within this way will be denoted as “closed-aperture” data.

In the case of the 2PA effect, the sample will change its absorption as a function from laser intensity. This will lead to power changes in transmitted light depending on the sample position. In this case, measuring the overall power of the transmitted beam is sufficient enough. In the experimental setup, this measurement is denoted as an “open-aperture” measurement. Here the only essential aspect is that beam size variations cannot lead to the laser beam exceeding detectors sensor size.

In many cases samples possess both effects – 2PA and Kerr effect. In general it is assumed that open-aperture measurements are indifferent to the Kerr effect and will always detect only absorption changes. At the same time closed-aperture measurements are influenced by both effects. To separate the Kerr effect from the 2PA effect, closed-aperture data are divided by open-aperture data (see Figure 2.4)

Analytically Z-scan experiment can be described using the following differential equations:

$$\begin{cases} \frac{d(\Delta\Phi)}{dz} = \Delta n(I) \cdot k \\ \frac{dI}{dz} = -\alpha(I) \cdot I \end{cases}, \tag{2.3}$$

where $\Delta\Phi$ is the phase change due to NLO effects and $\Delta n(I)$ and $\alpha(I)$ is the refractive index and the optical absorption change functions from the optical intensity, respectively. In this work, we will consider the “thin-sample” model, where sample thickness is smaller or comparable to Rayleigh length. A more detailed description of thick-sample cases can be found in the

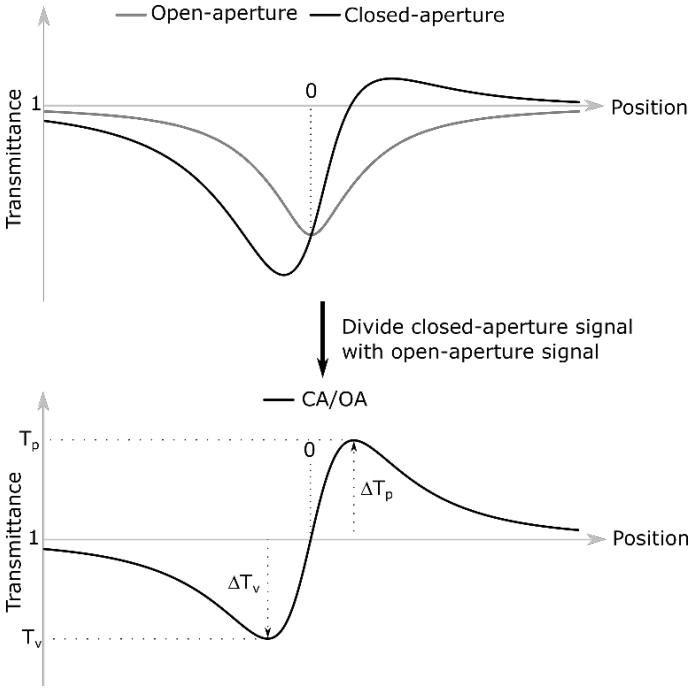

Figure 2.4: *Example of Z-scan measurement. The first graph shows experimental measurements of both detectors. The second graph shows separated Kerr influence.*

overview article about Z-scan theory[121]. Considering a case when "closed-aperture" measurement is influenced only by the Kerr effect and "open-aperture" measurement by the 2PA effect and the laser beam has a Gaussian profile, equations (2.3) can be solved analytically (See Appendix B):

$$\begin{cases} Open-aperture \ \rightarrow \ T(z) = \frac{\left(1+\frac{z^2}{{z_0}^2}\right)}{\sqrt{\pi}\cdot q} \cdot \int_{-\infty}^{+\infty} \ln\left(1+\frac{q}{\left(1+\frac{z^2}{{z_0}^2}\right)}\cdot e^{-\tau^2}\right) d\tau \\ Closed-aperture \ \rightarrow T(z) = \frac{\int_0^{r_a}\left|\sum_{m=0}^{\infty}\frac{\left(i\cdot\Delta\Phi_0(z)\right)^m}{m!}\frac{w_{m0}}{w_m(z)}e^{\left(-\frac{r^2}{{w_m(z)}^2}+i\cdot\theta_m-i\cdot\frac{k\cdot r^2}{2\cdot R_m(z)}\right)}\right|^2\cdot r dr}{{w_0}^2\cdot\left(1-e^{-\frac{2\cdot {r_a}^2}{w^2(z)}}\right)} \end{cases}, \quad (2.4)$$

Parameter q and $\Delta\Phi$ are defined as

$$\begin{cases} q = \alpha_2 \cdot L_{eff} \cdot I_0 \\ \Delta\Phi = n_2 \cdot k \cdot L_{eff} \cdot I_0 \end{cases} \quad (2.5)$$

where L_{eff} is the effective length and I_0 is the optical intensity at the focal point. Shapes of these functions can be seen in Figure 2.4. The main idea behind Z-scan data processing is that by fitting experimental transmittance data with equations (2.4) values for parameters of phase change $\Delta\Phi$ and absorption change q are acquired that are further used to calculate values of nonlinear refractive index and absorption coefficients. In cases when parameter $|q|<1$ and $|\Delta\Phi|<\pi$ (also known as weak nonlinear media condition) equation (2.4) can be simplified to form (See Appendix C):

$$\begin{cases} Open-aperture \ \rightarrow \ T(z) = \sum_{k=0}^{\infty}\frac{\left(-\frac{\alpha_2\cdot I_0\cdot L_{eff}}{\left(1+\left(\frac{z}{z_R}\right)^2\right)}\right)^k}{(k+1)^{\frac{3}{2}}} \\ Closed-aperture \ \rightarrow T(z) = 1-\frac{4\cdot\Delta\Phi\cdot\frac{z}{z_R}}{\left(\left(\frac{z}{z_R}\right)^2+9\right)\cdot\left(\left(\frac{z}{z_R}\right)^2+1\right)} \end{cases}, \quad (2.6)$$

While different models have been derived for cases of thin/thick samples as well as weak/strong nonlinearities a general theory for the Z-scan measurements can be acquired by using paraxial approximation and solving Helmholtz equation[122] that can be used for very specific cases where no simpler analytical model works. Also for the first approximation of the Z-scan data, a correlation between transmittance difference between peak and valley points can be used to calculate the phase change (see Figure 2.4):

$$T_p - T_v = \Delta T_{pv} = 0.406\cdot(1-S)^{0.25}\cdot|\Delta\Phi|, \quad (2.7)$$

where S is the ratio of transmitted light through aperture:

$$S_R = 1 - e^{\frac{-2\cdot r^2}{w^2}}, \quad (28)$$

where w is the beam size at closed-aperture detector and r is the aperture size. In most cases, aperture size influence is small enough to neglect. While generally this approach is not used for precise extraction of refractive index changes, it can be used for first approximations.

Special attention in the literature has been given how to correctly measure the Kerr effect in media with a strong 2PA effect[123,124]. This is usually characterized by coupling factor $\rho=\alpha_2/(2\cdot k\cdot n_2)$. A general formula for closed-aperture measurement taking into account both Kerr and 2PA effect can be expressed as[123]:

$$T = 1 - \frac{4\cdot\Delta\Phi\cdot\frac{z}{z_R}}{\left(\left(\frac{z}{z_R}\right)^2+9\right)\cdot\left(\left(\frac{z}{z_R}\right)^2+1\right)} - \frac{2\cdot\left(\left(\frac{z}{z_R}\right)^2+3\right)\cdot\Delta\Psi}{\left(\left(\frac{z}{z_R}\right)^2+9\right)\cdot\left(\left(\frac{z}{z_R}\right)^2+1\right)}, \tag{2.9}$$

where $\Delta\Psi=\rho\cdot\Delta\Phi$ and describes the 2PA contribution. The coupling factor also influences equation (2.7) that needs to be rewritten in form[124]:

$$\Delta T_{pv} = (0.406 + 0.268\cdot\rho^2)\cdot|\Delta\Phi|, \tag{2.10}$$

2PA also leads to asymmetry in the peak-valley shape of closed-aperture measurement. This asymmetry can be characterized by equation[124]:

$$\frac{\Delta T_p}{-\Delta T_v} = 1 - 3.4\cdot\rho + 2.88\cdot\rho^2, \tag{2.11}$$

Another essential parameter for closed-aperture measurement is the distance between peak and valley positions. This distance differs depending on what order effects induce refractive index changes. This is usually defined as the ratio of this distance to Rayleigh length. For third-order effects this distance is approximately $\Delta z_{pv}\approx1.7\cdot z_R$, while for higher orders it becomes shorter. For example, fifth-order effects will induce a similar shape with the peak-valley distance of $\Delta z_{pv}\approx1.2\cdot z_R$.[125] There is one more case where this distance can change and it is the accumulative thermo-optical effect. It is important to emphasize that this is only for cases where the pulse width is too short to induce a thermo-optical effect with a single pulse but the repetition rate is high enough to accumulate heat. Usually this can happen when using femtosecond or picosecond laser with a pulse repetition rate over 10 kHz. In this case, peak-valley separation distance can increase up to $\Delta z_{pv}\approx3.4\cdot z_R$ when measuring third-order effects. The exact distance depends on the ratio between illumination time and characterizing time for accumulative thermo-optical effect[125].

Till this moment an essential parameter of light has been ignored – polarization. When the Z-scan method was first introduced it was mainly implemented with linearly polarized light. The first experimental measurements for polarization dependence of nonlinear refractive index using Z-scan were presented by R. DeSalvo in 1993[126]. This was done by simply rotating light polarisation direction relative to the crystal crystallographic axis. In the case of solutions, this type of approach does not work due to isotropic media. This can be fixed by using a $\lambda/4$ plate that changes beam polarization from linear to circular and has already been widely applied in literature[127,128]. This allowed for a simple way to study different tensor elements of third-order susceptibility and determine the origins of refractive index changes in a sample. The ratio of n_2 values for linear and circular polarisations indicates what effect induces the refractive index (has been previously shown in Table 1.2). In general case n_2 value as a function of the angle between the slow axis of $\lambda/4$ plate and linear polarization direction can be written as:

$$n_2 = \pi\cdot(2\cdot A + B\cdot(\cos 2\theta)^2)\cdot\frac{|E|^2}{n_0}, \tag{2.12}$$

The main advantages of the Z-scan method compared to other methods for NLO studies are that it is easy to assemble, you can study Kerr and 2PA effects simultaneously as well as determine the sign of the Kerr effect. For example, degenerated four-wave mixing and Mach-Zehnder interferometric methods can measure only the amplitude of the Kerr effect coefficient. Measurement accuracy for the Z-scan method can reach up to λ/300 for phase changes.

According to the scientific literature, the Z-scan method has been widely applied for various types of third-order susceptibility studies. This includes:

Pulse duration. A wide spectrum of different studies for pulse duration influence on refractive index changes has been carried out. These studies can be divided mainly into two groups – study of different Kerr contributions and separation of thermo-optical and Kerr effects. Let's consider the first type of study. These mainly look at refractive index changes in the range from hundreds of femtosecond to few picosecond pulse duration. Scientific groups have shown that in this range refractive index decreases as the pulse duration is decreased for most organic solvents[129]. As the Kerr effect can be separated into electronic and nuclear contributions, time constants of these effects start to play a significant role at fs and ps pulse duration scale. For electronic response, it is mainly assumed that it is instant compared to pulse duration, but the molecular response time constant can wary from few hundreds of femtosecond to few picoseconds depending on the nuclear effect type. Two approaches are used for the molecular contribution characterization – giving an average time constant for all nuclear contributions or separating collision, libration, and diffusive components. Although the later type studies demand time-resolved measurements that can be either carried out by implementing different pulse width lasers or setting up pump-probe measurements with probe pulse being delayed in time relative to pump pulse. Pump-probe measurements with delay in time between pulses cannot be carried out with Z-scan setup and other types of methods for third-order NLO studies need to be employed for this, such as beam deflection method[45,53]. The average time constants can range from 0.8 to 4 ps for various solvents[129]. Time-dependent studies have also been carried out for various organic dyes[53]. The Z-scan method has mainly used to separate electronic and nuclear responses. Recently a scientific group showed that the nuclear component has a strong dependence on pulse duration compared to electronic response[7] using Z-scan. While this does not give as much information about molecular processes as the beam deflection method, Z-scan is sufficient to predict how molecules will respond in solid form, when diffusive components are reduced. This information is essential when solid form materials are incorporated into devices.

Polarisation measurements. Several publications have been published regarding how Z-scan measurements with linear and circular polarised light can be used to determine B/A ration and what effect induces refractive index changes. This has mainly been applied to various solutions, including chloroform[129] and CS_2[127–129]. While these papers mostly focus on separating electronic and molecular reorientation components, recently polarization-resolved measurements have also been used to separate also thermo-optical effect from the electronic response for organic dye[7]. Although this is essential for correct methodology, an extension of this work is still necessary that would also include: i) Separation of solute and solvent contributions (Melhado group[7] used solvent with weak NLO properties that do not reflect the

most popular experimental setup, where chloroform is used as a solvent and has significant influence); ii) Estimating both molecular and electronic contributions of organic dye. Few scientific groups have attempted to carry out polarization-resolved measurements for guest-host thin films with PMMA as a host material and some organic dye as guest material[130,131]. Mostly these works have implemented CW lasers and are studying photoisomerization that induces much stronger refractive index changes compared to the thermo-optical effect. This is one of the few cases when CW laser can be correctly implemented to study other refractive index changes inducing effects then thermo-optical effect.

Repetition frequency. The pulse repetition rate only influences the thermo-optical effect, as the Kerr effect is independent of this laser parameter. This allows for a way to separate the thermo-optical effect and the Kerr effect. Several works have been published regarding frequency-dependent Z-scan measurements, usually studying CS_2 properties[132–134]. The main conclusion from these works is, that even short pulse lasers (with an order of few 100 fs) can induce a thermo-optical effect in case of high-repetition-rate (more than >1 MHz). This effect can not only be influenced by the repetition rate, but also by implementing a lens with different focal length, leading to changes in beam size in the focal point. The thermo-optical effect time constant is strongly influenced by beam size at the focal point. N. Wickremasinghe and his group showed[134], that thermal effects can be "eliminated" by using a stronger lens. By changing the focusing lens from a 10x to 20x lens, they could eliminate the refractive index changes due to the pulse repetition rate that started to appear over 200 kHz frequency due to shifting threshold frequency for thermal effects to higher frequencies. Also, thermal effects can be induced not only by linear absorption but also by the 2PA effect. K. Kamada and his group[135] showed that measured refractive index changes due to the pulse repetition rate for femtosecond laser due to 2PA induced accumulative thermal effects.

Spectral dependence. Spectral studies of third-order NLO properties are very few in literature. Kerr and 2PA effect dependence has been measured for silicon[136] and water[137], while there are plenty of publications that can be found about just 2PA dispersion for organic compounds[18–20,112,113,138]. 2PA dispersion measurements in literature are mainly carried out by two methods – Z-scan and 2PA fluorescence measurements. In this work, only Z-scan measurements will be considered as it aligns more with the focus of this work. It is evident that literature is lacking works regarding Kerr effect spectral dependence.

Concentration dependence. Scientific groups have shown that 2PA coefficient values can depend on concentration. In this reference[54], the scientific group proposed that this could be due to aggregation that leads to 2PA dependence on concentration. This can also influence 2PA induced ESA and lead to concentration dependence for ESA cross-section[139]. While at high solution concentration (0.01 M of organic dye in solvent) will lead to a decrease in 2PA values for most of the reported materials, scientific groups have shown that the concentration at which this decrease begins can be altered through structural alterations of molecules[140].

Laser profile. While Gaussian type beams are the most common for Z-scan measurements, analytical models have been derived for various other types of lasers. This includes elliptical beams[141], top-hat beam[142,143], Bessel beam[144] as well as a general equation for beams with circular symmetry[145]. The main motivation for switching from the Gaussian beam to other

types of laser beams is increased sensitivity. For example, it is reported that by employing a laser with a top-hat beam profile Z-scan sensitivity can be increased up to 2.5 times[143].

2.3.2. Mach-Zehnder interferometer

Design for MZI was first proposed by Ludwig Zehnder in 1891 and later refined by Ludwig Mach in 1892, thus the name Mach-Zehnder interferometer. The experimental setup consists of two mirrors and two beam splitters. An incoming light beam is split into two beams that travel in separate "arms" of the interferometer and then are combined through the second beam splitter (see Figure 2.5). The output intensity of the interferometer will depend on the phase difference between both beams and can be expressed as:

$$I_{out} = \frac{I_1+I_2+2\cdot\sqrt{I_1\cdot I_2}\cdot\cos(\Delta\Phi)}{2}, \tag{2.13}$$

where I_1 and I_2 are the optical intensity of the first and the second beam and ΔΦ is the phase difference between both beams. If there is no phase difference (ΔΦ=0) between both beams constructive interference will be observed in output. If one beam is altered so the phase difference between both beams will be ΔΦ=π/2, destructive interference will be observed in output.

In the case of a pulsed laser source, it is also important to take into account the coherence length of the laser. In the case where the optical path difference between both arms is larger than the coherence length, it is difficult to acquire a stable interference pattern. Coherence length can be calculated as:

$$L_C = \frac{\lambda^2}{n\cdot\Delta\lambda}, \tag{2.14}$$

where λ is the optical wavelength, n is the refractive index of media and $\Delta\lambda$ is the spectral width of the optical signal. As for shorter pulse lasers spectral width increase, it becomes more essential to have the same path length for both arms of the interferometer. By placing a phase modulator with NLO properties in one of the interferometer "arm", the phase difference between both arms will change as a function from the optical intensity. This will influence phase changes in equation (2.13) in the following way:

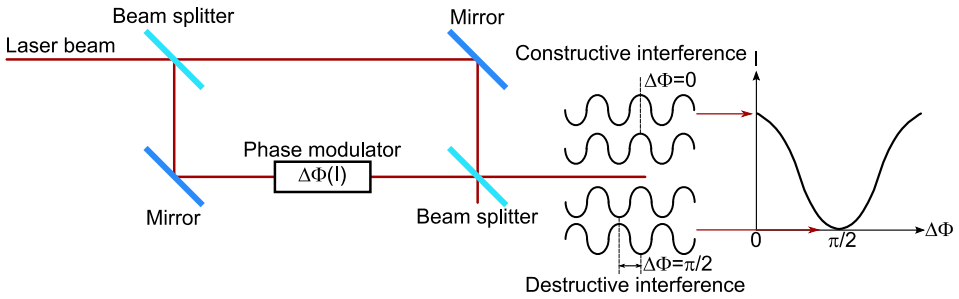

Figure 2.5. *Schematics of Mach-Zehnder interferometer.*

$$\Delta\Phi = \Delta\Phi_{NLO}(I) + \Delta\Phi_{Const}, \quad (2.15)$$

where $\Delta\Phi_{NLO}(I)$ describes the NLO changes in phase and $\Delta\Phi_{Const}$ is a constant. Depending on whether a single laser or two laser setup is used, equation (2.3) can be simplified in different forms. Although MZI has previously been used to study third-order NLO properties, it has not been used to demonstrate optical switching with two laser beams.

MZI has been widely used for second-order NLO effect studies, especially the electro-optical effect. As there are several similarities between the Kerr effect and electro-optical effect, in this work a more detailed comparison between Z-scan and MZI methods will be carried out.

2.3.3. Degenerated four-wave mixing

Another widely used method to study third-order NLO effects is the Degenerated four-wave mixing (DFWM)[146–149]. In general four-wave mixing is an NLO effect where three or two photons with specific frequencies interact, generating one or two new photons. Most of DFWM experimental works irradiate a sample with three beams of the same frequency, where two beams travel opposite to each other (forward pump and backward pump) and the third beam (probe beam) is tilted slightly compared to the other two beams (see Figure 2.6). Due to NLO interaction, a backward beam (DFWM signal) is formed traveling opposite to the probe beam. By measuring backward beams intensity as a function from the square root of product of both pump beam intensities, one can calculate the model of third-order susceptibility. Similar to the Z-scan, DFWM is also strongly influenced by the thermal, free carrier, and other effects that can complicate the procedure to correctly estimate third-order susceptibility[148]. For DFWM this issue is most commonly solved by time-resolved DFWM. In this case, the backward pump is delayed with respect to probe and forward pump beams. By measuring DFWM signal intensity as a function from this delay time, it is possible to determine what effect produces DFWM signal[150]. Previous research has already been done in comparing time-

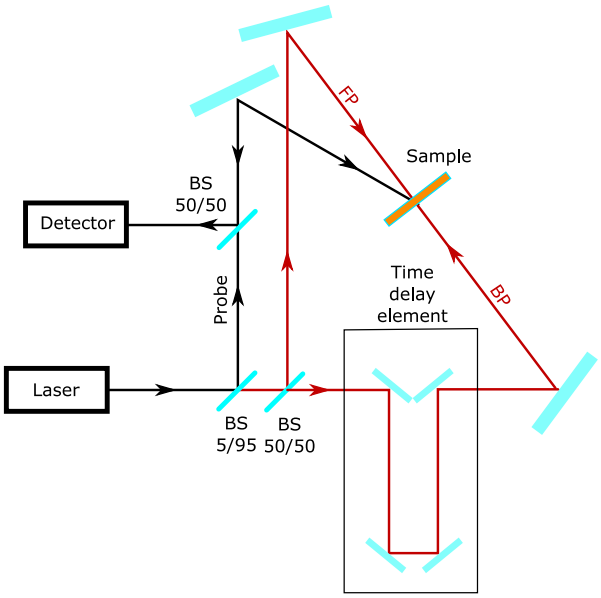

Figure 2.6: *Experimental setup for Degenerated four-wave mixing. FP denotes forward pump beam and BP – backward pump beam.*

resolved DFWM with the Z-scan method and has shown that both methods give equivalent results[5].

2.4. Quantum Chemical Calculations

Quantum Chemical calculations (QCC) are widely used for theoretical predictions of a molecule's linear and nonlinear optical properties. In this work, the main focus will be on QCC for linear polarizability and second-order hyperpolarizability. In literature, one can find various software's that are used for QCC – Gaussian 09[151], Gaussian 03[152], Dalton[153], and others. In this work, experimental results will be compared to values obtained by Gaussian 09 software as it is one of the most widely used QCC softwares, especially for linear polarizability and higher oreder hyperpolarizabilty calculations.

Gaussian software is a computational chemistry software with a wide scope of applications. Both Gaussian 03 and Gaussian 09 software's have been widely used in literature for Highest Occupied Molecular Orbital (HOMO) and Lowest Unoccupied Molecular Orbital (LUMO) energy levels[154–156], molecule geometry[155,157–159], linear polarizabilities[160,161], first-order hyperpolarizability[156,161] as well as second-order hyperplarizability[160,162,163]. The main motivation for the implementation of the correct QCC is to improve molecular structure screening for NLO applications. While various methods can be used to predict molecular properties, in this work we used density functional theory. Gaussian 09 has an inbuilt density functional theory model to calculate molecular properties with various sets of functionals depending on necessary variable[161,164]. The general density functional theory separates Hamiltonian into three parts: i) Kinetic energy element, ii) Potential energy due to nuclei, iii) electron-electron columbic interaction energy. In reality, this is not enough to accurately describe molecular properties and additional functionals, denoted as exchange-correlation functionals are employed. Additionally, a base set is used that defines what functions are used to express wave function. In this work, CAM-B3LYP functional was used for second-order hyperpolarizability calculations as it has been widely and successfully implemented in other works[160,162,163]. Compared to other functionals, CAM-B3LYP is under a Long-range corrected functional group that has been shown to fix the overestimation of electronic contribution to electrical dipole and molecular properties related to it[161]. It is important to note that second-order hyperpolarizability values are not calculated straightforward. Analytical calculations of the first-order hyperpolarizability are carried out that are then numerically differentiated according to the finite field methodology. This means that values acquired by QCC are Convention IV type values and specific coefficients need to be taken into account when comparing experimental and QCC values. To calculate solvent influence on molecular properties, a solvation model is implemented that can either continuum or atomistic solvent model. For the continuum case, also used in this work, usually, a polarizable continuum model is used in which solvent molecules are modeled as polarizable continuum[165]. This significantly simplifies the calculations and reduces the necessary time, as modeling each solvent molecule independently would be complicated. For this case a solute cavity is created in the solvent continuum, a specific molecule is placed in this cavity, and calculations are carried out.

3. Experimental section

3.1. Sample preparation

According to literature one of the most popular approaches to study third-order NLO properties of organic molecules is by dissolving the organic compound in small concentration in solvent (most often chloroform is used) and studied in form of solution. This approach allows us to use isotropic approximation when describing experimental results, at small enough concentration any aggregation effects can be avoided as well as such samples are easy to produce. For experimental measurements, organic compounds were dissolved in chloroform and filled in 2 mm thick photometric quartz cuvettes.

Chloroform. In this work chloroform was used as all of the studied compounds can be dissolved in it and it is one of the most widely used solutions in Z-scan measurements, making it a good choice to compare results in this work with literature. The density of chloroform is ρ=1488 kg/m^3, refractive index[166] n=1.4359 at 1064 nm and the Kerr coefficient is n_2=1.7 to 3.2·10^{-15} cm^2/W at 1064 nm measured with 30 ps laser[167,168]. The essential aspect here is pulse width as it significantly influences the nuclear contribution to nonlinear refractive index changes. Previous studies show that for liquid chloroform, refractive index changes can be divided into four parts[44]: i) Instantaneous electronic response, ii) Ultrafast libration effect with a time constant around 170 fs, iii) Intermediate collision effect with a time constant around 400-600 fs; iv) Slow diffusive reorientation with a time constant larger than 1.5 ps. Wider studies have shown that the ultrafast and slow responses are connected to the anisotropic nature of chloroform. Pulse width dependent measurements from 60 fs to 1 ps suggest that the electronic response of chloroform is of order n_2=0.54·10^{-15} cm^2/W.[129] Increase in nonlinear refractive index value can be observed by increasing pulse width and gives an insight into fast nuclear effects – such as libration and collision effects.

3.2. Optical absorption

Absorption measurements were carried out with the Ocean Optics HR4000CG-UV-NIR spectrometer. Using this spectrometer, the absorption spectrum from 300 to 1100 nm could be measured. Samples were prepared in the form of solutions and contained in 2 mm thick quartz cells. For absorption measurements firstly a reference measurement of pure chloroform was carried out after which a sample with organic compound diluted in chloroform was measured. The specific organic compound was dissolved in chloroform of concentration range from 10^{-5} to 10^{-6} mol/L solutions. Reference measurement was subtracted from sample measurement to separate any cell or solvent contribution to absorption.

3.3. Lasers

For material studies, six different lasers were implemented in this work – two ps lasers, one ns laser, and three CW lasers. For ps measurements at 1064 nm an Nd:YAG laser with 30 ps pulse duration and 10 Hz repetition rate was used (EKSPLA PL 2143A further denoted as PL ps). This laser provided high-intensity laser irradiation and was used to acquire precise results that could be compared to QCC results. Laser output power did not exceed 1

mW during all measurements. Literature suggests that usage of such laser should lead to only Kerr effect induced refractive index changes. A second ps laser with 15 ps pulse duration and variable pulse repetition rate from 10 to 1000 Hz (EKSPLA PL2210 Picosecond laser/PG400 Optical Parametric Generator) were used to acquire spectral dependences for NLO effects. For ns measurements an Nd:YAG laser with 8 ns pulse duration and variable pulse repetition rate from 200-40 000 Hz was used (EKSPLA NL 640). Three different CW lasers were used in this work He-Ne 632.8 nm laser and two diode lasers with 437 nm and 780 nm wavelengths. All of the laser beams had a Gaussian profile.

3.4. Z-scan setup

The experimental setup used in this work is shown in Figure (3.1). Laser beam power was controlled using Fresnel Rhomb placed in a motorized rotation stage (SM 1) and Glan-Taylor prism. The e-ray of the prism was used in setup while the o-ray was directed towards a beam dump (BD). A small part of the laser beam was reflected with a beam splitter (BS) and measured using the reference detector (Ref). In this case, a glass substrate was used as a beam splitter. The laser beam was focused using a lens with an 11 cm focal length. Transmitted light was measured using two detectors. Part of the transmitted beam was separated with a glass substrate (BS) and collected unto an open-aperture detector (OA) using a lens with a 20 cm focal length to measure the power of the transmitted beam. The rest of the beam was transmitted through an aperture with a diameter of 1 mm and measured with a detector closed-aperture detector (CA). Aperture transmittance in this setup was estimated to be less than 1 % that fits very well for the “closed-aperture” measurement model. The sample was positioned on the motorized stage (SM 2) that moved parallel to the laser beam. Both motorized stages could be controlled using a computer. The experimental setup was built on a metal plate to move the setup between different laser sources. An option of placing a quarter-wavelength plate (QWP) was implemented into setup to carry out measurements with circularly polarised light.

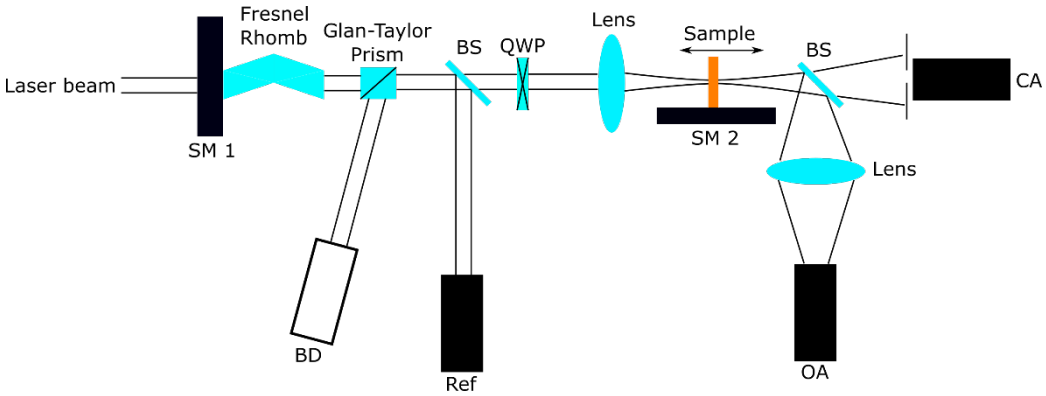

Figure 3.1: *Z-scan experimental setup. BD – Beam Dump; BS - Beam Splitter; QWP – Quarter-wavelength plate; SM – Step motor; Ref – Reference detector; CA – Closed-aperture detector; OA – Open-aperture detector.*

An additional electronic scheme was used for detector signal reading and step motor controlling (see Figure 3.2). Two controllers were used for device communication with a computer. One was a commercially available controller for the sample motorized stage (SM

2). The second was a specially made controller that could read all three detector signals and control the motorized rotation stage for Fresnel Rhomb (SM 1). This allowed for measurement automatization with batch type measurements of Z-scan at different laser intensities.

Various types of Z-scan measurements were carried out in this work that can be separated in the following groups:

1. Measurements with ns laser at different pulse repetition rates to study the influence of the thermo-optical effects,
2. Circular and linear polarisation measurements with ns laser to separate the thermo-optical and the Kerr contribution to refractive index changes,
3. Measurements with ps laser to study the Kerr and 2PA effects of different materials,
4. PS measurements at different polarizations to study the origins of the Kerr effect and calculate values of different third-order susceptibility tensor elements.

For experimental data fitting a *Matlab* and *Python* codes were created.

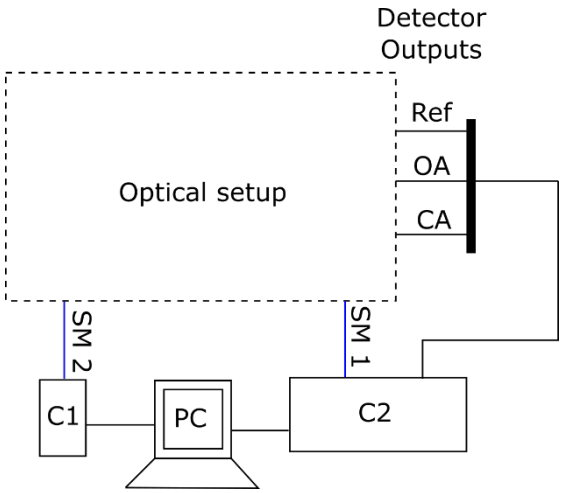

Figure 3.2: *Electronic scheme of the Z-scan setup. C1 – Controller 1; C2- Controller 2.*

3.5. Mach-Zehnder interferometer setup

MZI measurements were carried out in two forms – a single beam and a two beam setups (see Figure 3.3). For both cases, incoming beam was split into two beams using a beam splitter (BS) – sample and reference beams. The sample beam was guided through a lens that focused the beam onto the sample and through another lens that collimated the beam – both with a focal length of 8 cm. A motorized sample holder was placed in the focus of both lenses. To find the focal point a Z-scan type measurement could be carried out using a reference detector (Ref 2) as a closed-aperture measurement. This ensured that no beam size variation due to the Kerr effect should be present. A small part of this beam in the sample arm was separated using a glass slide and measured with a closed-aperture detector for two purposes: i) to measure any power changes that could be induced due to the 2PA effect; ii) detect beam size variation due to Kerr effect. An optical wedge was placed in reference beams way to

adjust the optical path difference between both beams to be smaller than the coherence length (very essential for ps laser measurements). To monitor the laser power, part of the reference beam was separated using a glass slide and measured using a reference detector (Ref 1). Both beams were guided towards the second BS where they interfered. The output signal was measured using another detector (Int). In the case of a two beam measurements, optical filters that separated probing and inducing beams were placed in front of detectors. In this case, no special setup was used to control the power of the laser source as various lasers were used and for each of them a different way to control laser power was used – some had an inbuilt power controller while for other optical filters were used. A similar electronic scheme as for Z-scan was used for this setup (see Figure 3.2), excluding the motorized rotation stage (SM 1) as only sample motorized stage was used for finding the correct sample position (more details in "Result and Discussion" section).

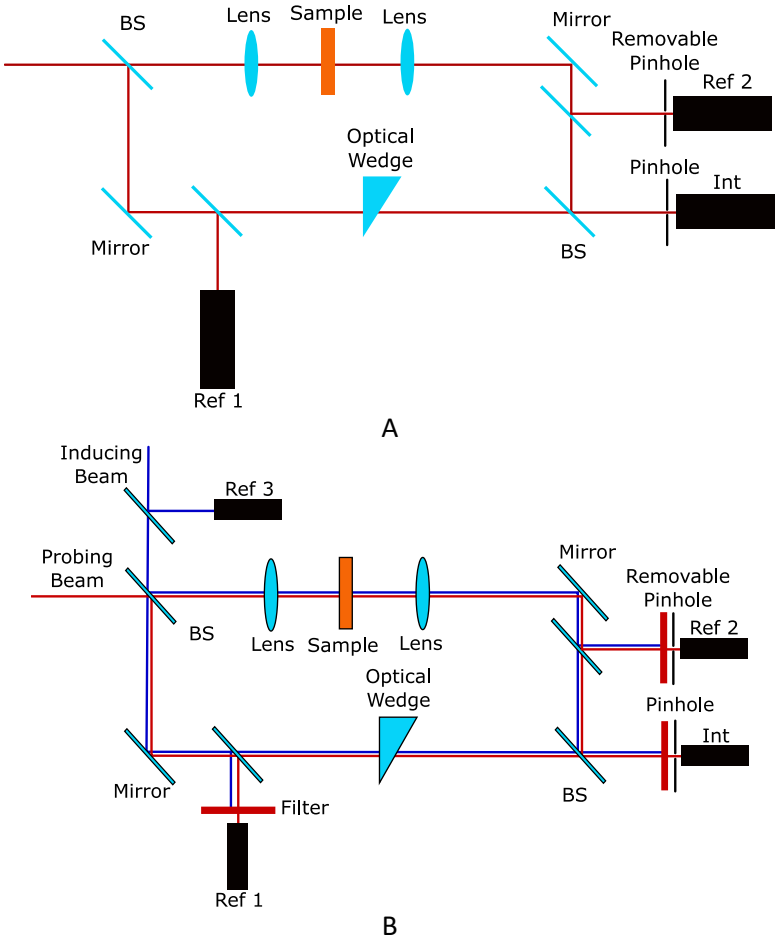

Figure 3.3: *Mach-Zehnder interferometer experimental setups. A – Single beam setup; B – Two-beam setup.*

3.6. Quantum Chemical calculation parameters

Similarly as in the Literature overview section, only a brief overview of parameters for QCC used in this work will be given here as it is not the main focus of this work. The first step for QCC was calculating molecular structures. Spatial molecular structures were calculated in vacuum using all the ωB97X-D density functional with empirical atomistic dispersion

correction and 6-311G(d,p) Pople-style basis set. Next, the first-order hyperpolarizability is calculated analytically using the Gaussian 09 coupled perturbed Kohn-Sham approach and then differentiated numerically using default settings to acquire values of second-order hyperpolarizability. CAM-B3LYP density functional was used with a 6-311G(d,p) base set. This base set means that internal electron orbital wavefunctions are expressed as six Gaussian functions with fixed parameters while valence orbital wavefunctions are expressed as three Gaussian functions with variable parameters. To calculate the solvent impact on the second-order hyperpolarizability CPCM continuum solvation model in the default nonequilibrium mode was used.

4. Results and Discussion

In this section the results of this work will be presented. This section will be separated into three main parts – NLO measurement methods, NLO properties of organic materials, and Experimental value comparison to Quantum Chemical calculations – as well as an additional section regarding Spectral measurements. The last section was separated from the three main as it does not contribute to the Thesis of this work, but gives additional information that allows explaining specific experimental observations.

4.1. Evaluation of NLO measurement methods

4.1.1. Z-scan

In this section various aspects of Z-scan experiments will be studied to give a workflow for the correct measurement method. This will include calibration of presented setup, pulsewidth influence and pulse repetition rate influence on measurments, polarisation-resolved measurements to separate molecular and electronic contribution, correct estimation of the electronic part of Kerr effect of organic dyes, and possible errors while measuring Kerr effect of organic dyes using ns laser.

Calibration. To calibrate the Z-scan setup, measurements of chloroform and CS_2 were carried out with PL ps laser. These compounds were chosen as CS_2 is a widely used reference sample for Z-scan calibration and chloroform will be used throughout work as solvent for organic samples. Experimental measurement data for chloroform can be seen in Figure 4.1. For chloroform acquired value was $n_2=(2.01\pm0.14)\cdot10^{-15}$ cm^2/W and for CS_2 - $n_2=(3.10\pm0.25)\cdot10^{-14}$ cm^2/W. Both values fit well with literature[133] giving strong enough evidence to conclude that it is possible to correctly evaluate the Kerr coefficient for a liquid sample with experimental setup implementing PL ps laser used in this work.

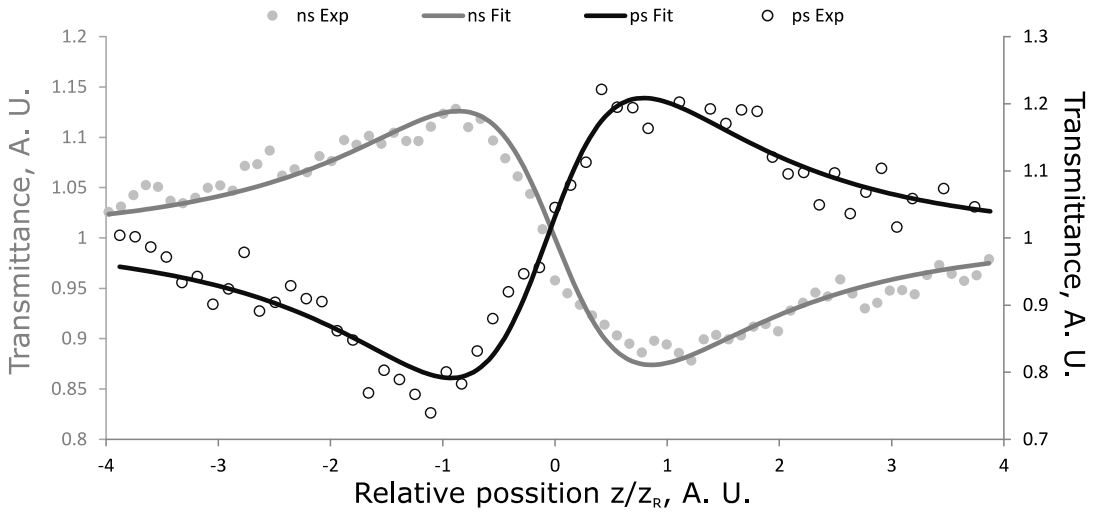

Figure 4.1: *Z-scan experimental measurement with ns and 30 ps lasers. From this graph, it is evident that both measurements have different signs of the Kerr coefficient.*

Pulse width influence. A comparison of measurements implementing either of lasers was carried out using chloroform. Firstly, the sample was measured using the ns laser at a 4 kHz repetition rate. Comparing acquired data to PL ps measurement (see Figure 4.1) we observed that experimental curves have inverse shapes. By calculating values of n_2 for both cases, we concluded, that PL ps measurements gave $n_2=(2.01\pm0.14)\cdot10^{-15}$ cm^2/W, while ns measurements gave $n_2=(-4.47\pm0.23)\cdot10^{-13}$ cm^2/W which has an opposite sign and much larger value than the Kerr coefficient for chloroform. This inconsistency can be explained by thermal effects. In the case of high repetition rate lasers, heat can accumulate and lead to a thermally induced variation of sample density and refractive index changes. For chloroform heat dissipation time is τ_S=15 ns (see equation 1.51) and thermal diffusion time is equal to τ_D=2.1 ms (calculated using equation 1.50), meaning that diffusion effects will strongly influence measurements that are carried out 500 Hz and higher laser pulse repetition rates. This indicates that for this specific measurement both single-pulse and accumulative effects could be present.

Pulse repetition rate influence. To investigate this further, experiment implementing ns laser with different pulse repetition rates were carried out. Acquired n_2 values are shown in Figure 4.2. While experimental data approaches constant value at small laser pulse repetition rates, as expected, this value still has a negative sign that does not fit values presented in the literature. The thermo-optical coefficient of chloroform is $dn/dT=6.3\cdot10^{-3}$ 1/K. From equation (1.52) we can see that this would give negative value for n_2 at thermal equilibrium which is in accordance with observed results. The frequency dependence indicates that in these measurements thermal equilibrium was not reached and equation (1.52) cannot be used for further analyses.

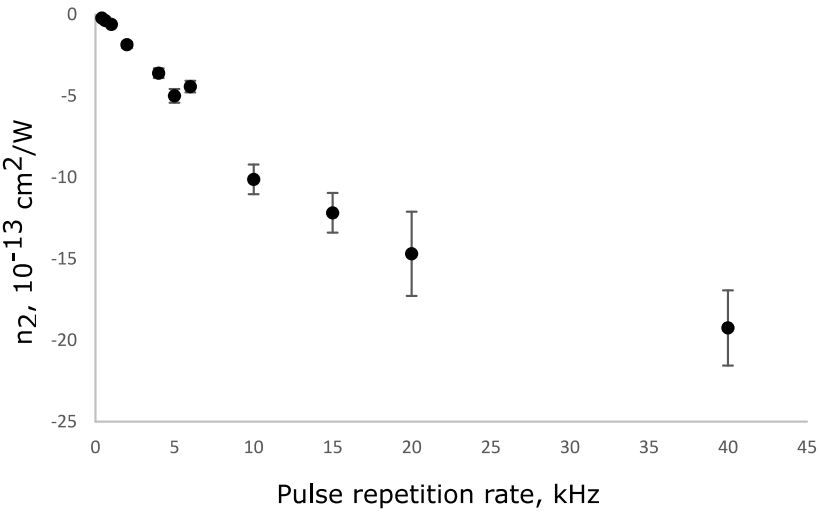

Figure 4.2: *Nonlinear refractive index of chloroform at a different pulse repetition rates.*

Polarisation measurements. To study origins of nonlinear refractive index changes in chloroform, measurements at different light polarisations – varying from circular to linear –

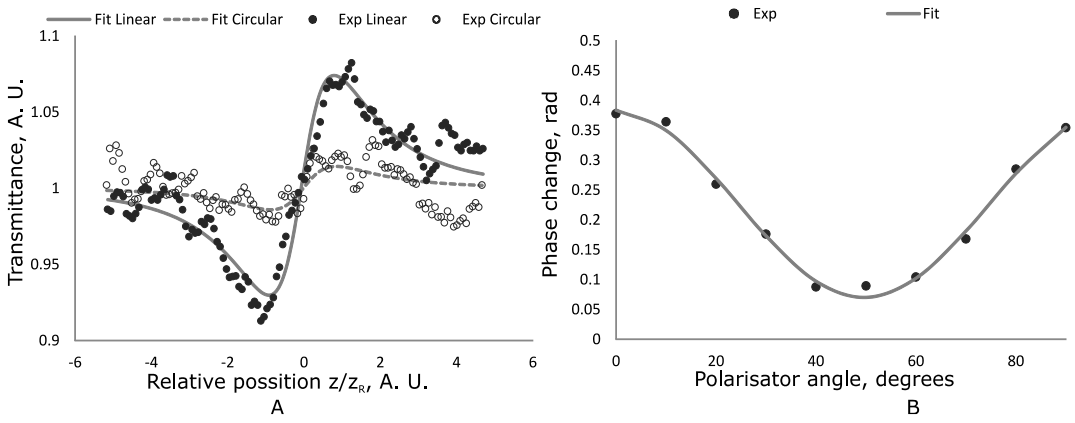

Figure 4.3: *Experimental measurements at different polarisations. A – The transmittance curve drastically changes when comparing linear and circular polarization measurements. B - To determine B/A ratio, phase changes were plotted as a function of Polarizers angle and fitted with equation (4.1).*

was carried out using the PL ps laser. Experimental results can be seen in Figure 4.3. Experimental data were fitted with function:

$$n_2 = C_1 + C_2 \cdot \cos^2(C_3 \cdot \varphi + C_4) \tag{4.1}$$

which is of a similar form as equation (3.2) where C_i are the fitting constants. Using equations (1.40) we can show that ratio *B/A* can be expressed as:

$$\frac{B}{A} = 2 \cdot \left(\frac{n_{2;linear}}{n_{2;Circular}} - 1 \right) \tag{4.2}$$

From acquired results, the *B/A* ratio was calculated giving a value of 6.09. This indicates that for pure chloroform this effect is solely due to molecular reorientation. Similar measurements were also carried out using ns laser at different repetition rates to distinguish between the Kerr and thermo-optical contributions to refractive index changes as both of these effects have different dependencies on polarisation. Experimental measurements were firstly carried out with ns laser at a 200 Hz pulse repetition rate. Phase change dependence on the polarizator angle can be seen in Figure 4.4. These data were fitted with equation (4.1). To separate the thermo-optical and Kerr contributions, we assumed that for the thermo-optical effect *B/A*=0 and for the Kerr effect *B/A*=6. This means that any difference in refractive index changes between values at linear and circular polarizations is only due to the Kerr effect. This difference will be equal to:

$$\frac{n_{2;linear}}{n_{2;Circular}} = 4 \;\rightarrow\; \Delta n_2 = n_{2;linear} - n_{2;Circular} = \frac{3}{4} \cdot n_{2;linear} \tag{4.3}$$

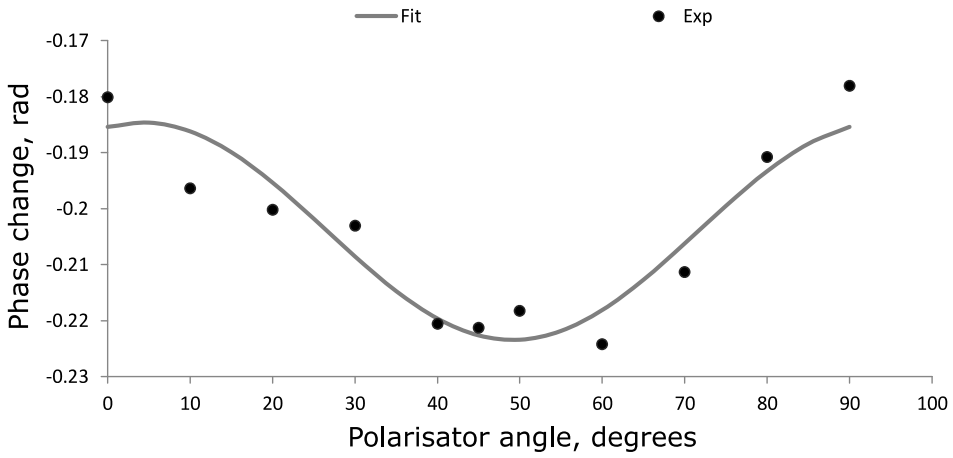

Figure 4.4: *Phase change polarisation dependence for ns measurements at 200 Hz.*

Using this equation we calculated thermo-optical effect contribution to be $n_{2;TO}$=-(7.56±0.65)·10^{-15} cm^2/W and Kerr contribution to be $n_{2;Kerr}$=(1.84±0.31)·10^{-15} cm^2/W. The Acquired Kerr value is close to PL ps measurement value, validating that polarization-dependent measurements can be used to separate both (Kerr and thermo-optical) contribution. But this method is limited by the laser repetition rate. When increasing the laser pulse repetition rate up to 1000 Hz any distinguishable dependence on polarization disappeared, due to a strong thermo-optical effect. To compare, at 200 Hz difference between linear and circular polarization was around 16 % of the measured value, while at 800 Hz the difference was around 5 %, becoming smaller than the average measurement error, complicating the correct evaluation of the Kerr value (see Table 4.1).

Table 4.1. *Polarisation measurement results at different pulse repetition rates*

Nr	ν, Hz	$\Delta\Phi_{Linear}$, rad	$\Delta\Phi_{Circular}$, rad	R*, %
1	200	-0.1801	-0.221311939	0.228828
2	400	-0.4771495	-0.519353424	0.08845
3	800	-1.1808504	-1.24165566	0.051493

** The value r denotes how large is the phase change between linear and circular measurements compared to linear measurement.*

Study of organic dyes. As the most popular approach to measuring the NLO properties of organic compounds is by diluting them in solvent and then measuring, the solvent can significantly influence measurement results depending on its own properties. There are examples in literature that by using methanol, solvents influence can be neglected[7]. Although this is a way to correctly measure organic chromophores NLO properties, the most popular approach is to use chloroform as a solvent which significantly contributes to the samples' NLO response. This gives a rise to a new problem – correctly separating solvents influence to determine the magnitude of organic chromophores Kerr effect as well as to separate the

nuclear and electronic parts. While the former has already been solved in literature, how to correctly analyze polarisation measurement results have yet to be presented. In this section guidelines of result analysis will be given. For Z-scan test measurements, two organic compounds were chosen – DMABI and MeSBI (see Figure 4.5). These molecules were chosen as they possess insignificant absorption at 532 nm and the 2PA effect should not influence experimental measurements (absorption properties of these compounds will be presented in section NLO properties of organic molecules). This could allow for a better understanding of how the type of laser (either PL ps or ns laser in this work) influences observed refractive index changes.

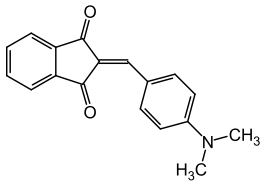

DMABI

2-[4-(N,N-dimethylamino)-benzylidene]
-2H-indene-1,3-dione

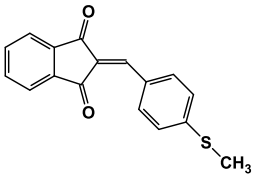

MeSBI

2-(4-methylsulphanylbenzylidene)
-indane-1,3-dione

Figure 4.5: *Organic compound structures and names.*

If studied media consists of multiple components, the overall nonlinear optical properties will be proportional to the component mass ratio. In general case it can be written as[5]:

$$n_{2;media} = \sum_{i=1}^{n} \frac{m_i}{m_{media}} \cdot n_{2;i}, \tag{4.4}$$

where m_{media} is the mass of studied media and m_i and $n_{2;i}$ are the mass and the Kerr coefficient of a component. For the case when a specific organic component is diluted in chloroform, equation (4.4) can be rewritten as:

$$n_{2;sample} = \frac{m_{chloroform}}{m_{sample}} n_{2;chlorform} + \frac{m_{organic}}{m_{sample}} n_{2;organic}, \tag{4.5}$$

where $m_{chloroform}$, $m_{organic}$, $n_{2;chloroform}$ and $n_{2;organic}$ are the mass and the Kerr coefficient of the chloroform and the organic compound.

Firstly Z-scan measurements for these compounds were carried out using PL ps laser to determine the Kerr coefficient for these molecules. The acquired values were $n_2=(2.49\pm0.22)\cdot10^{-13}$ cm^2/W for DMABI and $n_2=(2.52\pm0.62)\cdot10^{-13}$ cm^2/W for MeSBI. For DMABI polarization-resolved Z-scan measurements with PL ps were also carried out. An example of an experimental measurement of DMABI dissolved in chloroform can be seen in Figure 4.6. In this case, *B* to *A* ration was calculated to be *B/A*=4.39. By assuming that for pure chloroform *B/A*=6.09, the ratio value for the DMABI molecule was calculated to be *B/A*=2.85. This was acquired by solving the following equation:

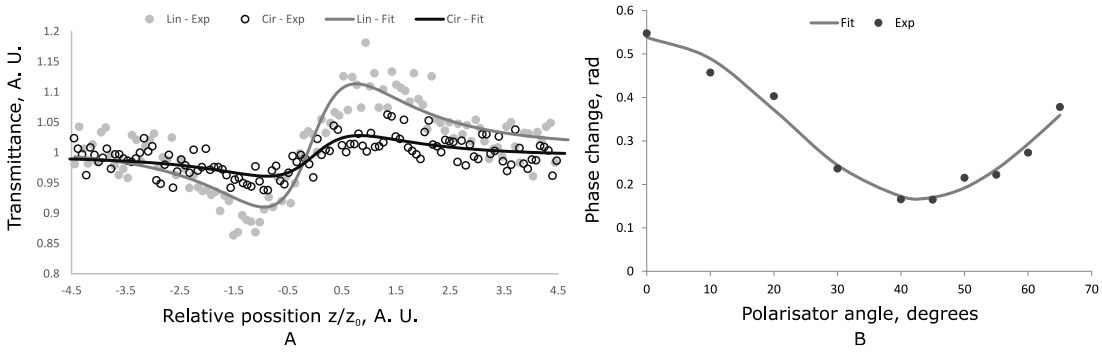

Figure 4.6: *Polarisation measurements for DMABI dissolved in chloroform. A) Transmittance measurements for linear and circular polarisations. B) Phase change dependence on polarizer angle.*

$$\frac{1}{2}\cdot\left(\frac{\mathrm{B}}{\mathrm{A}}\right)_{(\mathrm{Exp})}+1=\frac{n_{2;(\mathrm{C})}+n_{2;(\mathrm{Organic\ Dye})}}{\frac{1}{\frac{1}{2}\left(\frac{\mathrm{B}}{\mathrm{A}}\right)_{(\mathrm{C})}+1}\cdot n_{2;(\mathrm{C})}+\frac{1}{\frac{1}{2}\frac{\mathrm{B}}{\mathrm{A}}+1}\cdot n_{2;\mathrm{lin(Organic\ Dye)}}}\rightarrow$$

$$\begin{bmatrix}\left(\frac{\mathrm{B}}{\mathrm{A}}\right)_{(\mathrm{Exp})}=4.39\\ \left(\frac{\mathrm{B}}{\mathrm{A}}\right)_{(\mathrm{C})}=6.09\end{bmatrix}\rightarrow 3.95=\frac{n_{2;(\mathrm{C})}+n_{2;(\mathrm{Organic\ Dye})}}{\frac{1}{4.045}\cdot n_{2;(\mathrm{C})}+\frac{1}{\frac{1}{2}\frac{\mathrm{B}}{\mathrm{A}}+1}\cdot n_{2;\mathrm{lin(Organic\ Dye)}}} \tag{4.6}$$

The equation is written in such form to use *B/A* ratio as variables. Another option would be to use the nonlinear refractive index ratio at linear and circular polarisations, but *B/A* ratio is a more widespread approach. For further result analysis assumption is made that only molecular reorientation and electronic components influence refractive index changes, with molecular reorientation having ration *B/A*=6 and electronic response *B/A*=1. Using this assumption, measured n_2 value can be separated into both components. To acquire values of induced refractive index changes at linear polarisation for both effects, the following equation system needs to be solved:

$$\begin{cases} n_{2;lin}=n_{2;MR}+n_{2;E}\\ n_{2;cir}=\frac{1}{4}\cdot n_{2;MR}+\frac{2}{3}\cdot n_{2;E}\end{cases} \tag{4.7}$$

Using this equation nonlinear refractive index values were calculated to be $n_{2;MR}=1.52\cdot10^{-13}$ cm^2/W and $n_{2;E}=(9.71\pm0.22)\cdot10^{-14}$ cm^2/W. These values will be further used in comparison with QQC results to estimate how precise calculations can predict experimental results.

Errors of organic chromophore measurements with ns laser. The main issue with NLO measurements implementing ns laser is the thermo-optical effect due to either one- or two-photon absorption. One could assume that for materials that possess insignificant absorption at irradiation wavelength λ and $\lambda/2$, correct measurements of the Kerr effect should be possible with ns laser. To check this we measured DMABI and MeSBI solutions with ns laser. Firstly MeSBI was measured with ns laser at a 40 kHz repetition rate. A comparison of experimental measurements for pure chloroform and MeSBI solution is shown in Figure 4.7. From this graph, it is evident that MeSBI possesses a negative nonlinear refractive index as

peak-valley amplitude increases by adding MeSBI to chloroform. The calculated refractive index changes for MeSBI were n_2=(-2.8±0.3)·10^{-10} cm^2/W that is few orders higher than the value measured with PL ps laser. By measuring n_2 dependence on polarisation, no variation in nonlinear refractive index value was observed. Also, experiments at different pulse repetition rates were carried out and observed that the magnitude of the nonlinear refractive index increased with the repetition rate. This clearly indicates that these changes are only due to thermal effects, although MeSBI has no significant absorption at 1064 nm or 532 nm. This shows an important aspect of NLO measurements - even for materials with insignificant absorption at irradiance wavelength and at half of it, NLO properties can still be dominated by thermo-optical effects. For DMABI 8 ns measurements gave a positive value of n_2=(1.3±0.2)·10^{-10} cm^2/W, which is around three orders larger than the value acquired with 30 ps laser. Polarisation-resolved measurements gave a *B/A* ratio of 1.18 for DMABI, indicating that mostly electronic contribution dominates refractive index changes. This will be analyzed in further sections at this moment remaining as an open problem – why does Kerr effect electronic contribution for DMABI increase with pulse duration?

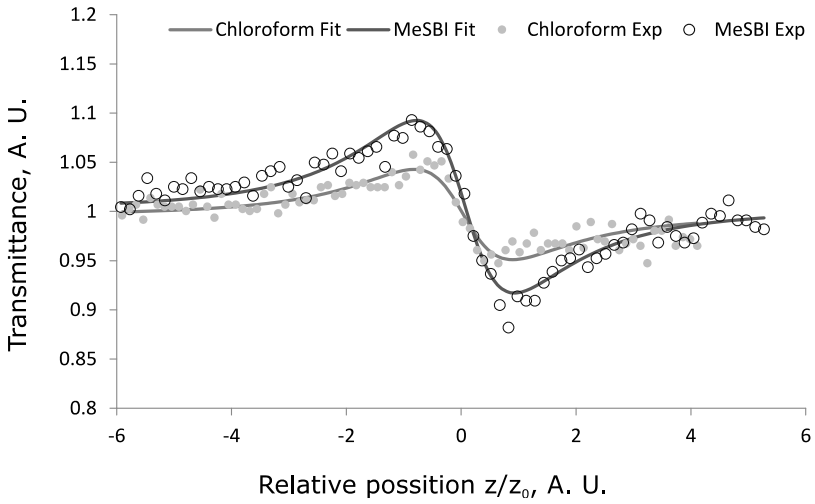

Figure 4.7: *Experimental measurements of MeSBI compared to chloroform with ns laser at 40 kHz pulse repetition rate.*

Summary. In conclusion, a wide spectrum of different measurements was carried out to test the limits of the Z-scan method for measuring the Kerr effect of liquids. The main conclusions from these sections are:

1. While ns laser pulse width should not be long enough to induce a thermal response from liquids, at a higher repetition rate this happens due to the accumulative thermo-optical effect and overwhelms the Kerr effect. This can lead to overestimation of the Kerr effect if not investigated properly,
2. When using ns laser Kerr effect contribution can be separated from the thermo-optical one using polarization-resolved Z-scan measurements, but only when the Kerr

effect contribution is larger than the experimental measurement error. This can become an issue when using a higher repetition rate lasers.

3. Polarisation-resolved Z-scan measurements can be used to determine the ratio of molecular and electronic contributions to the Kerr effect. This is an experimentally simpler approach than measuring the Kerr effect at different pulse widths. Although the separation is based only on the effect response to linear and circular polarisation beams that can limit its applicability. Theory suggests that collision effects and electronic will have a *B/A* ratio of 1 while libration and diffusive reorientation *B/A* ratio will be 6. While this method does not give a complete separation of all contributions, in specific cases this can be simplified. While collision effects are very profound when studying solvents, time-resolved measurements of specific organic compounds have shown that no collision effects are present due to organic compound[53]. At low concentrations, organic compounds are too far from each other in the solvent to influence each other's electron distribution, while the solvent is to "weak" compared to the organic compound to induce any collision effects. Due to this, polarisation resolved Z-scan can be used to correctly separate the electronic contribution of low concentration solutions. This can be assumed only when the organic dye has a much larger Kerr effect than the solvent. A more complicated aspect is the separation of libration and diffusive reorientation and would demand pulse width dependent measurements.
4. When measuring solutions of organic compounds dissolved in chloroform with ns laser, it is not straight forward answer whether the response is due to thermo-optical effects or the Kerr effect. Our measurements showed that it also does not correlate with linear absorption at irradiance wavelength or the 2PA effect.

4.1.2. Mach-Zehnder interferometer

The first step of MZI measurements was to ensure that sample is placed in the focal point of the setup. From the Z-scan theory, it is evident that by placing the sample exactly at the focal point of a lens, no beam size variations will be present and the Kerr effect will only induce a phase change in the beam and no other alterations. To find the correct sample position, a Z-scan type measurement was carried out with liquid chloroform that was contained in a 2 mm quartz cell and irradiated with ns laser. After that sample was placed at the focal point and transmitted lights dependence on input intensity was measured using the sample arms reference detector with an aperture in front of it. If any 2PA effect or size variation would be present in the sample, a closed-aperture measurement of this detector would pick it up. Similar measurements were carried out also with small deposition form focal point to test position influence on measurements. The results are shown in Figure 4.8. Although at focal point transmitted light should linearly depend on input intensity, a deviation from this trend was observed when input intensity was over 300 MW/cm^2 at the focal point. This can be explained due to higher-order elements of Z-scan analytical expression that needs to be taken into account when describing beam focusing that leads to changes of the coordinates where no changes in beam size are observed (see Appendix C). This shows the maximal intensity at which measurements can be carried out. By displacing the sample from the focal point, deviation started at smaller laser intensity as expected. After setup calibration,

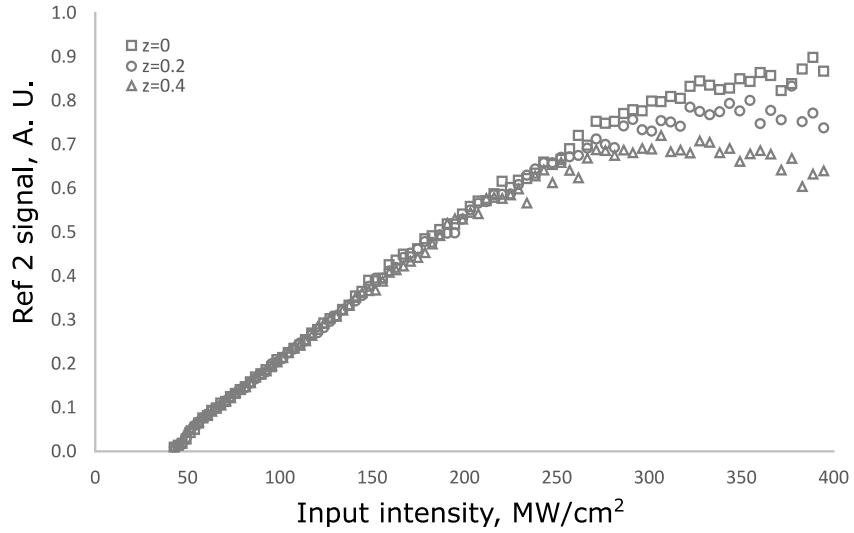

Figure 4.8. *Transmitted light as a function of laser beam intensity at the focal point. Z denotes position compared to the focal point. Squares indicate the measurement with the sample placed in the focal point, Circles with 0.2 mm deviation, and Triangles - 0.4 mm deviation. Transmitted light was measured using a reference detector (Ref 2) and is displayed in arbitrary units.*

interferometric measurements were carried out. The signal from output detector was measured as a function of laser power. For this case equation (2.2) can be simplified to form:

$$P_{out} = \mathrm{A}_1 \cdot P_1 \cdot (1 + A_2 \cdot \cos(\Delta\Phi^* \cdot P_1 + \Delta\Phi_0)), \tag{4.8}$$

where P_1 is the laser power of sample beam, A_1 and A_2 are the fitting coefficients, $\Delta\Phi_0$ is the phase coefficient, and $\Delta\Phi^*$- the nonlinear phase change coefficient (see Appendix D for the derivation of equation (4.8)). Experimental measurements were carried out with ps, ns, and CW lasers and will be presented in the same order in the following section.

Ps measurements. Measurements with ps laser for liquid chloroform were carried out to confirm that this setup can be used to study the Kerr effect. During experimental testing, there were difficulties to acquire a stable interference pattern. This was due to the small coherence length that for ps laser is equal to l=1.47 mm. To overcome this, the experimental setup was constructed so that both arm lengths were equal and an optical wedge was used to compensate path difference introduced by the quartz cell. This allowed getting a stable interference pattern and measuring the Kerr coefficient. An example of experimental data can be seen in Figure 4.9. Kerr coefficient was measured to be $n_2=(2.09\pm0.18)\cdot10^{-15}$ cm^2/W which is similar to values presented in the literature. Ps measurements highlighted an important limitation of the MZI method - by implementing shorter pulse duration lasers, the coherence length decreases and it becomes more difficult to acquire a stable interference pattern. To implement a 100 fs laser for MZI measurements, the path difference between both interferometer arms could not exceed a few microns significantly complicating experimental implementation. Taking into account that the Z-scan method has no such limitation this is an obvious shortcoming of MZI when compared to Z-scan.

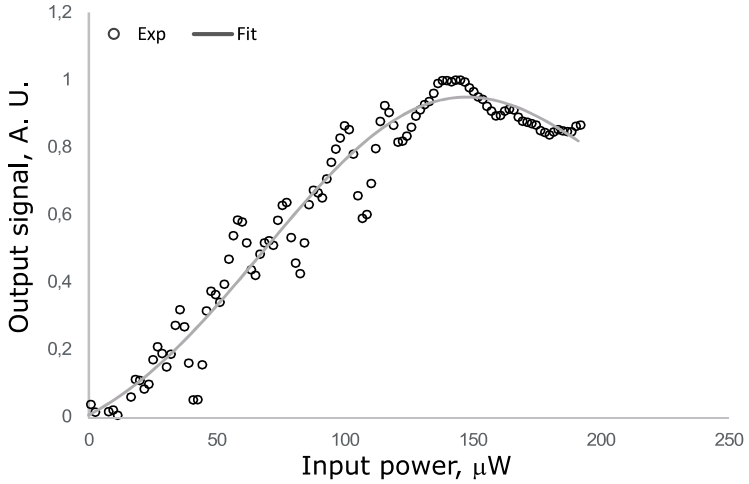

Figure 4.9: *Mach-Zehnder interferometer experimental data using 30 ps laser.*

Ns measurements. An example of experimental measurement can be seen in Figure 4.10 A. Here a phase change larger than 4π was measured. For Z-scan measuring such a large phase change would demand a more complicated analytical model while for MZI the same simple equation (4.8) could be used indicating an advantage for MZI over the Z-scan method. Measurements were carried out at different laser repetition rates. Acquired results were compared with Z-scan results to verify their credibility. From Figure 4.9 B it is evident that results from both methods fit very well.

CW measurements. For further thermo-optical effect studies, measurements using 437 nm CW laser were carried out. A significant difference between ns and CW measurements is that during CW measurements a significant signal fluctuation in time was observed during measurements. Due to this, measurements at each laser power was carried over time and averaged to get a data point at specific laser power. This also introduced a systematic error

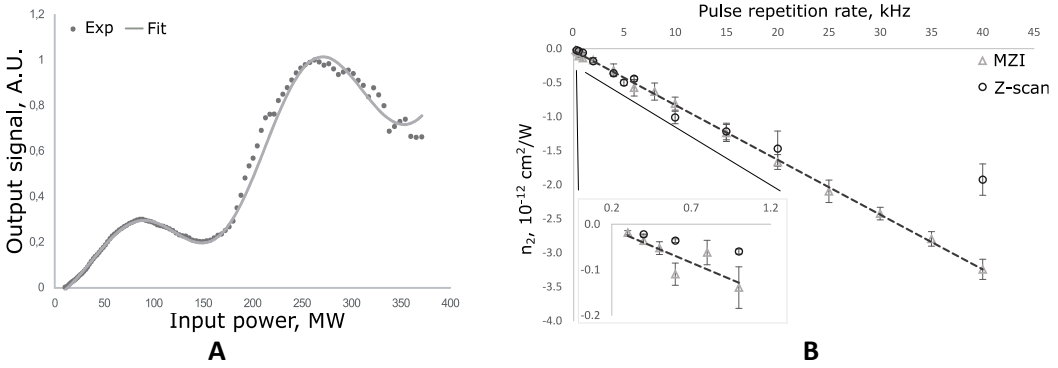

Figure 4.10: *A - Experimental measurement of chloroform using single beam Mach-Zehnder interferometer. Dots represent experimental measurements and line represents an analytical fit with equation (4.8). B - Pulse repetition rate measurements for both Mach-Zehnder interferometer and Z-scan method compared.*

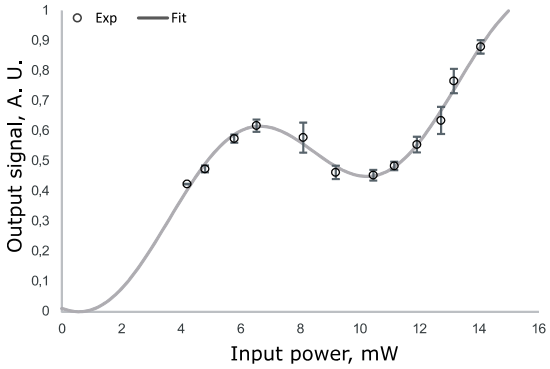

Figure 4.11: *Mach-Zehnder interferometer measurement using a 437 nm CW laser.*

for each data point. An example of experimental measurements can be seen in Figure 4.11. For the CW case we can assume that sample has reached thermal equilibrium and we can calculate the nonlinear refractive index from equation (1.53) using values of chloroforms thermo-optical coefficient and linear absorption presented in literature[166,169]. This gave us refractive index changes of n_2=-1.27·10^{-8} cm^2/W. Experimental measurements gave value n_2=(-5.06±0.32)·10^{-8} cm^2/W that is of the same order as the theoretical value.

The second part of MZI experiments used two laser beams for demonstration of all-optical switching using two beams – inducing and probing. In this setup, one laser induces refractive index changes, and the second one probes the changes. Ns laser was used as an inducing beam while different CW lasers with wavelengths of 437, 632.8, and 780 nm were used as probing beams. For this case equation (3.2) can be simplified to form (see Appendix D):

$$P_{out} = B_1 + B_2 \cdot \cos(\Delta\Phi^* \cdot P_i + \Delta\Phi_0), \tag{4.9}$$

where B_1 and B_2 are the fitting constants and P_i is the inducing beam power. An example of experimental data for 780 nm probing laser and ns laser at 30 kHz pulse repetition rate are shown in Figure (4.12 A). Experimental measurements were carried out at different repetition

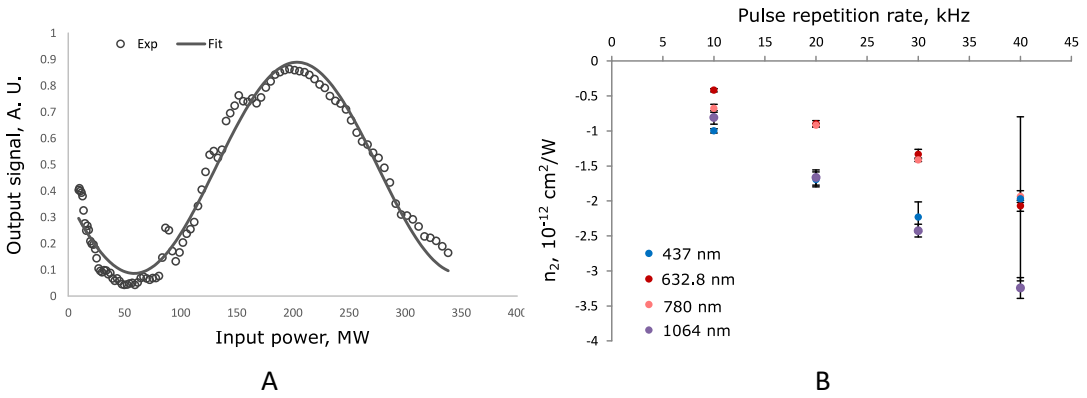

Figure 4.12: *A – Experimental data of two-beam Mach-Zehnder interferometer measurement using 780 nm laser as probing and ns laser with pulse repetition rate at 30 kHz as inducing beam. B – Comparison of probed refractive index changes with different lasers.*

rates for all lasers and results can be seen in Fig (4.12 B). It is essential to emphasize that in this case all-optical switching is mainly due to the thermo-optical effect. Taking this into account, all of the probing beams should theoretically give the same results as single laser measurements with ns laser as an interaction between laser beams is carried out through thermally induced density changes. From experimental results, it is evident that data with 437 nm probing laser are similar to single laser (ns laser) results, while 632.8 and 780 nm laser gave smaller n_2 values. This can be due to multiple factors: i) statistical error during approximation, ii) all lasers had different spot sizes in the focal point, iii) how precisely both beams were positioned respectively to each other and how well they overlapped. In Figure (4.12 B) only the statistical error part is represented. Regarding the second aspect, all of the probing beams had smaller beam sizes in the focal point compared to the inducing beam. Also, the data point for 437 nm laser at 40 kHz ns laser pulse repetition rate shows a very large error and falls out from the linear trend of other points. This was due to the fact, this specific measurement was difficult to acquire a stable interference pattern leading to a large error. This was not further studied as it didn't seem relevant to this work.

Measured nonlinear refractive index values at different pulse widths are shown in Table 4.2. For each class the following conclusion can be made: i) Using a CW laser gives a value that is similar to the theoretically predicted value of thermo-optical effect when the sample has reached equilibrium state; ii) 8 ns pulse width measurements at pulse repetition rate from 200 – 40 000 Hz are strongly influenced by thermo-optical effect, but it is still a small fraction of this effect when compared to CW measurements; iii) 30 ps pulse width measurements gives a value that fits the Kerr values given in the literature.

Table 4.2: *Nonlinear refractive index values of chloroform measured with Mach-Zehnder interferometer*

Laser	Dominant Effect	Value
CW laser	Thermo-optical effect	$(-5.06\pm0.32)\cdot10^{-8}$ cm^2/W
ns laser	Thermo-optical effect	Depends on laser repetition rate (− 0.0185… − 3.24 × 10^{-12} cm^2/W)
ps laser	Kerr effect	$(2.09\pm0.18)\cdot10^{-15}$ cm^2/W

In principle, this setup could be used to probe Kerr effect induced all-optical switching between two different laser beams and to determine χ(ω1; ω1, ω2,- ω2), although ps laser with few Hz repetition rate and fast detectors synchronized with the laser would be necessary.

Summary. In conclusion, the MZI method was tested as an alternative to the Z-scan method for NLO measurements. The following conclusions were made:

1. MZI simple analytical model can be used even for large phase changes (up to 3π) and is only limited by the change of location of sample position relative to the focal point at which no beam size variations are induced. Compared to Z-scan that demands more complicated analytical models to process measurements with large phase change (>π/2) this is a clear advantage.

2. In the case of short-pulse lasers (ps range) used in MZI measurements, coherence length becomes a limiting aspect. While for 30 ps laser we were able to adjust the optical length of both MZI arms with an optical wedge, this could become more complicated if measurements are carried out with femtosecond laser. On the other hand, such Z-scan has no such limitations.

4.1.3. Conclusions on NLO measurement methods

Through the study of Z-scan and MZI methods, clear advantages and disadvantages have become apparent. Each of the methods has its specific conditions at which they serve the best.

Z-scan. In summary, Z-scan is a good general method for NLO measurements that can be widely applied for material studies. The main limitation of the Z-scan method is the difficulty to study materials in which large phase changes are induced. While it is possible, the analytical models become complicated, and often numerical simulations need to be used. This is not an issue for general material studies as often low concentration samples are studied with small induced phase changes.

MZI. The main advantage of MZI is the simple analytical model for data fitting that extends even to large phase changes. On the other side, MZI is hard to implement experimentally for short-pulse lasers, which is essential for correct studies Kerr effect. Due to this, MZI is not the best method for general material studies but has its applicability in ns region measurements. One field, where MZI could be more applicable than Z-scan is in studying refractive index changes due to photoisomerization in thin-films as this effect can lead up to $n_2 \approx 10^{-4}$ cm^2/W and large induced phase changes in sample[170].

4.2. NLO properties of organic materials

In this section results of the Z-scan measurements for various organic compounds will be given. The study of NLO properties of various organic molecule groups allowed to derive conclusions independent of specific molecule structure and can be applied to organic materials in general. Three main material groups were studied in this work: i) Aminobenziliden-1,3-indandione (ABI) derivatives (13 compounds). Due to a wide range of different derivatives, this material group could give some insight into specific structure-property relations of the Kerr and 2PA effects with main focus on different donor and acceptor groups; ii) Triphenylamine (TPA) derivatives (8 compounds). This group includes materials with small structural alterations to study how angular positions of different molecular groups influence NLO properties; iii) 2,6-bis(4-aminobenzylidene)-s-indacene-1,3,5,7-tetraones (BIT) derivatives (6 compounds). These materials exhibit a strong 2PA effect and could be applicable for optical limiting applications. Each section will be divided into three parts: i) Compound description giving a short description about molecule structural form and linear optical properties; ii) NLO results presenting experimental results; iii) Observations giving a deeper analysis of results.

4.2.1. ABI derivatives

Compounds: Molecular structures and abbreviations for studied ABI derivatives are shown in Figure 4.13. The main structural variations between selected compounds can be summarized as follows: i) Molecules with the same indandione acceptor group but with different donor groups (DMABI-Ju, DAMBI-dph, DMABI, MeOBI, MeSBI, DMABI-OH, DMabi-Ph6); ii) Molecules with different amount of indandione acceptor groups attached to triphenylamino donor group (TPA – 0, DMABI-dph – 1; DiDMABI – 2; TriDMABI – 3). This group is also interesting due to changes in the symmetry of molecules, with DMABI-dph and DiDMABI being non-

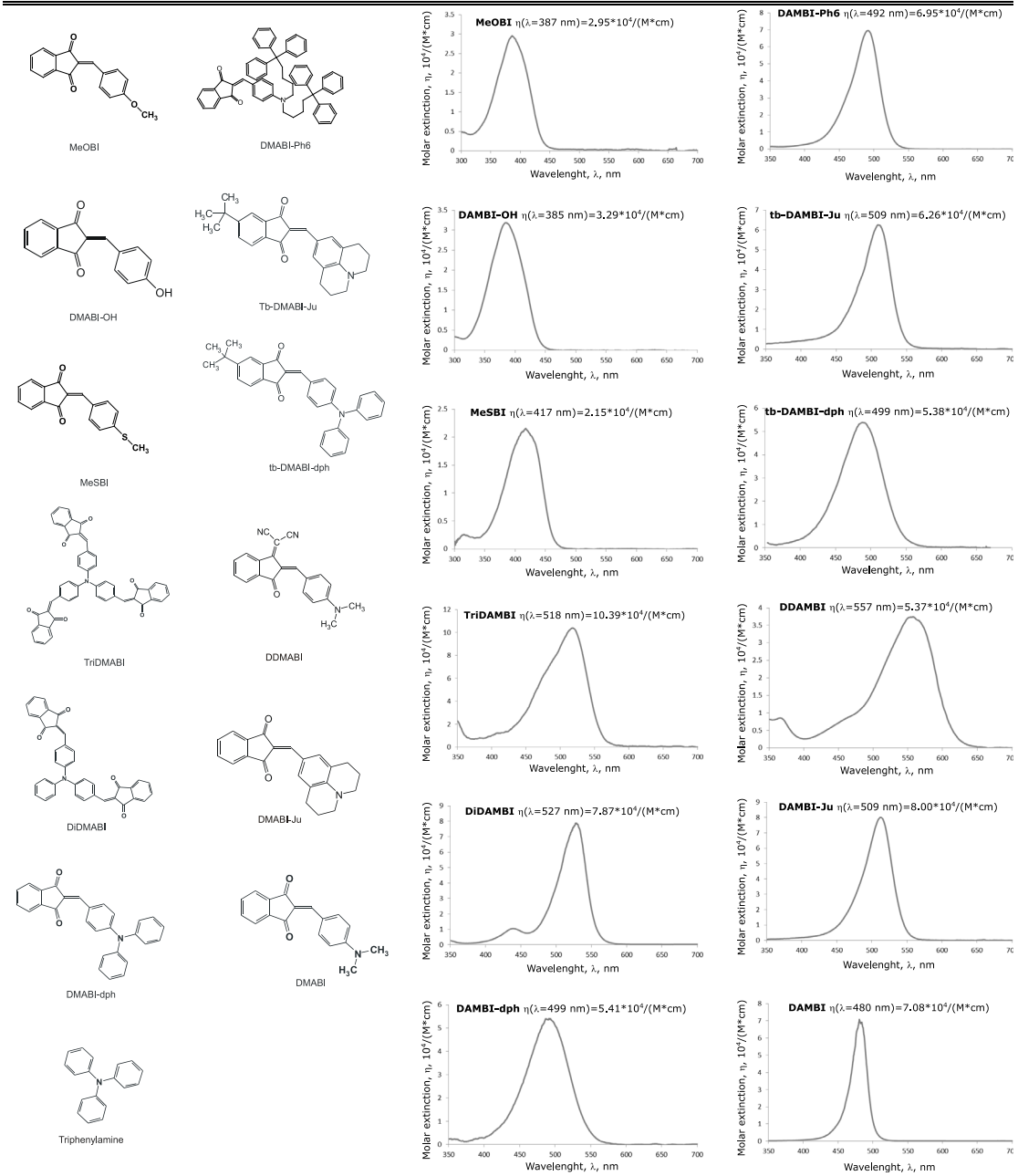

Figure 4.13: *Molecular structures,* abbreviations *and absorption spectrums of ABI derivatives.*

centrosymmetric and Tri-DMABI having a planar structure with no permanent dipole moment in the ground state; iii) For practical applications, it is beneficial if an organic compound can form thin-film molecular glass layer or at least allows to have a high concentration in a guest-host system with some polymer before crystallization. Several of these materials do not meet this condition (DMABI can have up to 10 wt% in PMMA guest-host system before it starts to crystalize). To solve this, we study how additional structural groups to increase the solubility of the organic compound in specifics polymer guest-host systems influence NLO properties of specific materials. If these groups lead to higher solubility but significantly lower the NLO efficiency, this alteration is not beneficial. The absorption maximum for these compounds is compiled in Table 4.3. Absorption spectra in chloroform solution for these compounds are shown in Figure 4.13. As TPA did not exhibit any significant absorption at the visible spectrum, absorption data for this compound is not presented. While none of the compounds possess significant absorption at 1064 nm, some of the molecules absorb 532 nm that could influence 2PA properties. While for centrosymmetric molecules linear absorption at half of the irradiation wavelength is not a strong indication about 2PA properties, for non-centrosymmetric molecules it is. As in this case, only molecules that do not possess any significant absorption at 532 nm are DMABI, DMABI-OH, MeOBI, and MeSBI it is expected that these molecules will have no 2PA effect.

Table 4.3: *Absorption maximum for ABI derivatives*

Compound	λ, nm	η, 1/(M*cm)
DMABI	480	70807
DMABI-Ju	509	80060
tb-DMABI-Ju	509	62564
DMABI-dph	499	54118
tb-DMABI-dph	499	53835
TriDMABI	518	103899
DiDMABI	527	78758
DMABI-OH	385	32905
DDMABI	557	53689
MeOBI	387	29473
MeSBI	417	21533
DMABI-Ph6	492	69544

NLO results: NLO properties for these compounds were measured using the 30 ps laser. Also to study pulse width influence on 2PA, some of the compounds with the most profound 2PA properties were also measured with ns laser. In this case, only open aperture data were studied as closed-aperture data was strongly influenced by thermo-optical effects due to absorption. Linear optical properties at 532 nm and acquired NLO values with ps laser are presented in Table 4.4. Results with ns laser will be discussed further in the text.

Table 4.4: *Nonlinear optical values of ABI derivatives measured with 30 ps laser*

Solute	Extinction coefficient at 532 nm	$\beta_{2;ps}$, cm/W · 10^{-7}	$\sigma_{2PA;ps}$, GM	n_2, $cm^2/W \cdot 10^{-12}$	δ_{NLR}, RGM
Chloroform	-	-	-	0.00201±0.00014	0.294±0.021
DMABI	1023	-	-	0.249±0.022	84.9±7.5
Triphenylamine	-	-	-	0.086±0.029	25.9±8.7
DMABI-dph	17578	0.519±0.056	434±47	-0.594±0.036	-293±18
DiDMABI	76692	1.23±0.18	1420±210	-1.35±0.20	-920±140
TriDMABI	81243	1.281±0.081	1900±120	-2.12±0.28	-1860±250
tb-DMABI-dph	14230	0.438±0.059	417±59	-0.493±0.066	-277±37
DMABI-Ju	38068	0.332±0.054	228±37	-0.67±0.10	271±41
tb-DMABI-Ju	26578	0.365±0.024	293±19	-0.261±0.036	-123±17
DMABIOH	-	-	-	2.75±0.34	840±110
DDMABI	30458	0.962±0.089	652±60	0.339±0.043	135±21
DMABI-Ph6	3577.823	-	-	-0.105±0.011	-109±11
MeSBI	-	-	-	0.252±0.062	96±24
MeOBI	-	-	-	0.220±0.054	80±20

*$\beta_{2;ps}$ – 2PA coefficient measured with 30 ps laser; $\sigma_{2PA;ps}$ – 2PA cross-section calculated from $\beta_{2;ps}$ values; n_2 – Kerr coefficient measured with 30 ps; δ_{NLR} – Nonlinear refractive cross-section calculated from n_2 values.

The first conclusion can be made regarding the sign of the Kerr effect. By looking at results, it can be seen that at for molecules with small absorption at 532 nm (around or less than 1000) Kerr coefficient is positive, with the only exception being DDMABI. For correct sign analysis information about 2PA spectral dependence is necessary to know how close measurements are to 2PA resonance. As most molecules, except TriDMABI, have a permanent dipole moment, we can use the two-level system to analyze these results. This also means that one-photon absorption should give a good idea about how close we are to 2PA resonance as there are no specific selection rules to transitions for one-photon or two-photon processes. Firstly for the group consisting of DMABI, DMABI-Ph6, MeOBI, MeSBI, and DMABI-OH we can apply the non-resonant case as no 2PA effect was observed. All of these molecules possess a positive sign for the Kerr effect except for DMABI-ph6. That means that for DMAB-ph6 the N term dominates and transition dipole moment are much larger than the difference between dipole moments in the ground and excited states while for the other molecules the D term dominates and the difference between dipole moments in the ground and excited states are much larger than transition dipole moment. This indicates that triphenylpentyl groups added to DMABI-Ph6 significantly influence the NLO properties of the molecule. It is difficult to say what induces these changes, but one of the reasons could be that triphenylpentyl groups twist around the molecule influencing the local-field effect that influences the NLO response of the molecule. Next, we can look at molecules that are closer to 2PA resonance. The second group is formed by DMABI-dph, DiDMABI, TriDMABI, tb-DMABI-dph, DMABI-Ju,tb-DMABI-Ju, and DDMABI. Special attention needs to be given to TriDMABI as it has no permanent dipole moment in ground state and DDMABI as 532 nm is a shorter wavelength than the maximum of its absorption. The rest of the second group molecules have a permanent dipole moment in the ground state and their maximum absorption is shorter than 532 nm. As for these molecules, the Kerr coefficient is negative, it indicates that N term dominates the Kerr effect.

On the other hand, DDMABI has a positive sign. As it is a non-centrosymmetric molecule, we can apply the two-level scheme to characterize its Kerr response. As measurements are carried out at wavelength shorter than the absorption maximum it should correspond to the rule that two-photon term is negative before crossing two-photon resonance. As the one-photon term is negative all the time, this should give an overall negative response. A positive value indicates that such a simple model cannot be used. The absorption spectrum of DDMABI shows multiple absorption bands close to each other that could contribute differently to 2PA processes. This will be further studied in spectral dependent measurements, as the main focus on this section is a comparison of various materials.

Observation 1: The first main conclusion from these results regards the correlation of 2PA effectwith the linear absorption at 532 nm. A somewhat linear trend between both parameters can be seen (see Figure 4.14). Also, TriDMABI fits in this trend although it has no permanent dipole moment in the ground state. This could indicate that its virtual state for 2PA transition is close to one-photon absorption.

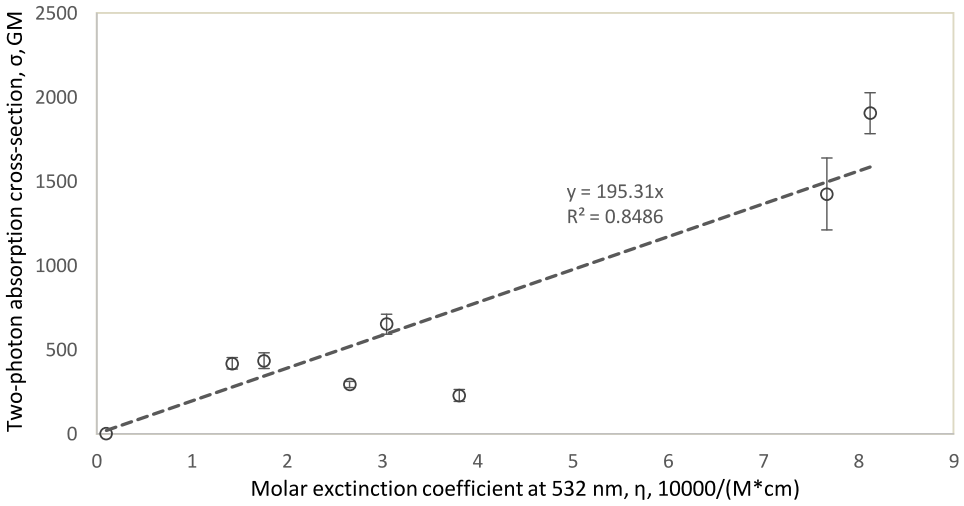

Figure 4.14: *Two-photon absorption cross-section at 1064 nm as function from the molar extinction coefficient at 532 nm.*

Observation 2: Next we will look at material group TPA, DMABI-dph, DiDMABI, and TriDMABI. This series of molecules represents how NLO properties change by increasing the ABI group number attached to TPA. Both 2PA and nonlinear-refractive cross-section is plotted as a function from the ABI group number in Figure 4.15. This figure shows that 2PA cross-section increases linearly with the number of ABI groups while nonlinear refractive cross-section increases quadratically with the number of ABI groups. This non-linear contribution could be through both number of ABI groups increasing the Dipolar contribution, and 2PA increasing corresponding two-photon term of Kerr effect. Both these terms increasing linearly with the number of branches lead to a quadratic increase in overall Kerr response.

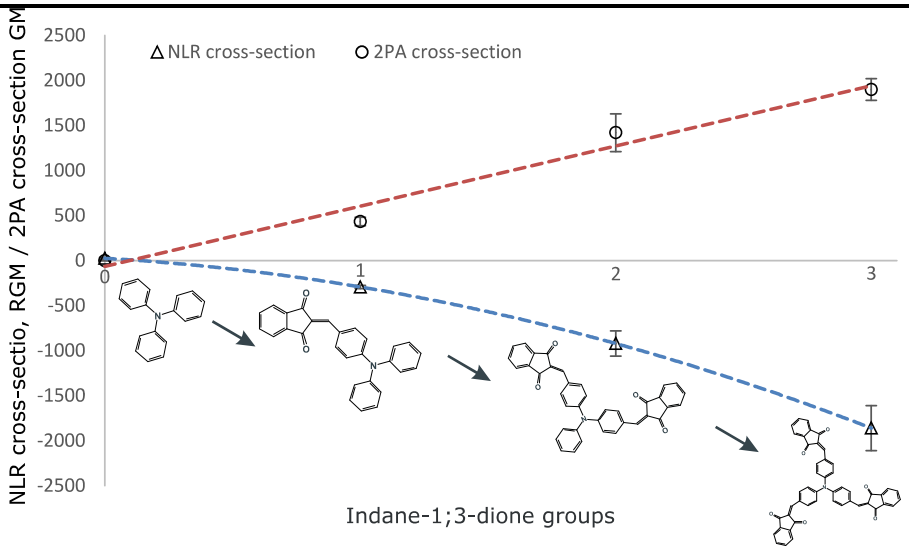

Figure 4.15: *Nonlinear refractive (NLR) cross-section and 2PA cross-section as functions of ABI groups.*

Observation 3: Lastly, when comparing ns and ps results for 2PA, it is evident that ns values are much larger (see Table 4.5). When looking at the difference between both values, it is around 10^3 that is close to the difference in laser pulse widths. Similar observations have been presented in the literature[171]. This indicates that 2PA scales with pulse width. During Z-scan calibration, we observed that the Kerr value for DMABI increases when comparing ns and ps measurements. If we look at the two-level model for molecule, the two-photon contribution to the Kerr effect is positive when measuring at a wavelength larger than 2PA resonance. As both 2PA values of various organic compounds and the Kerr effect of DMABI increased proportionally to pulse width (three orders of magnitude), this could be due to the two-photon term value increase for DMABI. This is also supported by polarisation measurements indicating that mainly electronic contribution is present during ns measurements compared to ps measurements. This was further studied by spectral measurements of 2PA and Kerr effect for DMABI.

Table 4.5: *Two-photon absorption comparison between ns and ps lasers*

Solute	$\beta_{2;ps}$, cm/W · 10^{-7}	$\beta_{2;ns}$, cm/W · 10^{-4}	$\sigma_{2PA;ps}$, GM	$\sigma_{2PA;ns}$, GM·10^6
DiDMABI	1.23±0.18	1.044±0.090	1420±210	3.23±0.28
TriDMABI	1.281±0.081	1.74±0.16	1900±120	5.41±0.51
tb-DMABI-Ju	0.365±0.024	0.480±0.029	293±19	1.491±0.090

*$\beta_{2;ps}$ – 2PA coefficient measured with 30 ps laser; $\sigma_{2PA;ps}$ – 2PA cross-section calculated from $\beta_{2;ps}$ values; $\beta_{2;ns}$ – 2PA coefficient measured with 8 ns laser; $\sigma_{2PA;ns}$ – 2PA cross-section calculated from $\beta_{2;ns}$ values.

4.2.2. Spectral measurements

To better understand if pulse duration influence on the Kerr effect is due to DMABI 2PA contribution to the Kerr effect additional spectral measurements for DMABI were carried out to study Kerr and 2PA effect spectral dispersion. This was done using a 15 ps tunable laser.

For DMABI the spectral measurements were carried out over a range from 630 to 1060 nm. Firstly let's look at 2PA results. The spectral dispersion of 2PA compared to linear absorption is shown in Figure 4.16. Here data is plotted as a function of photon energy in eV not wavelength for correct interpretation of results – a Gaussian distribution in energy scale converted to wavelength can show broadening that has no physical origins. To better compare results, linear absorption is plotted at half of the measured photon energy.

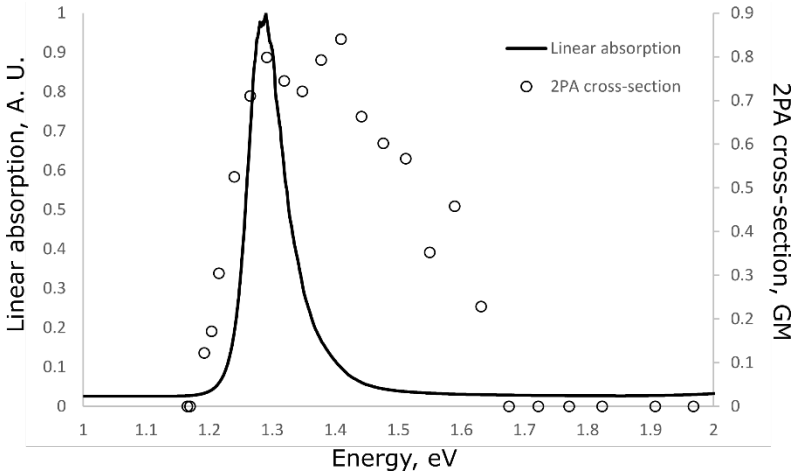

Figure. 4.16: *Two-photon absorption cross-sections spectral dispersion compared to linear absorption.*

2PA data indicates multiple peaks around the linear absorption spectrum. Here two main regions must be separated. One absorption peak can be identified around the linear absorption peak that is expected as non-centrosymmetric molecules do not have any special selection rules for one- and two- photon transitions. Two or more peaks at higher energies can be identified when looking at spectral data. These are transitions to vibrational coupled levels to the first excited state of DMABI. Although in the linear spectrum they are quite weak in the 2PA process they have a similar cross-section as a direct transition to an excited state. It has been previously reported that for non-centrosymmetric molecules the angle between transition dipole moment and difference between excited-state and ground-state dipole moments significantly influences the 2PA effect for a direct transition to an excited state. This could also be the case were such effects play a role.

Values of 2PA cross-section and nonlinear refraction cross-section are shown in Figure 4.17 for DAMBI. It can be seen that the Kerr effect changes its sign when approaching spectral diapasons where the 2PA effect can be observed – as observed for most ABI derivatives. Also, the tail of 2PA gives a positive contribution to the Kerr effect at larger wavelengths, explaining the increase of the Kerr effect with pulse length. Here we can return to the question about DDMABI that was the only ABI compound with a positive Kerr coefficient. An essential difference between DMABI and DDMABI is the second absorption peak for DDMABI at shorter wavelengths that can start to influence NLO spectral dispersion.

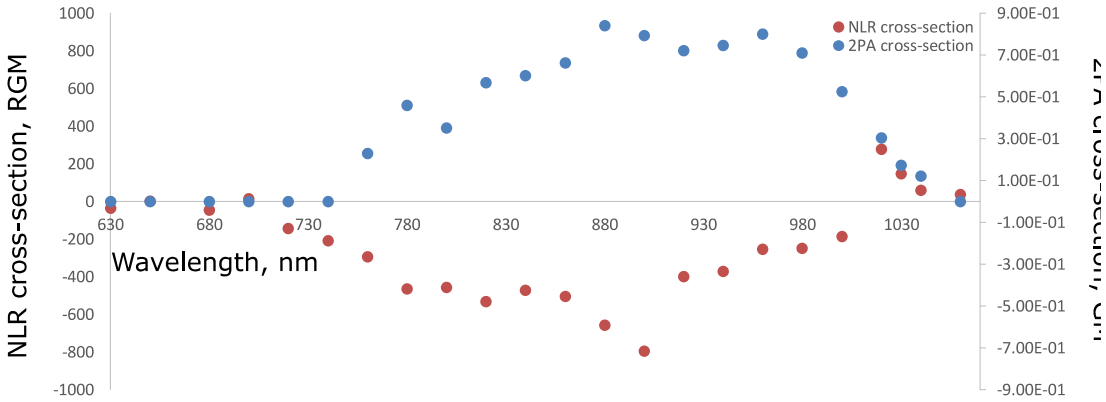

Figure 4.17: *Spectral dispersion of DMABI nonlinear refractive and two-photon absorption cross-sections spectral dispersions.*

4.2.3. TPA derivatives

Compounds: The next material group studied in this work was different TPA derivatives. This included materials with smaller or larger molecular groups attached to the TPA group. Structural forms as well as abbreviations for studied materials are shown in Figure 4.18. Only two of these compounds possessed any significant absorption at the visible range – TPA 7 and TPA 8. Normalized absorption spectrums are shown in Figure 4.18 with a maximum for TPA 7 – 24000 1/(M·cm) at 466 nm; TPA 8 – 18000 1/(M·cm) at 424 nm.

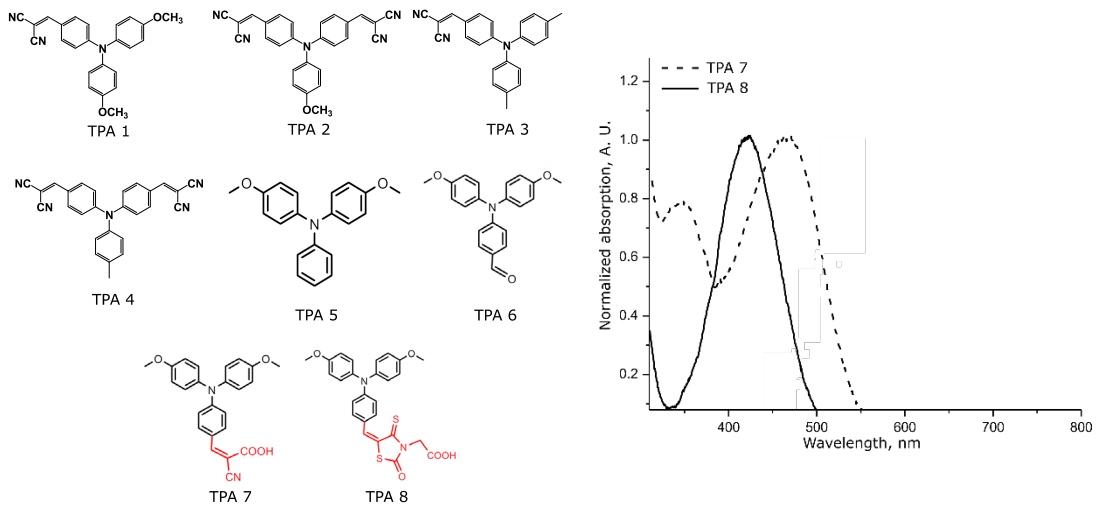

Figure 4.18: *Structural formulas and abbreviations of the TPA derivatives as well as absorption spectrums for TPA 7 and TPA 8.*

NLO results: Measured NLO values with 30 ps laser for all compounds are shown in Table 4.6. Only TPA 7 possessed any significant 2PA effect with a magnitude of $\alpha_2=(7.10\pm0.86)\cdot10^{-8}$ cm/W corresponding to $\sigma_{2PA}=592\pm72$ GM.

Table 4.6: *Nonlinear refractive index and its cross-section of TPA derivatives*

Solute	n_2, $cm^2/W \cdot 10^{-14}$	δ_{NLR}, RGM
Chloroform	0.201±0.014	0.294±0.021
Triphenylamine	8.6±2.9	25.9±8.7
TPA 1	11.19±0.95	52.5±4.5
TPA 2	19.7±3.0	104±16
TPA 3	21.3±2.1	91.5±9.0
TPA 4	13.4±1.8	67.8±9.1
TPA 5	10.6±2.3	39.8±8.6
TPA 6	24.9±3.5	102±14
TPA 7	-187±22	-920±110
TPA 8	-193±20	-1200±120

Firstly we will look at compounds TPA 1-4. These compounds can be divided into two groups – A-D structures (TPA 1 and TPA 3) and A-D-A structure (TPA 2 and TPA 4). For the first pair main alterations were made by strengthening the donor group with a methoxy group. Although this should increase the Kerr effect magnitude, experimental values contradict this. On the other hand, TPA 2 and TPA 4 followed very well the rule, that molecule with a stronger donor group had a larger Kerr effect value. A similar pattern can be observed with compounds TPA 5 and TPA 6 even further proving this rule. Two molecules that strongly differ from others were TPA 7 and TPA 8, with both possessing negative signs. They have more similarities with previously studied ABI derivatives as having a simpler acceptor/donor structure of D-A and having significant absorption in a visible range indicating possible 2PA contribution to the Kerr effect. These results will be further examined in the Experimental value comparison to the Quantum Chemical calculations section.

Observation 1: To explain these results in more detail we have looked at QCC results of spatial structures of TPA molecules. The essential difference was in the angle between either methyl (TPA 3) or methoxy (TPA 1) groups to the central NC_3 group. TPA 1 had an angle of 68^0, while TPA 3 had 63^0. We believe that this angle is the main reason behind differences in the Kerr effect, as it influences the electron flow between molecular groups. On the other hand QCC results for TPA 2 and TPA 4 (followed the rule that molecule with a stronger donor group had a larger Kerr effect value), the special structure showed that none of the phenyl rings were close to being in-plane with the central group (angels were between 85^0 and 80^0 degrees). This indicates that angles between molecular groups influence group conjugation and can influence how much the strength of separate molecule groups influence overall molecular properties.

4.2.4. BIT derivatives

Compounds: The last molecule group studied in this work was 2,6-bis(4-aminobenzylidene)-s-indacene-1,3,5,7-tetraones (BIT) derivatives. First reports of NLO properties of such

materials can be traced back to R. D. Breuker group[172] that presented novel material for NLO applications with high 2PA for optical limiting. In this work, specific derivatives of this base compound were studied that possessed stronger acceptor groups (dicyanomethylene), as well as 3-oxo-3-(2,2,2-triphenylalkoxy)propyl groups that allow forming higher-concentration homogeneous guest-host thin films to find more efficient materials for optical limiting applications. These molecules have a centrosymmetric structure of form D-A-D. Structures of studied compounds as well as abbreviations can be seen in Figure 4.19. BIT 0 represents the original compound studied by R. D. Breuker group. Absorption spectrums are shown in Figure 4.19. Absorption maximums for these compounds are compiled in Table 4.7.

Table 4.7: *Absorption maximum for BIT derivatives.*

Compound	λ, nm	η, 10^4/(M*cm)
BIT 0	578	196000
BT 1	547	200000
BIT 2	625	99000
BIT 3	704	76000
BIT 4	583	103000
BIT 5	638	130000

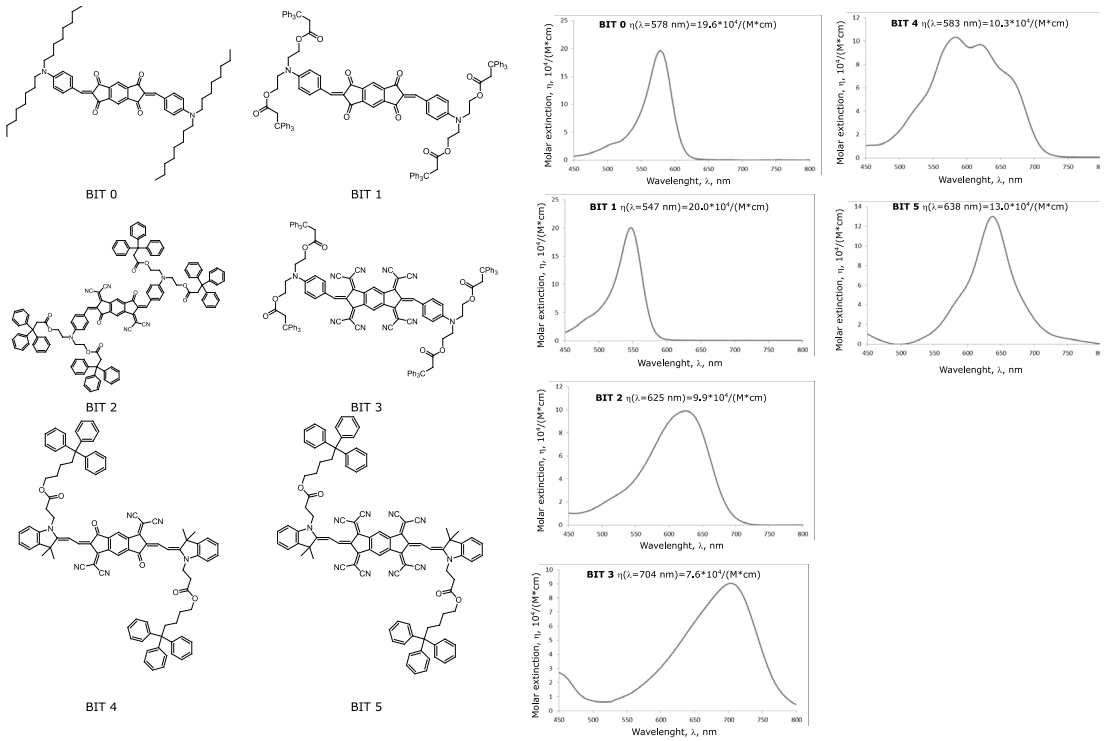

Figure 4.19: *Structures, abbreviations, and absorption spectrum of studied BIT derivatives.*

NLO results: Results of NLO measurements are compiled in Table 4.8.

Table 4.8: *Nonlinear optical values of BIT derivatives*

Solute	β_2, cm/W · 10^{-7}	σ_{2PA}, GM	n_2, cm^2/W · 10^{-13}	δ_{NLR}, RGM
BIT 0	3.66±0.95	6629±1721	-19.5±2.3	-2090±250
BIT 1	1.07±0.14	3846±523	-4.41±0.51	-940±110
BIT 2	2.99±0.31	11378±1182	19.47±0.73	4380±1600
BIT 3	1.09±0.17	4330±678	-8.4±1.1	-1980±260
BIT 4	2.53±0.24	7320±700	12.5±1.9	2140±320
BIT 5	1.09±0.10	3372±314	-5.4±1.4	-990±260

*$\beta_{2;ps}$ – 2PA coefficient measured with 30 ps laser; $\sigma_{2PA;ps}$ – 2PA cross-section calculated from $\beta_{2;ps}$ values; n_2 – Kerr coefficient measured with 30 ps; δ_{NLR} – Nonlinear refractive cross-section calculated from n_2 values.

Observation 1: BIT derivatives possess quiet large NLO coefficient values and can be used to study how well analytical models fit experimental measurements of 2PA and Kerr effect. In Figure 4.20 Z-scan measurement data for BIT 0 is shown for different concentration samples. Two things can be derived from this figure. First, measured NLO properties have a linear dependence on the concentration that fits the theory. Second, for larger *q* values general equation for the 2PA effect in Z-scan (equation (2.7)) needs to be used as simplified models (equation (2.8)) can lead to incorrect results indicating some kind of saturation effect. This can be observed as orange dots representing the simplified sum approach diverges from the linear trend for larger q values. For measurements where q<1 both models give the same values.

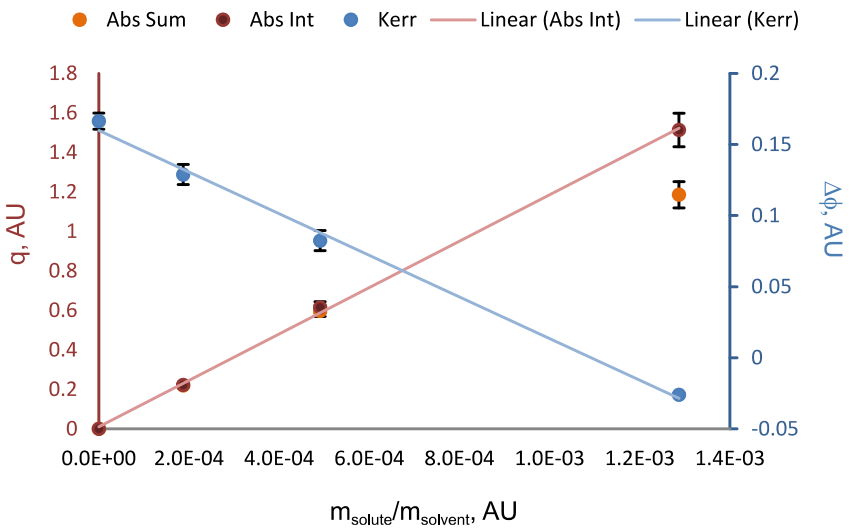

Figure 4.20: *ΔΦ (phase changes) and q (two-photon absorption induced absorption changes charecteraizing parameter) parameters for different BIT 0 concentration samples. Blue dots – ΔΦ values; Red dots – q values acquired with the general integral equation for open-aperture data (equation (2.6)); Orange dots – q values acquired with the simplified open-aperture model (equation (2.7)).*

Observation 2: When looking at the acquired values, the molecules can be separated into two groups – negative Kerr effect (BIT 0, BIT 1, BIT 3, and BIT 5) and positive Kerr effect (BIT 2 and

BIT 4). From a structural point of view, the main difference between these molecules is in the central acceptor group. While all of the BIT molecules have symmetry center molecules with a negative Kerr effect have a central acceptor group with mirror symmetry while positive molecules lack this symmetry. This could be an indication that third-order NLO properties for these molecules are not only influenced by dipolar properties of the whole molecule, but also by dipolar and quadrupole properties of separate groups – in this case, the central acceptor group. It is also important to emphasize that all molecules have their first absorption peak at a longer wavelength than 532 nm. All of these molecules can be considered centrosymmetric and needs to be studied using the three-level model. At first, this should mean that the Kerr effect is negative for all molecules as the two-photon term is negative at shorter wavelengths than resonance wavelength and positive for larger. On the other hand, centrosymmetric molecules cannot be excited to the same state through one-photon absorption and two-photon process, with exclusion being the vibrationally coupled levels. This means that the first peak of linear absorption cannot be used as an indicator of 2PA properties. There are two main ways to approach these results:

1. State that the sign indicates on which side of two-photon resonance the measurements were done. This would mean that for BIT 0, BIT 1, BIT 3 and BIT 5 2PA resonance is at a longer wavelength, while for BIT 2 and BIT 4 has a shorter wavelength. This conclusion can be made if we assume that one-photon contribution is negligible.
2. On the other hand, we can use equation (1.25) that showed that the sign of the Kerr effect for centrosymmetric molecule indicates which contribution – one- or two-photon – is dominant for the Kerr effect.

In reality, both of these statements are true and additional information regarding the spectral dispersion of 2PA is necessary for further analysis.

4.3. Experimental value comparison to Quantum Chemical calculations

Comparison between experimental and QCC values was done in two ways:

- From linear polarizability values acquired with the QCC molecular reorientation contribution was acquired and compared with experimental results,
- Experimental values of the Kerr coefficient was converted to second-order hyperpolarizability and compared to the QCC results.

First, let's will consider linear polarizability values acquired with the QCC and compare how well they predict the molecular reorientation contribution to refractive index changes. First, let's look at chloroform. QCC gave to different linear polarizability values for chloroform - $\alpha_{xx}=\alpha_{yy}$=56 Bohr^3, α_{zz}=29 Bohr^3. Gaussian 09 gives values in CGS system and converts linear polarizability from cm^3 to Bohr^3 where Bohr stands for the Bohr radius with 1 Bohr = $5.29\cdot10^{-9}$ cm. By using equation (1.46) molecular reorientation contribution was calculated to be n_2=$2.0\cdot10^{-15}$ cm^2/W which is close to the experimental value. As polarization-resolved measurements showed that for pure chloroform refractive index changes are mainly due to reorientation, this was expected and confirms the QCC precision for the case of chloroform.

Similar calculations were also carried out for DMABI. For DMABI linear polarizability had different values in each of the directions for which QCC gave the following values - α_{xx}=609 Bohr^3, α_{yy}=277 Bohr^3, and α_{zz}=111 Bohr^3. Molecular reorientation contribution was calculated to be n_2=2.0·10^{-13} cm^2/W. After separating electronic and molecular reorientation response by polarisation dependent measurement, the experimental value for molecular reorientation contribution to refractive index changes at 30 ps scale was n_2=(1.5±0.1)·10^{-13} cm^2/W. This value is smaller than the QCC result. This could be due to two factors: i) QCC is not able to preciously calculate linear polarizability; ii) Molecular reorientation effect has a longer time constant than 30 ps and has not reached an equilibrium state.

Next, a detailed comparison of experimental values and QCC values of the Kerr effect from Gaussian 09 will be compared. With QCC values of molecules second-order hyperpolarizability was calculated. Results for second-order hyperpolarizability, nonlinear refractive cross-section, 2PA cross-section, and the ratio of the nonlinear refractive cross-section to second-order hyperpolarizability are presented in Table 4.9.

Table 4.9: *Quantum Chemical calcualtion results for second-order hyperpolarizability*

Molecule	γ_{QQC}, 10^{-36} esu	δ_{NLR}, RGM	$\sigma_{2PA;ps}$, GM	$\delta_{NLR}/\gamma_{QQC}$, 10^{36} RGM/esu
Chloroform	2.4	0.294±0.021	-	0.12
DMABI	292.73	84.9±7.5	-	0.29
TPA	57.17	25.9±8.7	-	0.45
DMABI-dph	726.34	-293±18	434±47	0.40
DiDMABI	1701.67	-920±140	1420±210	0.54
TriDMABI	2562.50	-1860±250	1900±120	0.73
tb-DMABI-dph	765.66	-277±37	417±59	0.36
DMABI-Ju	346.18	271±41	228±37	0.78
tb-DMABI-Ju	387.31	-123±17	293±19	0.32
DMABIOH	136.93	840±110	-	6.18
DDMABI	466.82	135±21	652±60	0.29
TPA 1	520	52.5±4.5	-	0.10
TPA 2	1040	104±16	-	0.10
TPA 3	980	91.5±9.0	-	0.09
TPA 4	460	67.8±9.1	-	0.15
TPA 5	109	39.8±8.6	-	0.37
TPA 6	203	102±14	-	0.50
TPA 7	547	-920±110	592±72	1.68
TPA 8	1084	-1200±120	-	1.11
BIT 0	1973.22	-2090±250	6629±1721	1.06
BIT 1	1843.47	-940±110	3846±523	0.51
BIT 2	2507.21	4380±1600	11378±1182	1.75
BIT 3	2998.73	-1980±260	4330±678	0.66
BIT 4	1626.06	2140±320	7320±700	1.31
BIT 5	1814.43	990±260	3372±314	0.54

By looking at ratio value $\delta_{NLR}/\gamma_{QQC}$ the value various quite a lot from 0.12 to1.74 with a special exception of DMABI-OH of 6.18. One of the reasons for this large divergence from general values could be due to photochemical processes present during measurement. One of the explanations could be that the –OH group can be easily ionized with laser irradiation by removing a proton. By plotting the absolute ratio value $\delta_{NLR}/\gamma_{QQC}$ as a function from 2PA cross-section, a linear trend can be observed (see Figure 4.21). Red dots indicate compounds TPA 7 and TPA 8 that differ from the general trend. This could be due to aggregation effects as they can lead to an increase in the Kerr effect. Previously in the literature there have been observations that aggregation can lead to an increase in Kerr effect around 2 to 3 times[173] that correlates with over observed results. The rest of the molecules fits a linear trend.

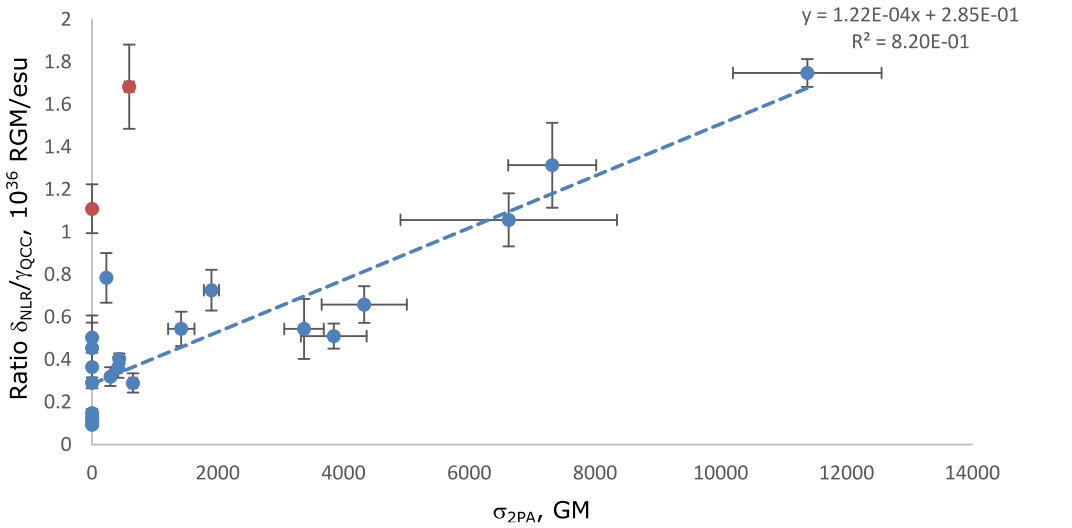

Figure 4.21: *Two-photon absorption influence on the ratio between experimental data and Quantum Chemical calculation results.*

To better understand this linear dependence, we will look in more detail of the ratio between experimental and QCC values for second-order hyperpolarizability. Firstly let's consider pure chloroform. In Table 4.10 values for experimental, QCC, and QCC values converted from convention IV to I of second-order hyperpolarizability are shown.

Table. 4.10: *Second-order hyperpolarizability of chloroform and DMABI*

Compound	γ_E, esu · 10^{-36}	$\gamma_{A,IV}$, esu · 10^{-36}	$\gamma_{A,I}$, esu · 10^{-36}
Chloroform	1.92±0.10	2.45	0.41
DMABI	3.07±0.69	2.97	0.495

Other literature works that have measured the Kerr effect for chloroform in fs range to determine fast component gives values in the range from 0.52-0.89·10^{-34} esu indicating larger values than QCC values. This also is a bit contradictory to experimental results that gave mainly reorientation contribution to refractive index changes. One of the reasons could be as through

this work, and also in literature, when describing experimental results – two main assumptions are made:

1. Solution is an isotropic media that gives specific relation to effective third-order susceptibility,
2. The induced effect is instantaneous compared to the laser pulse duration.

It could be possible that in this case both of these assumptions are broken and a new analytical model needs to be used to better fit experimental data. Some works show that when not taking into account laser pulse temporal shape, an underestimation of the Kerr effect can happen[174]. This could be an explanation for the discrepancy in electronic contributions.

Next, let's look at DMABI results in more detail. Nonlinear refractive index and second-order hyperpolarizability values for DMABI are also shown in Table 4.10. For DMABI the second-order hyperpolarizability values are quite close to each other, but when changing the Convention the values are an order apart. Both chloroform and DMABI show that it is very complicated to straightforwardly analyze the ratio between experimental and calculation results and all further analysis will only be carried based on the comparison between different molecules.

Now let's compare results for different organic components. DAMBI-OH, TPA 7, and TPA 8 were excluded as their NLO properties seem to be strongly influenced by other effects excluding the Kerr effect. Firstly comparison of second-order hyperpolarizability will be carried out for molecules that possessed no significant 2PA and one-photon absorption at half-wavelength and acquired value is closer to the non-resonant case. All molecules possessed positive Kerr coefficient and values are shown in Table 4.11.

Table 4.11: *Second-order hyperpolarizability values of materials with non-resonant Kerr effect*

Molecule	γ_E, 10^{-36} esu	γ_{QQC}, 10^{-36} esu	γ_E/γ_{QCC}	$\Delta\gamma$, 10-36 esu
Chloroform	1.92±0.10	2.4	0.80±0.06	-0.48±0.10
DMABI	783±69	292.73	2.67±0.24	490±69
Triphenylamine	169±57	57.17	2.9±1.0	112±57
TPA 1	2210±190	520	4.25±0.36	1690±190
TPA 2	3670±560	1040	3.53±0.54	2630±560
TPA 3	4000±390	980	4.08±0.40	3020±390
TPA 4	2030±270	460	4.4±0.59	1570±270
TPA 5	374±81	109	3.43±0.74	265±81
TPA 6	960±130	203	4.73±0.66	757±130

For these molecules, the ratio between experimental and QCC results is around 2.6-4.7 and seems indifferent to the absolute value of second-order hyperpolarizability (see Figure 4.22). When carrying out the transition between conventions IV to I, the QCC value decreases even further increasing the difference even further. This indicates that for this type of molecules the main problem between the correlation of QCC and experimental results is a coefficient by

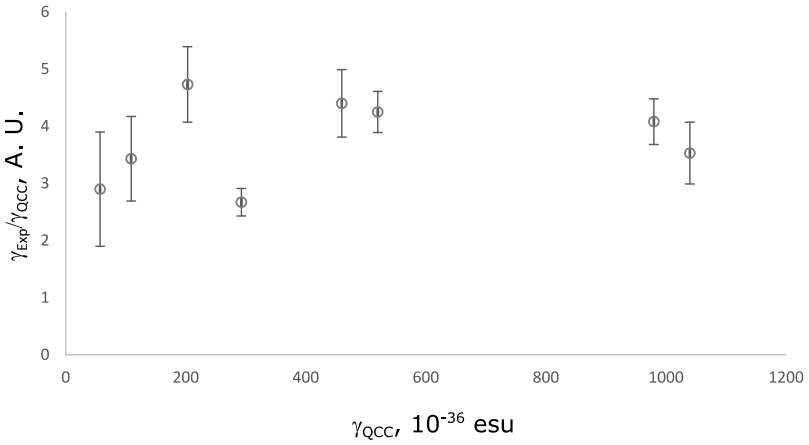

Figure. 4.22: *Ratio (experimental and Quantum Chemical calcualtion values of second-order hyperpolarizability) as a function from Quantum Chemical calcualtion values.*

which QCC values need to be multiplied. But more importantly, this shows that QCC values for these molecules can be used to estimate which molecules will have a larger Kerr response.

Next, let's consider molecules with pronounced 2PA effect and one-photon absorption at half-wavelength. In this case, a bigger focus will be given to the difference between experimental and QCC results compared to 2PA cross-section values. Second-order hyperpolarizability values for these molecules are shown in Table 4.12.

Table 4.12: *Second-order hyperpolarizability and two-photon absorption values of Two-photon absorption materials*

Molecule	γ_E, 10^{-36} esu	$\sigma_{2PA;ps}$, GM	γ_{QQC}, 10^{-36} esu	γ_E/γ_{QCC}	$\Delta\gamma$, 10^{-36} esu
DMABI-dph	-2700±160	434±47	726	3.72±0.22	3426±160
DiDMABI	-8500±1300	1420±210	1701	5.00±0.74	10201±1300
TriDMABI	-17100±2200	1900±120	2562	6.67±0.88	19662±2200
tb-DMABI-dph	-2560±340	417±59	766	3.34±0.44	3325±340
DMABI-Ju	-1770±260	228±37	346	5.11±0.76	2116±260
tb-DMABI-Ju	-1390±190	293±19	387	3.59±0.50	1777±190
DDMABI	1250±200	652±60	467	2.68±0.41	783±200
BIT 0	-28000±3400	6629±1721	1973	14.6±1.7	30899±3400
BIT 1	-13000±1500	3846±523	1843	7.09±0.82	14918±1500
BIT 2	60900±2300	11378±1182	2507	24.30±0.91	58429±2300
BIT 3	-27600±3600	4330±678	2999	9.12±1.2	30582±3600
BIT 4	29700±4500	7320±700	1626	18.2±2.7	28057±4500
BIT 5	-13600±3500	3372±314	1814	7.5±1.9	15382±3500

These results can be examined in two ways: i) ratio γ_E/γ_{QCC} value depending on the 2PA cross-section; ii) $\Delta\gamma$ value depending on the 2PA cross-section. These two types of correlations were carried out to better understand if 2PA influence can be accounted through either multiplying the QCC value by a specific coefficient that is proportional to 2PA magnitude or adding a shift

value to QCC value that is proportional to 2PA. The sign of experimental value was taken into account when calculating Δγ values. For ratio γ_E/γ_{QCC} the absolute value was used. Both correlations are shown in Figure 4.23. From these graphs it is evident that for molecules with a strong 2PA better correlation is between ratio γ_E/γ_{QCC} values and 2PA cross-section values.

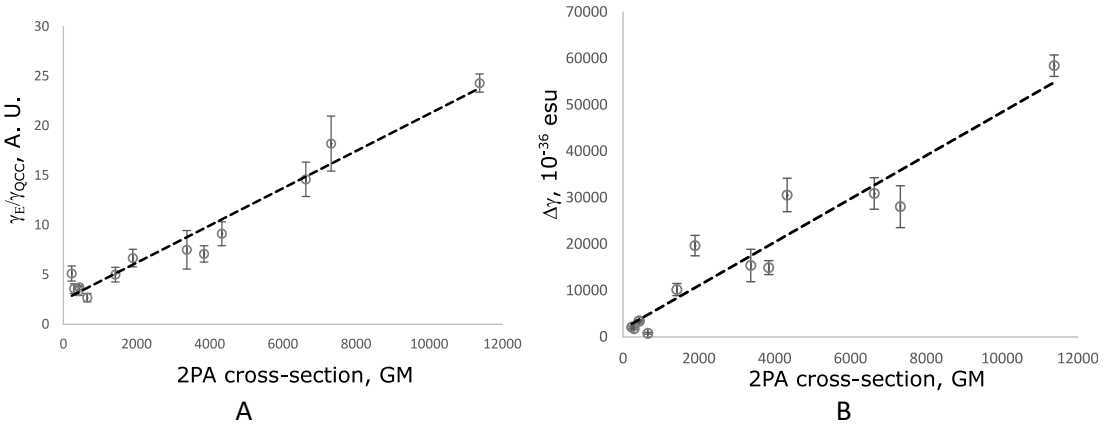

Figure 4.23: *A – Ratio of experimental and QCC values of second-order hyperpolarizability as a function from Two-photon absorption cross-section values. B – Difference between experimental and Quantum Chemical calculation values as a function from Two-photon absorption cross-section values.*

Comparing both molecule groups a distinctive difference can be observed:

- Molecules that do not possess any 2PA at irradiation wavelength and linear absorption at half-wavelength have a linear correlation between QCC values and experimental values, indicated by a scaling factor around 3.6±1,
- Molecules that possess 2PA irradiation wavelength and/or linear absorption at half-wavelength have a linear correlation between the ratio of experimental to QCC values and 2PA cross-section.

These conclusions can be used to further tune QCC methods to better predict experimental results and step towards material screening through QCC. It is important to stress again that here experimental value consists of both molecular reorientation and electronic contributions. For some compounds, molecular reorientation was evaluated through QCC results of linear polarizability. The QCC results for 2PA molecules are shown in Table 4.13. While the molecular reorientation contribution is quite significant for molecules with a small 2PA coefficient and respectively also Kerr coefficient values (ABI compounds excluding DiDMABI and TriDMABI), it becomes insignificant for larger ones. When taking into account QCC prediction of molecular reorientation to Kerr response average γ_E/γ_{QCC} scaling factor and its error for molecules with small Kerr values changes from 4.52±1.3 to 5.7±1.0 that is still in the limits of error of scaling factor. While this could be considered significant changes it is so only for lower values and does not explain the overall linear trend observed in Figure 4.23 A. There is one exception between these compounds – DDMABI. Here the main issue is that

DDMABI NLO response was influenced by two absorption peaks as discussed before, making this an exception.

Table 4.13: *Quantum Chemical calcualtion results for molecular reorientation contribution to refractive index changes*

Molecule	$n_{2;QCC/MR}$,$cm^2/W \cdot 10^{-12}$	$n_{2;Exp}$,$cm^2/W \cdot 10^{-12}$	$n_{2;QCC/MR}/n_{2;Exp}$
DMABI-Ju	0.19	-0.67±0.10	0.29
DMABI-dPh	0.154	-0.594±0.036	0.26
DiDMABI	0.21	-1.35±0.20	0.15
TriDMABI	0.17	-2.12±0.28	0.08
DDMABI	0.254	0.339±0.043	0.75
tB-DMABI-Ju	0.169	-0.261±0.036	0.34
tB-DMABI-dPh	0.143	-0.493±0.066	0.55

Conclusions

Here the main conclusions of this work will be presented. Conclusions will be divided into three parts – NLO measurement methods, NLO properties of organic materials, and experimental result comparison to QCC.

Methods: Regarding third-order NLO measurement methods two different methods were tested in this work – the Z-scan and the MZI. Both methods were tested with 8 ns and 30 ps 1064 nm lasers. By comparing both methods the following conclusions were made:

- *Z-scan* - a good general method for NLO measurements. The main limitation of the Z-scan method is measuring samples with large induced phase changes due to complicated analytical models. This is not an issue for general material studies as often low concentration samples are studied with weak NLO signals.
- *MZI - t*he main advantage of MZI is the simple analytical model for data fitting that can be used for small or large phase changes (around 3π). For phase changes larger than 3π the beam size variation starts to influence results. Also, MZI is hard to implement experimentally when short pulse lasers (ps scale) are used. Due to this, MZI is not the best method for Kerr effect studies where short pulse lasers are preferred but has its applicability in ns region measurements in a case when large phase change takes place, for example, photoisomerization in thin-films.

A more in-depth study of the Z-scan method was carried out to give general guidelines for correct Kerr effect evaluation with the main focus on separating molecular reorientation contribution from the electronic response of organic compounds when they are dissolved in chloroform. The main conclusions from this section were:

- In general ns laser pulse width should not be long enough to induce a thermal response from liquids with no significant linear absorption or 2PA at irradiation wavelength. But at higher pulse repetition rates this can happen due to accumulative thermo-optical effect and can overwhelm the Kerr effect. This holds up for pure organic solvents as well as for organic dyes dissolved in solvents. To be sure whether measured refractive index changes of organic dyes are due to Kerr or thermo-optical effect, polarisation dependent Z-scan measurements need to be implemented, especially for ns or longer pulse lasers,
- Polarisation resolved Z-scan measurements can be used to determine the ratio of molecular and electronic contributions to the Kerr effect. This is a simpler approach than measuring the Kerr effect at different pulse widths. While electronic response can be separated this way, a more complicated aspect is the separation of the nuclear response into libration and diffusive reorientation components and would demand pulse width dependent measurements to do this correctly.

Materials: Next a brief overview of conclusions from organic material measurements will be given.

- ABI derivatives: i) A correlation between linear absorption and 2PA cross-section was observed, indicating that the virtual state for 2PA transition and first excited state could be located close to each other; ii) 2PA effect increases when using lasers with longer pulse widths and scales proportionally to pulse width. A similar effect was observed for the Kerr effect in the case of DMABI that could be due to two-photon contribution to the Kerr effect increasing; iii) By increasing the ABI branch number attached to the TPA group 2PA effect increased linearly while the Kerr effect increased quadratically. This is because both dipolar and the two-photon contributions of the Kerr effect increased with the number of ABI groups.
- TPA derivatives – Angle between methyl or methoxy groups to central NC_3 group significantly influences the Kerr coefficient value. A smaller angle leads to a larger Kerr effect.
- BIT derivatives – These materials have large 2PA cross-sections indicating that they could be applicable for optical limiting in the infra-red region.

Experiment vs QCC: From the comparison of experimental values to QCC the main conclusions regarding organic materials were:

- Molecules that do not possess any 2PA at irradiation wavelength and linear absorption at half-wavelength have a linear correlation between scaling factor between experimental/QCC values and QCC values, indicated by a ratio of both values around 3.6±1.0,
- For that possess 2PA irradiation wavelength and/or linear absorption at half-wavelength scaling factor grows 2PA cross-section.
- Also, QCC results for molecular reorientation show, that this contribution is significant only for a molecule with small Kerr values ($\approx 2 \cdot 10^{-13}$ cm^2/W).

Thesis

- Separation of Kerr and thermo-optical contributions to refractive index changes by the Z-scan method can be done by polarisation and pulse repetition rate-dependent measurements. This can allow studying the Kerr effect using up to ns pulse width lasers.

- To correctly separate the electronic and the molecular contributions to the Kerr coefficient for organic chromophores dissolved in solvents polarization-resolved measurements must be used.

- When using Quantum Chemical calculations for predicting Kerr effect values for organic chromophores, molecular reorientation contribution can be calculated accurately from values of linear polarizability while a significant error for electronic contribution arises due to disregard of two-photon contribution.

References

1. Meyers, F. *et al.* Electric field modulated nonlinear optical properties of donor-acceptor polyenes: sum-over-states investigation of the relationship between molecular polarizabilities (alpha ,beta , and gamma) and bond length alternation. *Journal of the American Chemical Society B*, **116**, 10703–10714 (1994).

2. CISCO. Cisco Visual Networking Index: Forecast and Trends, 2017–2022. *https://www.cisco.com/c/en/us/solutions/collateral/service-provider/visual-networking-index-vni/white-paper-c11-741490.pdf* 1–38 (2019).

3. Franken, P. A., Hill, A. E., Peters, C. W. & Weinreich, G. Generation of optical harmonics. *Physical Review Journals*, **7**, 118–119 (1961).

4. Boyd, R. W. Nonlinear Optics. *Elsevier,* (2003).

5. Samoc, M. *et al.* Femtosecond Z-scan and degenerate four-wave mixing measurements of real and imaginary parts of the third-order nonlinearity of soluble conjugated polymers. *Journal of the Optical Society of America B*, **15**, 817 (1998).

6. Sheik-Bahae, M., Said, A. A., Wei, T.-H., Hagan, D. J. & Van Stryland, E. W. Sensitive measurement of optical nonlinearities using a single beam. *IEEE J. Quantum Electron.* **26**, 760–769 (1990).

7. Melhado, M. S., de Souza, T. G. B., Zilio, S. C., Barbano, E. C. & Misoguti, L. Discrimination between two distinct nonlinear effects by polarization-resolved Z-scan measurements. *Optics Express,* **28**, 3352 (2020).

8. Nitiss, E. *et al.* Review and comparison of experimental techniques used for determination of thin film electro-optic coefficients. *Physica status solidi (a) applications and materials science,* **212**, 1867–1879 (2015).

9. Miller, R. C. OPTICAL SECOND HARMONIC GENERATION IN PIEZOELECTRIC CRYSTALS. *Applied Physics Letters,* **5**, 17–19 (1964).

10. Mizrahi, V. & Shelton, D. P. Dispersion of Nonlinear Susceptibilities of Ar, N2, and O2 Measured and Compared. *Physical Review Letters,* **55**, 696–699 (1985).

11. Wynne, J. J. Optical third-order mixing in GaAs, Ge, Si, and InAs. *Physical Review,* **178**, 1295–1303 (1969).

12. Wynne, J. J. & Boyd, G. D. Study of optical difference mixing in Ge and Si using A CO2 gas laser. *Applied Physics Letters,* **12**, 191–192 (1968).

13. Rustagi, K. C. & Ducuing, J. Third-order optical polarizability of conjugated organic molecules. *Optics Communications,* **10**, 258–261 (1974).

14. Hermann, J. P., Ricard, D. & Ducuing, J. Optical nonlinearities in conjugated systems: β-carotene. *Applied Physics Letters,* **23**, 178–180 (1973).

15. Hermann, J. P. & Ducuing, J. Third-order polarizabilities of long-chain molecules. *Journal of Applied Physics,* **45**, 5100–5102 (1974).

16. Gorman, C. B. & Marder, S. R. An investigation of the interrelationships between linear

and nonlinear polarizabilities and bond-length alternation in conjugated organic molecules. *Proceedings of the National Academy of Sciences of the United States of America,* **90**, 11297–11301 (1993).

17. Zojer, E. Tuning the two-photon absorption response of quadrupolar organic molecules. *Journal of Chemical Physics*, **116**, 3646 (2002).

18. Webster, S. *et al.* Comparison of nonlinear absorption in three similar dyes: Polymethine, squaraine and tetraone. *Chemical Physics,* **348**, 143–151 (2008).

19. Fu, J. *et al.* Experimental and theoretical approaches to understanding two-photon absorption spectra in polymethine and squaraine molecules. *Journal of the Optical Society of America B,* **24**, 67 (2007).

20. Padilha, L. A. *et al.* Nonlinear absorption in a series of Donor–π–Acceptor cyanines with different conjugation lengths. *Journal of Materials Chemistry,* **19**, 7503 (2009).

21. Students, O. Optika. *Zvaigzne*, (1971).

22. Thompson, B. Characterization Techniques and Tabulations for Organic Nonlinear Optical Materials. *Routledge,* (2018).

23. Levine, B. F. & Bethea, C. G. Second and third order hyperpolarizabilities of organic molecules. *Journal of Chemical Physics,* **63**, 2666–2682 (1975).

24. Oudar, J. L. & Chemla, D. S. Hyperpolarizabilities of the nitroanilines and their relations to the excited state dipole moment. *Journal of Chemical Physics,* **66**, 2664–2668 (1977).

25. Ward, J. F. & New, G. H. C. Optical Third Harmonic Generation in Gases by a Focused Laser Beam. *Physical Review.* **185**, 57–72 (1969).

26. Orr, B. J. & Ward, J. F. Perturbation theory of the non-linear optical polarization of an isolated system. *Molecular Physics,* **20**, 513–526 (1971).

27. Kwak, C. H. & Kim, G. Y. Rigorous theory of molecular orientational nonlinear optics. *AIP Advances,* **5**, 017124, (2015).

28. Kajzar, F. & Messier, J. Third-harmonic generation in liquids. *Physical Review A,* **32**, 2352–2363 (1985).

29. Neher, D., Wolf, A., Bubeck, C. & Wegner, G. Third-harmonic generation in polyphenylacetylene: Exact determination of nonlinear optical susceptibilities in ultrathin films. *Chemical Physics Letters,* **163**, 116–122 (1989).

30. Bishop, D. M. Molecular vibrational and rotational motion in static and dynamic electric fields. *Reviews of Modern Physics,* **62**, 343–374 (1990).

31. Waite, J., Papadopoulos, M. G. & Nicolaides, C. A. Calculations of induced moments in large molecules. III. Polarizabilities and second hyperpolarizabilities of some aromatics. *Journal of Chemical Physics,* **77**, 2536–2539 (1982).

32. Boyd, R. W., Shi, Z. & De Leon, I. The third-order nonlinear optical susceptibility of gold. *Optics Communications,* **326**, 74–79 (2014).

33. Shelton, D. P. & Rice, J. E. Measurements and Calculations of the Hyperpolarizabilities of Atoms and Small Molecules in the Gas Phase. *Chemical Reviews,* **94**, 3–29 (1994).

34. Karna, S. P. & Yeates, A. T. Nonlinear Optical Materials: Theory and Modeling. *ACS Symposium Series*, **1**, 1–22 (1996).

35. Zhao, M. T., Singh, B. P. & Prasad, P. N. A systematic study of polarizability and microscopic third-order optical nonlinearity in thiophene oligomers. *Journal of Chemical Physics,* **89**, 5535–5541 (1988).

36. Kuzyk, M. G., Singer, K. D. & Stegeman, G. I. Theory of Molecular Nonlinear Optics. *Advances in Optics and Photonics,* **5**, 4 (2013).

37. Stegeman, G., Kuzyk, M., Papazoglou, D. G. & Tzortzakis, S. Off-resonance and non-resonant dispersion of Kerr nonlinearity for symmetric molecules [Invited]. *Optics Express,* **19**, 22486 (2011).

38. Kuzyk, M. G. Fundamental limits on third-order molecular susceptibilities. *Optics Letters,* **25**, 1183 (2000).

39. Lytel, R. Physics of the fundamental limits of nonlinear optics: a theoretical perspective [Invited]. *Journal of the American Chemical Society B,* **33**, E66 (2016).

40. Hutchings, D. C., Hagan, D. J. & Van Stryland, E. W. Kramers-Kronig relations in nonlinear optics. *Optical and Quantum Electronics volume*, **24**, 1–30 (1992).

41. del Coso, R. & Solis, J. Relation between nonlinear refractive index and third-order susceptibility in absorbing media. *Journal of the American Chemical Society B,* **21**, 640 (2004).

42. Ferdinandus, M. R. *et al.* Dual-arm Z-scan technique to extract dilute solute nonlinearities from solution measurements. *Optical Materials Express,* **2**, 1776 (2012).

43. Kivelson, D. & Madden, P. A. Light Scattering Studies of Molecular Liquids. *Annual Review of Physical Chemistrym,* **31**, 523–558 (1980).

44. Mcmorrow, D., Lotshaw, W. T. & Kenney-Wallace, G. A. Femtosecond Optical Kerr Studies on the Origin of the Nonlinear Responses in Simple Liquids. *IEEE Journal of Quantum Electronics*, **24**, 443–454 (1988).

45. Reichert, M. *et al.* Temporal, spectral, and polarization dependence of the nonlinear optical response of carbon disulfide. *Optica* **1**, 436 (2014).

46. Bucaro, J. A. & Litovitz, T. A. Rayleigh Scattering: Collisional Motions in Liquids. *Journal of Chemical Physics,* **54**, 3846–3853 (1971).

47. Cubeddu, R., Polloni, R., Sacchi, C. A. & Svelto, O. Self-phase modulation and 'rocking' of molecules in trapped filaments of light with picosecond pulses. *Physical Review A,* **2**, 1955–1963 (1970).

48. Close, D. H. *et al.* 8A2—The Self-Focusing of Light of Different Polarizations. *IEEE Journal of Quantum Electronics*, **2**, 553–557 (1966).

49. Shelton, D. P. Hyperpolarizability dispersion measured for CO_2. *Journal of Chemical Physics,* **85**, 4234–4239 (1986).

50. Fernandez, R. N. & Shelton, D. P. Hyperpolarizability dispersion measured for CS 2 vapor. *Journal of the American Chemical Society B,* **37**, 1769 (2020).

51. Bishop, D. M., Luis, J. M. & Kirtman, B. Additional compact formulas for vibrational dynamic dipole polarizabilities and hyperpolarizabilities. *Journal of Chemical Physics,* **108**, 10013–10017 (1998).

52. Kielich, S. Optical second-harmonic generation by electrically polarized isotropic media. *IEEE Journal of Quantum Electron,* **5**, 562–568 (1969).

53. Zhao, P., Reichert, M., Benis, S., Hagan, D. J. & Van Stryland, E. W. Temporal and polarization dependence of the nonlinear optical response of solvents. *Optica,* **5**, 583 (2018).

54. Ajami, A. *et al.* Evidence of concentration dependence of the two-photon absorption cross section: Determining the "true" cross section value. *Optical Materials,* **47**, 524–529 (2015).

55. Udayakumar, D. *et al.* Third-order nonlinear optical studies of newly synthesized polyoxadiazoles containing 3,4-dialkoxythiophenes. *Chemical Physics,* **331**, 125–130 (2006).

56. Tutt, L. W. & Boggess, T. F. A review of optical limiting mechanisms and devices using organics, fullerenes, semiconductors and other materials. *Progress in Quantum Electronics,* **17**, 299–338 (1993).

57. Shetty, T. C. S. *et al.* Structural and optical properties of a new organic crystal 3-(2-chloro-5-(trifluoromethyl) phenyl)-1-(3,4-dimethoxyphenyl)prop-2-en-1-one for nonlinear optical applications. *Materials Technology,* **32**, 140–147 (2017).

58. Quan, C. *et al.* Transition from saturable absorption to reverse saturable absorption in MoTe2 nano-films with thickness and pump intensity. *Applied Surface Science,* **457**, 115–120 (2018).

59. Saad, N. A., Dar, M. H., Ramya, E., Naraharisetty, S. R. G. & Narayana Rao, D. Saturable and reverse saturable absorption of a Cu2O–Ag nanoheterostructure. *Journal of Materials Science,* **54**, 188–199 (2019).

60. Roy, S. & Yadav, C. Femtosecond all-optical parallel logic gates based on tunable saturable to reverse saturable absorption in graphene-oxide thin films. *Applied Physics Letters,* **103**, 241113 (2013).

61. Weaire, D., Wherrett, B. S., Miller, D. A. B. & Smith, S. D. Effect of low-power nonlinear refraction on laser-beam propagation in InSb. *Optics Letters,* **4**, 331 (1979).

62. Wang, C. C. Empirical relation between the linear and the third-order nonlinear optical susceptibilities. *Physical Review B,* **2**, 2045–2048 (1970).

63. Bassani, F. & Lucarini, V. General properties of optical harmonic generation from a simple oscillator model. *Il Nuovo Cimento D,* **20**, 1117–1125 (1998).

64. Hu, B. Y. Kramers–Kronig in two lines. *American Journal of Physics,* **57**, 821–821 (1989).

65. Sharnoff, M. Validity Conditions for the Kramers-Kronig Relations. *American Journal of Physics,* **32**, 40–44 (1964).

66. Soh, D. B. S., Hamerly, R. & Mabuchi, H. Comprehensive analysis of the optical Kerr coefficient of graphene. *Physical Review A* **94**, 023845 (2016).

67. Brée, C., Demircan, A. & Steinmeyer, G. Kramers-Kronig relations and high-order nonlinear susceptibilities. *Physical Review A* **85**, 033806 (2012).

68. Boyd, G. D. & Kleinman, D. A. Parametric interaction of focused Gaussian light beams. *Journal of Applied Physics,* **39**, 3597–3639 (1968).

69. Kleinman, D. A. & Miller, R. C. Dependence of second-harmonic generation on the position of the focus. *Physical Review,* **148**, 302–312 (1966).

70. Peterson, G. E., Ballman, A. A., Lenzo, P. V. & Bridenbaugh, P. M. Electro-optic properties of LiNbO3. *Applied Physics Letters,* **5**, 62–64 (1964).

71. Boyd, G. D., Miller, R. C., Nassau, K., Bond, W. L. & Savage, A. LiNbO3: An efficient phase matchable nonlinear optical material. *Applied Physics Letters,*. **5**, 234–236 (1964).

72. Yamada, M., Nada, N., Saitoh, M. & Watanabe, K. First-order quasi-phase matched LiNbO3 waveguide periodically poled by applying an external field for efficient blue second-harmonic generation. *Applied Physics Letters,* **62**, 435–436 (1993).

73. Minakata, M. LiNbO3 optical waveguide devices. *Electronics and Communications in Japan (Part II: Electronics),* **77**, 37–51 (1994).

74. Sheik-Bahae, M., Hagan, D. J. & Van Stryland, E. W. Dispersion and band-gap scaling of the electronic Kerr effect in solids associated with two-photon absorption. *Physical Review Letters,* **65**, 96–99 (1990).

75. Hendry, E., Hale, P. J., Moger, J., Savchenko, a. K. & Mikhailov, S. a. Coherent Nonlinear Optical Response of Graphene. *Physical Review Letters,* **105**, 097401 (2010).

76. Zhang, H. *et al.* Z-scan measurement of the nonlinear refractive index of graphene. *Optics Letters,* **37**, 1856 (2012).

77. Sun, Z. *et al.* Graphene mode-locked ultrafast laser. *ACS Nano,* **4**, 803–810 (2010).

78. Phare, C. T., Daniel Lee, Y.-H., Cardenas, J. & Lipson, M. Graphene electro-optic modulator with 30 GHz bandwidth. *Nature Photonics* **9**, 511–514 (2015).

79. Li, W. *et al.* Ultrafast All-Optical Graphene Modulator. *Nano Letters,* **14**, 955–959 (2014).

80. Bikorimana, S. *et al.* Nonlinear optical responses in two-dimensional transition metal dichalcogenide multilayer: WS_2, WSe_2, MoS_2 and $Mo_{0.5}W_{0.5}S_2$. *Optics Express* **24**, 20685 (2016).

81. Fu, X., Qian, J., Qiao, X., Tan, P. & Peng, Z. Nonlinear saturable absorption of vertically stood WS_2 nanoplates. *Optics Letters,* **39**, 6450 (2014).

82. Wang, K. *et al.* Ultrafast Saturable Absorption of Two-Dimensional MoS_2 Nanosheets. *ACS Nano,* **7**, 9260–9267 (2013).

83. Zhang, H. *et al.* Molybdenum disulfide (MoS_2) as a broadband saturable absorber for ultra-fast photonics. *Optics Express,* **22**, 7249 (2014).

84. Zheng, X. *et al.* Z-scan measurement of the nonlinear refractive index of monolayer WS_2. *Optics Express,* **23**, 15616 (2015).

85. Luo, Z. *et al.* Two-dimensional material-based saturable absorbers: towards compact visible-wavelength all-fiber pulsed lasers. *Nanoscale,* **8**, 1066–1072 (2016).

86. Liang, G. *et al.* Optical limiting properties of a few-layer MoS_2/PMMA composite under excitation of ultrafast laser pulses. *Journal of Materials Chemistry C,* **7**, 495–502 (2019).

87. Gu, B. *et al.* Molecular nonlinear optics: recent advances and applications. *Advances in Optics and Photonics,* **8**, 328 (2016).

88. Mingabudinova, L. R., Vinogradov, V. V., Milichko, V. A., Hey-Hawkins, E. & Vinogradov, A. V. Metal-organic frameworks as competitive materials for non-linear optics. *Chemical Society Reviews,* **45**, 5408–5431 (2016).

89. Guloy, A. M., Tang, Z., Miranda, P. B. & Srdanov, V. I. A New Luminescent Organic–Inorganic Hybrid Compound with Large Optical Nonlinearity. *Advanced Materials,* **13**, 833–837 (2001).

90. Ni, B. *et al.* Tailoring the Linear and Second-Order Nonlinear Optical Responses of the Titanium-MIL-125 Metal–Organic Framework through Ligand Functionalization: A First Principles Study. *Journal of Physical Chemistry C,* **123**, 653–664 (2019).

91. Babaeian, M. *et al.* Nonlinear optical properties of chalcogenide hybrid inorganic/organic polymers (CHIPs) using the Z-scan technique. *Optical Materials Express,* **8**, 2510 (2018).

92. Ticha, H. & Tichy, L. Semiempirical relation between non-linear susceptibility (refractive index), linear refractive index and optical gap and its application to amorphous chalcogenides. *Journal of Optoelectronics and Advanced Materials*, **4**, 381–386 (2002).

93. Noginov, M. A. *et al.* Enhancement of surface plasmons in an Ag aggregate by optical gain in a dielectric medium. *Optics Letters,* **31**, 3022 (2006).

94. Falamas, A., Tosa, V. & Farcau, C. Hybrid architectures made of nonlinear-active and metal nanostructures for plasmon-enhanced harmonic generation. *Optical Materials,* **88**, 653–666 (2019).

95. Hamanaka, Y., Hayashi, N., Nakamura, A. & Omi, S. Dispersion of third-order nonlinear optical susceptibility of silver nanocrystal-glass composites. *Journal of Luminescence,* **87**–**89**, 859–861 (2000).

96. Sivapalan, S. T. *et al.* Off-resonant two-photon absorption cross-section enhancement of an organic chromophore on gold nanorods. *The Journal of Physical Chemistry Letters,* **4**, 749–752 (2013).

97. Walters, G. *et al.* Two-Photon Absorption in Organometallic Bromide Perovskites. *ACS Nano,* **9**, 9340–9346 (2015).

98. Stoumpos, C. C. *et al.* Hybrid germanium iodide perovskite semiconductors: Active lone pairs, structural distortions, direct and indirect energy gaps, and strong nonlinear optical properties. *Journal of the American Chemical Society,* **137**, 6804–6819 (2015).

99. Geng, F. J. *et al.* Perovskite-type organic-inorganic hybrid NLO switches tuned by guest cations. *Journal of Materials Chemistry C,* **5**, 1529–1536 (2017).

100. Mushtaq, A., Kushavah, D., Ghosh, S. & Pal, S. K. Nonlinear optical properties of benzylamine lead(II) bromide perovskite microdisks in femtosecond regime. *Applied Physics Letters,* **114**, (2019).

101. Yuan, C. *et al.* Chiral Lead Halide Perovskite Nanowires for Second-Order Nonlinear Optics. *Nano Letters,* **18**, 5411–5417 (2018).

102. Litchinitser, N. M. & Sun, J. Optical meta-atoms: Going nonlinear. *Science,* **350**, 1033–1034 (2015).

103. Suchowski, H. *et al.* Phase mismatch-free nonlinear propagation in optical zero-index materials. *Science,* **342**, 1223–1226 (2013).

104. Popov, A. K., Shalaev, M. I., Myslivets, S. A., Slabko, V. V. & Nefedov, I. S. Enhancing coherent nonlinear-optical processes in nonmagnetic backward-wave materials. *Applied Physics A,* **109**, 835–840 (2012).

105. Nicholls, L. H. *et al.* Designer photonic dynamics by using non-uniform electron temperature distribution for on-demand all-optical switching times. *Nature Communications,* **10**, (2019).

106. Lapine, M., Shadrivov, I. V. & Kivshar, Y. S. Colloquium: Nonlinear metamaterials. *Reviews of Modern Physics,* **86**, 1093–1123 (2014).

107. O'Brien, K. *et al.* Predicting nonlinear properties of metamaterials from the linear response. *Nature Materials,* **14**, 379–383 (2015).

108. Hales, J. M. *et al.* Design of Organic Chromophores for All-Optical Signal Processing Applications. *Chemistry of Materials,* **26**, 549–560 (2014).

109. Padilha, L. A. *et al.* Nonlinear absorption in a series of Donor–π–Acceptor cyanines with different conjugation lengths. *Journal of Materials Chemistry,* **19**, 7503 (2009).

110. Belfield, K. D. *et al.* Synthesis, Characterization, and Optical Properties of New Two-Photon-Absorbing Fluorene Derivatives. *Chemistry of Materials,* **16**, 4634–4641 (2004).

111. Scherer, D. *et al.* Two-photon states in squaraine monomers and oligomers. *Chemical Physics,* **279**, 179–207 (2002).

112. Fu, J. *et al.* Molecular structure—two-photon absorption property relations in polymethine dyes. *Journal of the Optical Society of America B*, **24**, 56 (2007).

113. Fu, J. *et al.* Two-photon anisotropy: Analytical description and molecular modeling for symmetrical and asymmetrical organic dyes. *Chemical Physic,* **321**, 257–268 (2006).

114. Pawlicki, M., Collins, H. A., Denning, R. G. & Anderson, H. L. Two-Photon Absorption and the Design of Two-Photon Dyes. *Angewandte Chemie International Edition,* **48**, 3244–3266 (2009).

115. Boudebs, G., Sanchez, F., Duverger, C. & Boulard, B. Improvement of Mach-Zehnder interferometry technique for third-order susceptibility measurement. *Optics Communications*, **199**, 257–265 (2001).

116. Boudebs, G., Chis, M. & Phu, X. N. Third-order susceptibility measurement by a new Mach-Zehnder interferometry technique. *Journal of the Optical Society of America B*, **18**, 623 (2001).

117. Boudebs, G., Sanchez, F., Troles, J. & Smektala, F. Nonlinear optical properties of chalcogenide glasses: Comparison between Mach-Zehnder interferometry and Z-scan techniques. *Optics Communications,* **199**, 425–433 (2001).

118. Xia, T., Hagan, D. J., Sheik-Bahae, M. & Van Stryland, E. W. Eclipsing Z-scan measurement of λ/10^4 wave-front distortion. *Optics Letters,* **19**, 317 (1994).

119. Marcano, A., Loper, C. & Melikechi, N. Pump–probe mode-mismatched thermal-lens Z scan. *Journal of the Optical Society of America B,* **19**, 119 (2002).

120. Ma, H., Gomes, A. S. L. & de Araujo, C. B. Measurements of nondegenerate optical nonlinearity using a two-color single beam method. *Applied Physics Letters,* **59**, 2666–2668 (1991).

121. Chapple, P. B., Staromlynska, J., Hermann, J. A., Mckay, T. J. & Mcduff, R. G. Single-Beam Z-Scan: Measurement Techniques and Analysis. *Journal of Nonlinear Optical Physics & Materials,* **06**, 251–293 (1997).

122. Pálfalvi, L., Tóth, B. C., Almási, G., Fülöp, J. A. & Hebling, J. A general Z-scan theory. *Applied Physics B,* **97**, 679–685 (2009).

123. Gaur, A. *et al.* Study of transmittance dependence closed-aperture Z-scan curves in the materials with nonlinear refraction and strong absorption. *Optik,* **123**, 1583–1587 (2012).

124. Liu, X., Guo, S., Wang, H. & Hou, L. Theoretical study on the closed-aperture Z-scan curves in the materials with nonlinear refraction and strong nonlinear absorption. *Optics Communications,* **197**, 431–437 (2001).

125. Falconieri, M. Thermo-optical effects in Z -scan measurements using high-repetition-rate lasers. *Journal of Optics A: Pure and Applied Optics,* **1**, 662–667 (1999).

126. DeSalvo, R., Sheik-Bahae, M., Said, A. A., Hagan, D. J. & Van Stryland, E. W. Z-scan measurements of the anisotropy of nonlinear refraction and absorption in crystals. *Optics Letters,* **18**, 194 (1993).

127. Liu, Z.-B., Yan, X.-Q., Tian, J.-G., Zhou, W.-Y. & Zang, W.-P. Nonlinear ellipse rotation modified Z-scan measurements of third-order nonlinear susceptibility tensor. *Optics Express* **15**, 13351 (2007).

128. Yan, X.-Q., Liu, Z.-B., Zhang, X.-L., Zhou, W.-Y. & Tian, J.-G. Polarization dependence of Z-scan measurement: theory and experiment. *Optics Express,* **17**, 6397 (2009).

129. Miguez, M. L., De Souza, T. G. B., Barbano, E. C., Zilio, S. C. & Misoguti, L. Measurement of third-order nonlinearities in selected solvents as a function of the pulse width. *Optics Express,* **25**, 3553 (2017).

130. Mohan, P. D. & Dhar, R. Polarization-dependent Z-scan characterization for optical nonlinearity in pyran dye. *Laser Physics,* **23**, (2013).

131. Liang, J., Zhao, H., Zhou, X., Wang, H. & Z-scan, A. S. Polarization-dependent effects of refractive index change associated with photoisomerization investigated with Z-scan technique. *Journal of Applied Physics,* **101**, 4–7 (2007).

132. Couris, S. *et al.* An experimental investigation of the nonlinear refractive index (n 2) of

carbon disulfide and toluene by spectral shearing interferometry and z-scan techniques. *Chemical Physics Letters,* **369**, 318–324 (2003).

133. Ganeev, R. A. *et al.* Nonlinear refraction in CS_2. *Applied Physics B,*. **78**, 433–438 (2004).

134. Wickremasinghe, N., Wang, X., Schmitzer, H. & Wagner, H. P. Eliminating thermal effects in z-scan measurements of thin PTCDA films. *Optics Express,* **22**, 23955–64 (2014).

135. Kamada, K., Matsunaga, K., Yoshino, A. & Ohta, K. Two-photon-absorption-induced accumulated thermal effect on femtosecond Z-scan experiments studied with time-resolved thermal-lens spectrometry and its simulation. *Journal of the Optical Society of America B,* **20**, 529 (2003).

136. Lin, Q. *et al.* Dispersion of silicon nonlinearities in the near infrared region. *Applied Physics Letters,* **91**, 2–4 (2007).

137. Marble, C. B. *et al.* Z-scan measurements of water from 1150 to 1400 nm. *Optics Letters,* **43**, 4196 (2018).

138. Gaur, A., Syed, H., Yendeti, B. & Soma, V. R. Experimental evidence of two-photon absorption and its saturation in malachite green oxalate: a femtosecond Z-scan study. *Journal of the Optical Society of America B,* **35**, 2906 (2018).

139. Gu, B., Ji, W., Huang, X. Q., Patil, P. S. & Dharmaprakash, S. M. Concentration-dependent two-photon absorption and subsequent excited-state absorption in 4-methoxy-2-nitroaniline. *Journal of Applied Physics,* **106**, 2–5 (2009).

140. Elim, H. I. *et al.* Large concentration-dependent nonlinear optical responses of starburst diphenylaminofluorenocarbonyl methano[60]fullerene pentads. *Journal of Materials Chemistry.* **17**, 1826 (2007).

141. Mian, S. M., Taheri, B. & Wicksted, J. P. Effects of beam ellipticity on Z-scan measurements. *Journal of the Optical Society of America B*, **13**, 856 (1996).

142. Zhao, W. & Palffy-Muhoray, P. Z-scan measurement of χ(3) using top-hat beams. *Applied Physics Letters,* **65**, 673–675 (1994).

143. Gu, B. *et al.* Determinations of third- and fifth-order nonlinearities by the use of the top-hat-beam Z scan: theory and experiment. *Journal of the Optical Society of America B*, **22**, 446 (2005).

144. Hughes, S. & Burzler, J. M. Theory of Z-scan measurements using Gaussian-Bessel beams. *Physical Review A,* **56**, R1103–R1106 (1997).

145. Rhee, B. K., Byun, J. S. & Van Stryland, E. W. Z scan using circularly symmetric beams. *Journal of the Optical Society of America B,* **13**, 2720 (1996).

146. Abrams, R. L. & Lind, R. C. Degenerate four-wave mixing in absorbing media. *Optics Letters,* **2**, 94 (1978).

147. Jain, R. K., Klein, M. B. & Lind, R. C. High-efficiency degenerate four-wave mixing of 106-μm radiation in silicon. *Optics Letters,* **4**, 328 (1979).

148. Jain, R. K. & Lind, R. C. Degenerate four-wave mixing in semiconductor-doped glasses. *Journal of the Optical Society of America,* **73**, 647 (1983).

149. Yariv, A. & Pepper, D. M. Amplified reflection, phase conjugation, and oscillation in degenerate four-wave mixing. *Optics Letters,* **1**, 16 (1977).

150. Rao, S. V. *et al.* Studies of third-order optical nonlinearity and nonlinear absorption in tetra tolyl porphyrins using degenerate four wave mixing and Z-scan. *Optics Communications,* **182**, 255–264 (2000).

151. Frisch, M. J. *et al.* Gaussian 09, Revision D.01. *Gaussian Inc., Wallingfor CT* (2016).

152. Frisch, M. J. *et al.* Gaussian 03, Revision C.02. *Gaussian Inc., Wallingfor CT.* (2004).

153. Aidas, K. *et al.* The Dalton quantum chemistry program system. *WIREs Computational Molecular Science,* **4**, 269–284 (2014).

154. McCormick, T. M. *et al.* Conjugated polymers: Evaluating DFT methods for more accurate orbital energy modeling. *Macromolecules,* **46**, 3879–3886 (2013).

155. Pir, H., Günay, N., Avci, D. & Atalay, Y. Molecular structure, vibrational spectra, NLO and NBO analysis of bis(8-oxy-1-methylquinolinium) hydroiodide. *Spectrochimica Acta Part A,* **96**, 916–924 (2012).

156. Sathya, K., Dhamodharan, P. & Dhandapani, M. Computational, spectral and structural studies of a new non linear optical crystal: 2-hydroxy pyridinium 3,5-dinitrobenzoate. *Journal of Molecular Structure,* **1130**, 414–424 (2017).

157. Liu, H., Li, G. & Hu, C. Selective ring C - H bonds activation of toluene over Fe/activated carbon catalyst. *Journal of Molecular Catalysis A: Chemical,* **377**, 143–153 (2013).

158. Ma, Z. *et al.* Synthesis and characterization of benzodithiophene-isoindigo polymers for solar cells. *Journal of Materials Chemistry,* **22**, 2306–2314 (2012).

159. Pastore, M., Mosconi, E., De Angelis, F. & Grätzel, M. A computational investigation of organic dyes for dye-sensitized solar cells: Benchmark, strategies, and open issues. *The Journal of Physical Chemistry C,* **114**, 7205–7212 (2010).

160. Marcano, E., Squitieri, E., Murgich, J. & Soscún, H. Theoretical investigation of the static (dynamic) polarizability and second hyperpolarizability of DAAD quadrupolar push–pull molecules. A comparison among HF (TD-HF), DFT (TD-B3LYP), and MP2 (TD-MP2) methods. *Computational and Theoretical Chemistry,* **985**, 72–79 (2012).

161. Bulik, I. W. *et al.* Performance of density functional theory in computing nonresonant vibrational (hyper)polarizabilities. *Journal of Computational Chemistry,* **34**, 1775–1784 (2013).

162. Limacher, P. A., Mikkelsen, K. V. & Lüthi, H. P. On the accurate calculation of polarizabilities and second hyperpolarizabilities of polyacetylene oligomer chains using the CAM-B3LYP density functional. *Journal of Chemical Physics,* **130**, (2009).

163. Lu, S.-I. On the performance of range-separated hybrid in computations of dynamic quadratic polarizability of solution-phase organic molecules: a comparison to MP2(Full) calculation. *Theoretical Chemistry Accounts,* **134**, 1589 (2015).

164. Avramopoulos, A., Otero, N., Reis, H., Karamanis, P. & Papadopoulos, M. G. A computational study of photonic materials based on Ni bis(dithiolene) fused with benzene, possessing gigantic second hyperpolarizabilities. *Journal of Materials Chemistry C,* **6**, 91–110 (2018).

165. Mennucci, B. *et al.* Polarizable continuum model (PCM) calculations of solvent effects on optical rotations of chiral molecules. *The Journal of Physical Chemistry A,* **106**, 6102–6113 (2002).

166. Samoc, A. Dispersion of refractive properties of solvents: Chloroform, toluene, benzene, and carbon disulfide in ultraviolet, visible, and near-infrared. *Journal of Applied Physics,* **94**, 6167–6174 (2003).

167. Cassano, T., Tommasi, R., Ferrara, M., Babudri, F. & Farinola, G. M. Substituent-dependence of the optical nonlinearities in investigated by the Z -scan technique. *Chemical Physics,* **272**, 111–118 (2001).

168. Iliopoulos, K. *et al.* Ultrafast third order nonlinearities of organic solvents. *Optics Express* **23**, 24171 (2015).

169. Cabrera, Marcano & Castellanos. Absorption coefficient of nearly transparent liquids measured using thermal lens spectrometry. *Condensed Matter Physics,* **9**, 385 (2006).

170. Liang, J., Zhao, H., Zhou, X. & Wang, H. Polarization-dependent effects of refractive index change associated with photoisomerization investigated with Z-scan technique. *Journal of Applied Physics,* **101**, 013106 (2007).

171. Gel'mukhanov, F., Baev, A., Macák, P., Luo, Y. & Ågren, H. Dynamics of two-photon absorption by molecules and solutions. *Journal of the Optical Society of America B,* **19**, 937 (2002).

172. Breukers, R. D. *et al.* Investigation of third order nonlinear optical properties in s-indacene-1,3,5,7(2H,6H)-tetraone based D-π-A-π-D chromophores by z-scan. *Proceedings of SPIE - The International Society for Optical Engineering,* **8827**, 88270N (2013).

173. Yang, L. *et al.* The tunable third-order optical nonlinearities of a diarylethene-zinc phthalocyanine hybrid. *Dyes and Pigments,* **102**, 251–256 (2014).

174. Gu, B., Ji, W. & Huang, X.-Q. Analytical expression for femtosecond-pulsed Z scans on instantaneous nonlinearity. *Applied Optics,* **47**, 1187 (2008).

Authors list of publications

Incorporated in this work:

1. **A. Bundulis**, E. Nitiss, I. Mihailovs, J. Busenbergs, M. Rutkis, *Study of Structure–Third-Order Susceptibility Relation of Indandione Derivatives*, The Journal of Physical Chemistry C, **120**, 27515–27522, 2016.

2. D. Gudeika, **A. Bundulis**, I. Mihailovs, D. Volyniuk, M. Rutkis, J. V. Grazulevicius, *Donor and acceptor substituted triphenylamines exhibiting bipolar charge-transporting and NLO properties,* Dyes and Pigments, **140**, 431–440, 2017.

3. **A. Bundulis**, I. Mihailovs, E. Nitiss, J. Busenbergs, M. Rutkis, *Determination of Kerr and two-photon absorption coefficients of indandione derivatives*, Proceedings SPIE, Nonlinear Optics and Applications, **10228**, 1022804, 2017.

4. **A. Bundulis**, E. Nitiss, J. Busenbergs, M. Rutkis, *Mach–Zehnder interferometer implementation for thermo-optical and Kerr effect study*, Applied Physics B, **124**, 56, 2018.

5. **A. Bundulis**, E. Nitiss, M. Rutkis, *Determination of Kerr and two-photon absorption coefficients of ABI thin films*, Proceedings SPIE, Nonlinear Optics and Applications, **10684**, 1068426, 2018.

6. **A. Bundulis**, M. Rutkis, *Determination of Third-order Nonlinear Optical Properties of ABI Derivatives*, Sensors & Transducers Journal, **233**, 46–50, 2019.

7. D. Gudeika, **A. Bundulis**, S. Benhattab, M. Ben Manaa, N. Berton, J. Bouclé, F. Tran Van, B. Schmaltz, D. Volyniuk, M. Rutkis, J. V. Grazulevicius, *Multifunctional derivatives of dimethoxy-substituted triphenylamine containing different acceptor moieties*, SN Applied Sciences, **2,** 327, 2020.

8. **A. Bundulis**, I. Mihailovs, M. Rutkis, *Origin of the Kerr effect: investigation of solutions by polarization-dependent Z-scan*, Journal of the Optical Society of America B, **37**, 1806–1811, 2020.

Other publications:

- E. Nitiss, **A. Bundulis**, A. Tokmakov, J. Busenbergs, E. Linina, M. Rutkis, *Review and comparison of experimental techniques used for determination of thin film electro-optic coefficients*, Physica Status Solidi (A) Applications and Materials Science, **212**, 1867–1879, 2015.

- E. Linina, **A. Bundulis**, E. Nitiss, M. Rutkis*, Poling dynamics of an EO active material using parallel-plate electrodes,* Proceedings SPIE, Nonlinear Optics and Applications, **10228**, 1022816 2017.

- K. Traskovskis, **A. Bundulis**, I. Mihailovs, *Unusual response to environmental polarity in a nonlinear-optical benzylidene-type chromophore containing a 1,3-bis(dicyanomethylidene)indane acceptor fragment*, Physical Chemistry Chemical Physics, **20**, 404–413, 2018.
- E. Nitiss, **A. Bundulis**, A. Tokmakov, J. Busenbergs, M. Rutkis, All-*Organic Waveguide Sensor for Volatile Solvent Sensing*, **9**, 356–366 Photonic Sensors, 2019.

Thesis in Conferences

1) **A. Bundulis**, E. Nitiss, J. Busenbergs, M. Rutkis, Implementation of Z-scan method for determinatio of non-linear optical material Two-photon absorption and optical Kerr coefficients, Institute of Solid State Physics University of Latvia 32nd Scientific Conference, Riga, Latvia, February 17–19, 2016, page 31.
2) **A. Bundulis**, E. Nitiss, J. Busenbergs, M. Rutkis, Determination of electro optic coefficient of thin films by Teng-Man, ATR and MZI techniques, Developments in Optics and Communications 2014, Riga, Latvia, April 9–12, page 27.
3) **A. Bundulis**, E. Nitiss, J. Busenbergs, M. Rutkis, Determination of two-photon absorption and Kerr effect of organic materials by z-scan method, Developments in Optics and Communications 2016, Riga, Latvia, March 21–23, page 10.
4) **A. Bundulis**, E. Nitiss, M. Rutkis, Implementation of Mach-Zehnder interferometric method for study of third order nonlinear properties, Institute of Solid State Physics University of Latvia 33rd Scientific Conference, Riga, Latvia, February 22–24, 2017, page 6.
5) **A. Bundulis**, E. Nitiss, M. Rutkis, Study of thermo-optical processes by Mach-Zehnder interferometric method, Developments in Optics and Communications 2017, Riga, Latvia, April 6–7, page 7.
6) **A. Bundulis**, E. Nitiss, M. Rutkis, I. Mihailovs, Determination of Kerr and two-photon absorption coefficients of indandione derivatives, SPIE Optics + Optoelectronics, Prague, Czech Republic, April 24–27, 2017, page 15.
7) **A. Bundulis**, E. Nitiss, M. Rutkis, Third-order nonlinear optical properties of thin organic films and solutions, Developments in Optics and Communications 2018, Riga, Latvia, April 12–13, page 40.
8) **A. Bundulis**, E. Nitiss, M. Rutkis, I. Mihailovs, Determination of Kerr and two-photon absorption coefficients of ABI thin films, SPIE Photonics Europe, Strasbourg, France, April 22–26, 2018, page 123.
9) **A. Bundulis**, Study of structure and nonlinear optical property relations of SIT derivatives, 10th Optoelectronics and Photonics winter school, Andalo, Italy, January 20–26, 2019.
10) **A. Bundulis,** M. Rutkis, Study of Nonlinear Optical Properties of Novel Indandion Derivatives, 2nd International Conference on Optics, Photonics and Lasers (OPAL' 2019), Amsterdam, The Netherlands, April 24–26, 2019, Conference Proceeding p. 34–35.
11) **A. Bundulis**, M. Rutkis, Third-order nonlinear optical measurement methodology using Z-scan, Institute of Solid State Physics University of Latvia 36th Scientific Conference, Riga, Latvia, February 11–13, 2020, page 25.

Acknowledgments

I would like to thank my supervisor Martins Rutkis for his consultations and guidance during these four years of making this work. Also, thank Igors Mihailovs for help with Quantum Chemical calculations and advice on result interpretation as well as Janis Busenbergs for help with the creation of electronic components for experimental setups. I would also like to express my special thanks to Edgars Nitiss for the support, advice and guidence in science that helped to overcome many challenges during this work.

I want to thank all the colleagues from the Laboratory of Organic Materials for advice and inspiration when it was most needed.

I would like to thank ISSP for the possibility to carry my work here as well as colleagues from RTU for synthesizing novel organic materials studied in this work.

Finally, I would like to thank everyone else who helped in the process of making this work.

This work could not be carried out without financial support from the following projects:

- Scientific Research Project for Students and Young Researchers Nr. SJZ2015/16 realized at the Institute of Solid State Physics, University of Latvia,
- The National Research program IMIS2 project “Photonics and Materials for Photonics”,
- Scientific Research Project for Students and Young Researchers Nr. SJZ/2016/10 realized at the Institute of Solid State Physics, University of Latvia
- ERDF 1.1.1.1 activity project Nr. 1.1.1.1/16/A/046 “Application assessment of novel organic materials by prototyping of photonic devices".

Appendix

Appendix A: Sum-over-states expression

In the general case, the third-order susceptibility can be written as follows:

$$\chi^{(3)}_{ijkl}(\omega_\sigma = \omega_p + \omega_q + \omega_r; \omega_p, \omega_q, \omega_r) = \frac{N}{\varepsilon_0 \cdot \hbar^3} \cdot L(\omega_p) \cdot L(\omega_q) \cdot L(\omega_r) \cdot L(\omega_\sigma) \cdot$$

$$\cdot \Bigg[\sum\nolimits'_{v,n,m} \Bigg\{ \frac{\mu_{gv,i}(\mu_{vn,l} - \mu_{gg,l})(\mu_{nm,k} - \mu_{gg,k})\mu_{mg,j}}{(\widehat{\omega}_{vg} - \omega_\sigma)(\widehat{\omega}_{ng} - \omega_q - \omega_p)(\widehat{\omega}_{mg} - \omega_p)} + \frac{\mu_{gv,j}(\mu_{vn,k} - \mu_{gg,k})(\mu_{nm,i} - \mu_{gg,i})\mu_{mg,l}}{(\widehat{\omega}^*_{vg} + \omega_p)(\widehat{\omega}^*_{ng} + \omega_q + \omega_p)(\widehat{\omega}_{mg} - \omega_r)}$$
$$+ \frac{\mu_{gv,l}(\mu_{vn,i} - \mu_{gg,i})(\mu_{nm,k} - \mu_{gg,k})\mu_{mg,j}}{(\widehat{\omega}^*_{vg} + \omega_r)(\widehat{\omega}_{ng} - \omega_q - \omega_p)(\widehat{\omega}_{mg} - \omega_p)}$$
$$+ \frac{\mu_{gv,j}(\mu_{vn,k} - \mu_{gg,k})(\mu_{nm,l} - \mu_{gg,l})\mu_{mg,i}}{(\widehat{\omega}^*_{vg} + \omega_p)(\widehat{\omega}^*_{ng} + \omega_q + \omega_p)(\widehat{\omega}^*_{mg} + \omega_\sigma)} \Bigg\}$$
$$- \sum\nolimits'_{n,m} \Bigg\{ \frac{\mu_{gn,i}\mu_{ng,l}\mu_{gm,k}\mu_{mg,j}}{(\widehat{\omega}_{ng} - \omega_\sigma)(\widehat{\omega}_{ng} - \omega_r)(\widehat{\omega}_{mg} - \omega_p)}$$
$$+ \frac{\mu_{gn,i}\mu_{ng,l}\mu_{gm,k}\mu_{mg,j}}{(\widehat{\omega}^*_{mg} + \omega_q)(\widehat{\omega}_{ng} - \omega_r)(\widehat{\omega}_{mg} - \omega_p)} + \frac{\mu_{gn,l}\mu_{ng,i}\mu_{gm,j}\mu_{mg,k}}{(\widehat{\omega}^*_{ng} + \omega_r)(\widehat{\omega}^*_{mg} + \omega_p)(\widehat{\omega}_{mg} - \omega_q)}$$
$$+ \frac{\mu_{gn,l}\mu_{ng,i}\mu_{gm,j}\mu_{mg,k}}{(\widehat{\omega}^*_{nfg} + \omega_r)(\widehat{\omega}^*_{mg} + \omega_p)(\widehat{\omega}^*_{ng} + \omega_\sigma)} \Bigg\} \Bigg]$$

The first special case to consider is the third-order susceptibility equation for the two-level model in the case of the Kerr effect. The general expression for third-order susceptibility can be written as:

$$\chi^{(3)}_{ijkl}(\omega_\sigma = \omega_p + \omega_q + \omega_r; \omega_p, \omega_q, \omega_r) = \frac{N}{\varepsilon_0 \cdot \hbar^3} \cdot L(\omega_p) \cdot L(\omega_q) \cdot L(\omega_r) \cdot L(\omega_\sigma) \cdot$$

$$\cdot \Bigg[\Bigg\{ \frac{\mu_{01,i}(\mu_{11,l} - \mu_{00,l})(\mu_{11,k} - \mu_{00,k})\mu_{10,j}}{(\widehat{\omega}_{10} - \omega_\sigma)(\widehat{\omega}_{10} - \omega_q - \omega_p)(\widehat{\omega}_{10} - \omega_p)} + \frac{\mu_{01,j}(\mu_{11,k} - \mu_{00,k})(\mu_{11,i} - \mu_{00,i})\mu_{10,l}}{(\widehat{\omega}^*_{10} + \omega_p)(\widehat{\omega}^*_{10} + \omega_q + \omega_p)(\widehat{\omega}_{10} - \omega_r)}$$
$$+ \frac{\mu_{01,l}(\mu_{11,i} - \mu_{00,i})(\mu_{11,k} - \mu_{00,k})\mu_{10,j}}{(\widehat{\omega}^*_{10} + \omega_r)(\widehat{\omega}_{10} - \omega_q - \omega_p)(\widehat{\omega}_{10} - \omega_p)}$$
$$+ \frac{\mu_{01,j}(\mu_{11,k} - \mu_{00,k})(\mu_{11,l} - \mu_{00,l})\mu_{10,i}}{(\widehat{\omega}^*_{10} + \omega_p)(\widehat{\omega}^*_{10} + \omega_q + \omega_p)(\widehat{\omega}^*_{10} + \omega_\sigma)} \Bigg\}$$
$$- \Bigg\{ \frac{\mu_{01,i}\mu_{01,l}\mu_{01,k}\mu_{01,j}}{(\widehat{\omega}_{10} - \omega_\sigma)(\widehat{\omega}_{10} - \omega_r)(\widehat{\omega}_{10} - \omega_p)} + \frac{\mu_{01,i}\mu_{01,l}\mu_{01,k}\mu_{01,j}}{(\widehat{\omega}^*_{10} + \omega_q)(\widehat{\omega}_{10} - \omega_r)(\widehat{\omega}_{10} - \omega_p)}$$
$$+ \frac{\mu_{01,l}\mu_{01,i}\mu_{01,j}\mu_{01,k}}{(\widehat{\omega}^*_{10} + \omega_r)(\widehat{\omega}^*_{10} + \omega_p)(\widehat{\omega}_{10} - \omega_q)} + \frac{\mu_{01,l}\mu_{01,i}\mu_{01,j}\mu_{01,k}}{(\widehat{\omega}^*_{10} + \omega_r)(\widehat{\omega}^*_{10} + \omega_p)(\widehat{\omega}^*_{10} + \omega_\sigma)} \Bigg\} \Bigg]$$

For the three-level scheme third-order susceptibility only transitions represented in “Third-order susceptibility” Figure 1.2 will be considered. The first sum is interpreted in two ways – as D and T terms:

$$\chi^{(3)}_{ijkl}(\omega_\sigma = \omega_p + \omega_q + \omega_r; \omega_p, \omega_q, \omega_r) = \frac{N}{\varepsilon_0 \cdot \hbar^3} \cdot L(\omega_p) \cdot L(\omega_q) \cdot L(\omega_r) \cdot L(\omega_\sigma) \cdot$$

$$\cdot \Bigg[\Bigg\{ \frac{\mu_{01,i}(\mu_{12,l} - \mu_{00,l})(\mu_{21,k} - \mu_{00,k})\mu_{10,j}}{(\widehat{\omega}_{10} - \omega_\sigma)(\widehat{\omega}_{20} - \omega_q - \omega_p)(\widehat{\omega}_{10} - \omega_p)} + \frac{\mu_{01,j}(\mu_{12,k} - \mu_{00,k})(\mu_{21,i} - \mu_{00,i})\mu_{10,l}}{(\widehat{\omega}^*_{10} + \omega_p)(\widehat{\omega}^*_{20} + \omega_q + \omega_p)(\widehat{\omega}_{10} - \omega_r)}$$
$$+ \frac{\mu_{01,l}(\mu_{12,i} - \mu_{00,i})(\mu_{21,k} - \mu_{00,k})\mu_{10,j}}{(\widehat{\omega}^*_{10} + \omega_r)(\widehat{\omega}_{20} - \omega_q - \omega_p)(\widehat{\omega}_{10} - \omega_p)}$$
$$+ \frac{\mu_{01,j}(\mu_{12,k} - \mu_{00,k})(\mu_{21,l} - \mu_{00,l})\mu_{10,i}}{(\widehat{\omega}^*_{10} + \omega_p)(\widehat{\omega}^*_{20} + \omega_q + \omega_p)(\widehat{\omega}^*_{10} + \omega_\sigma)} \Bigg\}$$
$$+ \Bigg\{ \frac{\mu_{01,i}(\mu_{11,l} - \mu_{00,l})(\mu_{11,k} - \mu_{00,k})\mu_{10,j}}{(\widehat{\omega}_{10} - \omega_\sigma)(\widehat{\omega}_{10} - \omega_q - \omega_p)(\widehat{\omega}_{10} - \omega_p)}$$
$$+ \frac{\mu_{01,j}(\mu_{11,k} - \mu_{00,k})(\mu_{11,i} - \mu_{00,i})\mu_{10,l}}{(\widehat{\omega}^*_{10} + \omega_p)(\widehat{\omega}^*_{10} + \omega_q + \omega_p)(\widehat{\omega}_{10} - \omega_r)}$$
$$+ \frac{\mu_{01,l}(\mu_{11,i} - \mu_{00,i})(\mu_{11,k} - \mu_{00,k})\mu_{10,j}}{(\widehat{\omega}^*_{10} + \omega_r)(\widehat{\omega}_{10} - \omega_q - \omega_p)(\widehat{\omega}_{10} - \omega_p)}$$
$$+ \frac{\mu_{01,j}(\mu_{11,k} - \mu_{00,k})(\mu_{11,l} - \mu_{00,l})\mu_{10,i}}{(\widehat{\omega}^*_{10} + \omega_p)(\widehat{\omega}^*_{10} + \omega_q + \omega_p)(\widehat{\omega}^*_{10} + \omega_\sigma)} \Bigg\}$$
$$- \Bigg\{ \frac{\mu_{01,i}\mu_{01,l}\mu_{01,k}\mu_{01,j}}{(\widehat{\omega}_{10} - \omega_\sigma)(\widehat{\omega}_{10} - \omega_r)(\widehat{\omega}_{10} - \omega_p)} + \frac{\mu_{01,i}\mu_{01,l}\mu_{01,k}\mu_{01,j}}{(\widehat{\omega}^*_{10} + \omega_q)(\widehat{\omega}_{10} - \omega_r)(\widehat{\omega}_{10} - \omega_p)}$$
$$+ \frac{\mu_{01,l}\mu_{01,i}\mu_{01,j}\mu_{01,k}}{(\widehat{\omega}^*_{10} + \omega_r)(\widehat{\omega}^*_{10} + \omega_p)(\widehat{\omega}_{10} - \omega_q)} + \frac{\mu_{01,l}\mu_{01,i}\mu_{01,j}\mu_{01,k}}{(\widehat{\omega}^*_{10} + \omega_r)(\widehat{\omega}^*_{10} + \omega_p)(\widehat{\omega}^*_{10} + \omega_\sigma)} \Bigg\} \Bigg]$$

Compared to the two-level case, this equation has an additional element that ensures a two-photon component even if the molecule does not possess any dipole moment in the ground or first excited state. As this case gives a more in-depth view of third-order susceptibility and two-level scheme can be expressed by removing the first term from equation () we will now derive the full third-order susceptibilities equation. For the Kerr effect, it is important to take in account all possible combinations of input frequencies: χ(ω; ω, ω, -ω), χ(ω; ω, -ω, ω), and χ(ω; -ω, ω, ω) as for each of these susceptibilities equation (..) will yield a different outcome. Firstly let's study the diagonal element χ_{1111}. To make it simpler for notation, we will further use x index to identify tensor elements – χ_{xxxx}. The three elements can be written as:

$$\boldsymbol{I)}\ \chi^{(3)}_{xxxx}(\omega; \omega, \omega, -\omega) = \frac{N}{\varepsilon_0 \cdot \hbar^3} \cdot L(\omega)^3 \cdot L(-\omega) \cdot$$

$$\Big[\big|\mu_{01,x}\big|^2\big(\mu_{12,y}-\mu_{00,x}\big)^2\Big\{\frac{1}{(\widehat{\omega}_{10}-\omega)^2(\widehat{\omega}_{20}-2\omega)}+\frac{1}{(\widehat{\omega}^*_{10}+\omega)^2(\widehat{\omega}^*_{20}+2\omega)(\widehat{\omega}_{10}+\omega)}$$
$$+\frac{1}{(\widehat{\omega}^*_{10}-\omega)(\widehat{\omega}_{20}-2\omega)(\widehat{\omega}_{10}-\omega)}+\frac{1}{(\widehat{\omega}^*_{10}+\omega)^2(\widehat{\omega}^*_{20}+2\omega)}\Big\}$$
$$+\big|\mu_{01,x}\big|^2\big(\mu_{11,x}-\mu_{00,x}\big)^2\Big\{\frac{1}{(\widehat{\omega}_{10}-\omega)^2(\widehat{\omega}_{10}-2\omega)}$$
$$+\frac{1}{(\widehat{\omega}^*_{10}+\omega)^2(\widehat{\omega}^*_{10}+2\omega)(\widehat{\omega}_{10}+\omega)}+\frac{1}{(\widehat{\omega}^*_{10}-\omega)(\widehat{\omega}_{10}-2\omega)(\widehat{\omega}_{10}-\omega)}$$
$$+\frac{1}{(\widehat{\omega}^*_{10}+\omega)^2(\widehat{\omega}^*_{10}+2\omega)}\Big\}$$
$$-\big(\mu_{01,x}\big)^4\Big\{\frac{1}{(\widehat{\omega}_{10}-\omega)^2(\widehat{\omega}_{10}+\omega)}+\frac{1}{(\widehat{\omega}^*_{10}+\omega)(\widehat{\omega}_{10}+\omega)(\widehat{\omega}_{10}-\omega)}$$
$$+\frac{1}{(\widehat{\omega}^*_{10}-\omega)(\widehat{\omega}^*_{10}+\omega)(\widehat{\omega}_{10}-\omega)}+\frac{1}{(\widehat{\omega}^*_{10}-\omega)(\widehat{\omega}^*_{10}+\omega)^2}\Big\}\Big]$$

$$\textbf{\textit{II}})\ \chi^{(3)}_{xxxx}(\omega;\omega,-\omega,\omega)=\frac{N}{\varepsilon_0\cdot\hbar^3}\cdot L(\omega)^3\cdot L(-\omega)\cdot$$

$$\Big[\big|\mu_{01,x}\big|^2\big(\mu_{12,x}-\mu_{00,x}\big)^2\Big\{\frac{1}{(\widehat{\omega}_{10}-\omega)^2\widehat{\omega}_{20}}+\frac{1}{(\widehat{\omega}^*_{10}+\omega)\widehat{\omega}^*_{20}(\widehat{\omega}_{10}-\omega)}+\frac{1}{(\widehat{\omega}^*_{10}+\omega)\widehat{\omega}_{20}(\widehat{\omega}_{10}-\omega)}$$
$$+\frac{1}{(\widehat{\omega}^*_{10}+\omega)^2\widehat{\omega}^*_{20}}\Big\}$$
$$+\big|\mu_{01,x}\big|^2\big(\mu_{11,x}-\mu_{00,x}\big)^2\Big\{\frac{1}{(\widehat{\omega}_{10}-\omega)^2\widehat{\omega}_{10}}+\frac{1}{(\widehat{\omega}^*_{10}+\omega)\widehat{\omega}^*_{10}(\widehat{\omega}_{10}-\omega)}$$
$$+\frac{1}{(\widehat{\omega}^*_{10}+\omega)\widehat{\omega}_{10}(\widehat{\omega}_{10}-\omega)}+\frac{1}{(\widehat{\omega}^*_{10}+\omega)^2\widehat{\omega}^*_{10}}\Big\}$$
$$-\big(\mu_{01,x}\big)^4\Big\{\frac{1}{(\widehat{\omega}_{10}-\omega)^3}+\frac{1}{(\widehat{\omega}^*_{10}-\omega)(\widehat{\omega}_{10}-\omega)^2}+\frac{1}{(\widehat{\omega}_{10}+\omega)(\widehat{\omega}^*_{10}+\omega)^2}$$
$$+\frac{1}{(\widehat{\omega}^*_{10}+\omega)^3}\Big\}\Big]$$

$$\textbf{\textit{III}})\ \chi^{(3)}_{xxxx}(\omega;-\omega,\omega,\omega)=\frac{N}{\varepsilon_0\cdot\hbar^3}\cdot L(\omega)^3\cdot L(-\omega)\cdot$$

$$\Big[\big|\mu_{01,x}\big|^2\big(\mu_{12,x}-\mu_{00,x}\big)^2\Big\{\frac{1}{\big(\widehat{\omega}_{10}{}^2-\omega^2\big)\widehat{\omega}_{20}}+\frac{1}{(\widehat{\omega}^*_{10}-\omega)\widehat{\omega}^*_{20}(\widehat{\omega}_{10}-\omega)}$$
$$+\frac{1}{(\widehat{\omega}^*_{10}+\omega)\widehat{\omega}_{20}(\widehat{\omega}_{10}+\omega)}+\frac{1}{\big(\widehat{\omega}^*_{10}{}^2+\omega^2\big)\widehat{\omega}^*_{20}}\Big\}$$
$$+\big|\mu_{01,x}\big|^2\big(\mu_{11,x}-\mu_{00,x}\big)^2\Big\{\frac{1}{\big(\widehat{\omega}_{10}{}^2-\omega^2\big)\widehat{\omega}_{10}}+\frac{1}{(\widehat{\omega}^*_{10}-\omega)\widehat{\omega}^*_{10}(\widehat{\omega}_{10}-\omega)}$$
$$+\frac{1}{(\widehat{\omega}^*_{10}+\omega)\widehat{\omega}_{10}(\widehat{\omega}_{10}+\omega)}+\frac{1}{\big(\widehat{\omega}^*_{10}{}^2+\omega^2\big)\widehat{\omega}^*_{10}}\Big\}$$
$$-\big(\mu_{01,x}\big)^4\Big\{\frac{1}{(\widehat{\omega}_{10}-\omega)^2(\widehat{\omega}_{10}+\omega)}+\frac{1}{(\widehat{\omega}^*_{10}+\omega)\big(\widehat{\omega}_{10}{}^2-\omega^2\big)}$$
$$+\frac{1}{(\widehat{\omega}^*_{10}+\omega)\big(\widehat{\omega}^*_{10}{}^2-\omega^2\big)}+\frac{1}{(\widehat{\omega}^*_{10}+\omega)(\widehat{\omega}^*_{10}-\omega)^2}\Big\}\Big]$$

Compared to the relation (1.23) mentioned in the main text we can see the origins for D, N, and T terms. Here we can see that instead of just μ_{12} element we see a difference μ_{12}-μ_{00} in the first term (T term). This gives rise to two-photon contribution from ground level to the second excited state. In practice, this element is only considered for symmetrical molecules

for which μ_{00} element is equal to zero. For non-symmetrical molecules, it rarely involves more than two levels and the second term (D Term) Gives rise to two-photon contribution through the first excited state.

In this work main focus is on solutions where the following relation can be used to calculate any third-order susceptibility tensor element:

$$\chi_{ijkl}^{(3)} = \chi_{\mathrm{xxyy}}^{(3)} \cdot \delta_{ij} \cdot \delta_{kl} + \chi_{\mathrm{xyxy}}^{(3)} \cdot \delta_{ik} \cdot \delta_{jl} + \chi_{\mathrm{xyyx}}^{(3)} \cdot \delta_{il} \cdot \delta_{jk}$$

Each of these elements can be divided into three parts that differ with frequency notation:

$$\begin{cases} \chi_{xyyx}^{(3)} = \chi_{xyyx}^{(3)}(\omega;\omega,\omega,-\omega) + \chi_{xyyx}^{(3)}(\omega;\omega,-\omega,\omega) + \chi_{xyyx}^{(3)}(\omega;-\omega,\omega,\omega) \\ \chi_{xxyy}^{(3)} = \chi_{xxyy}^{(3)}(\omega;\omega,\omega,-\omega) + \chi_{xxyy}^{(3)}(\omega;\omega,-\omega,\omega) + \chi_{xxyy}^{(3)}(\omega;-\omega,\omega,\omega) \\ \chi_{xyxy}^{(3)} = \chi_{xyxy}^{(3)}(\omega;\omega,\omega,-\omega) + \chi_{xyxy}^{(3)}(\omega;\omega,-\omega,\omega) + \chi_{xyxy}^{(3)}(\omega;-\omega,\omega,\omega) \end{cases}$$

This is also how the degeneracy term $D^{(3)}$ gets its value. For the Kerr effect, it is 3 as three unique frequency combinations arise. Depending on what Convention is used for third-order susceptibility this separation is accounted for or not. In the case of Convention I third-order susceptibility represents the sum of all possible combinations.

Appendix B: Derivation of open-aperture expression

In this section, a detailed derivation of open-aperture expression for Z-scan in case of media possessing the 2PA effect will be given. To describe the 2PA effect we can use a differential expression:

$$\frac{dI}{dz} = -(\alpha_0 + \alpha_2 \cdot I) \cdot I \qquad \text{(C1)}$$

where α_0 is the linear absorption, α_2 is the 2PA coefficient and I is optical intensity. To solve this we leave the sample position on one side and everything else on the other side. This equation is integrated in limits of *z:0->L*, where L is sample thickness, and *I:I->I_e*, where I is the input intensity and I_e is the output intensity:

$$\int_{\mathrm{I}}^{\mathrm{I_e}} \frac{\mathrm{dI}}{(\alpha_0+\alpha_2\cdot\mathrm{I})\cdot\mathrm{I}} = -\int_0^{\mathrm{L}} \mathrm{dz} \;\rightarrow\; \frac{\ln(\mathrm{I_e})-\ln(\alpha_0+\alpha_2\cdot\mathrm{I_e})}{\alpha_0} - \frac{\ln(\mathrm{I})-\ln(\alpha_0+\alpha_2\cdot\mathrm{I})}{\alpha_0} = \mathrm{L} \;\rightarrow$$

$$\rightarrow \frac{\mathrm{I_e}}{\alpha_0+\alpha_2\cdot\mathrm{I_e}} \cdot \frac{\alpha_0+\alpha_2\cdot\mathrm{I}}{\mathrm{I}} = \mathrm{e}^{-\alpha_0\cdot\mathrm{L}} \rightarrow \mathrm{I_e} = \mathrm{e}^{-\alpha_0\cdot\mathrm{L}} \cdot \frac{(\alpha_0+\alpha_2\cdot\mathrm{I_e})\cdot\mathrm{I}}{\alpha_0+\alpha_2\cdot\mathrm{I}} \qquad \text{(C2)}$$

$$\mathrm{I_e} = \frac{\mathrm{I}\cdot\mathrm{e}^{-\alpha_0\cdot\mathrm{L}}}{1+\alpha_2\cdot\mathrm{I}\cdot\frac{\left(1-\mathrm{e}^{-\alpha_0\cdot\mathrm{L}}\right)}{\alpha_0}} = \frac{\mathrm{I}\cdot\mathrm{e}^{-\alpha_0\cdot\mathrm{L}}}{1+\alpha_2\cdot\mathrm{I}\cdot\mathrm{L_{eff}}}$$

Here we introduce effective thickness L_{eff}. This derivation is true only in cases when beam size variation through the sample is negligible, also called the “thin-sample” approximation. Next, let’s consider a pulsed laser beam with a Gaussian profile. In this case beams intensity can be written as:

$$\mathrm{I(z,r,t)} = \mathrm{I_0} \cdot \left(\frac{\mathrm{w_0}}{\mathrm{w(z)}}\right)^2 \cdot \mathrm{e}^{-\frac{2\cdot\mathrm{r}^2}{\mathrm{w}^2(\mathrm{z})}} \cdot \mathrm{e}^{-\frac{\mathrm{t}^2}{\tau^2}} \text{ where } \mathrm{w}^2(\mathrm{z}) = {\mathrm{w_0}}^2 \cdot \left(1+\left(\frac{\mathrm{z}}{\mathrm{z_R}}\right)^2\right) \qquad \text{(C3)}$$

Here w_0 is the beam waist at the focal point, z_R is the Rayleigh length and τ is the pulse duration. To calculate laser power, equation (C2) must be integrated over the beam surface. In this case, a spherical coordination system can be used:

$$P_e = \int_0^{2\pi}\int_0^{\infty} \frac{I\cdot e^{-\alpha_0\cdot L}}{1+\alpha_2\cdot I\cdot L_{eff}}\cdot r\cdot drd\varphi = I_0\cdot {w_0}^2\cdot e^{-\alpha_0\cdot L}\cdot \int_0^{2\pi}\int_0^{\infty} \frac{\frac{r}{w^2(z)}\cdot drd\varphi}{e^{\frac{2\cdot r^2}{w^2(z)}}\cdot e^{\frac{t^2}{\tau^2}}+\alpha_2\cdot I_0\cdot\left(\frac{w_0}{w(z)}\right)^2\cdot L_{eff}} \quad (C4)$$

The first integration is carried over the radial dimension while the second over the angular dimension.

$$P_e = I_0\cdot\frac{{w_0}^2}{4}\cdot e^{-\alpha_0\cdot L}\cdot\int_0^{2\pi}\int_0^{\infty}\frac{d\left(\frac{2\cdot r^2}{w^2(z)}\right)d\varphi}{e^{\frac{2\cdot r^2}{w^2(z)}}\cdot e^{\frac{t^2}{\tau^2}}+\alpha_2\cdot I_0\cdot\left(\frac{w_0}{w(z)}\right)^2\cdot L_{eff}} =$$

$$= I_0\cdot\frac{{w_0}^2}{4}\cdot e^{-\alpha_0\cdot L}\cdot\int_0^{2\pi}\frac{\ln\left(\alpha_2\cdot I_0\cdot\left(\frac{w_0}{w(z)}\right)^2\cdot L_{eff}\cdot e^{-\frac{t^2}{\tau^2}}+1\right)d\varphi}{\alpha_2\cdot I_0\cdot\left(\frac{w_0}{w(z)}\right)^2\cdot L_{eff}} = \quad (C5)$$

$$I_0\cdot\frac{\pi\cdot{w_0}^2}{2}\cdot e^{-\alpha_0\cdot L}\cdot\frac{\ln\left(\frac{\alpha_2\cdot I_0\cdot L_{eff}}{\left(1+\left(\frac{z}{z_R}\right)^2\right)}\cdot e^{-\frac{t^2}{\tau^2}}+1\right)}{\frac{\alpha_2\cdot I_0\cdot L_{eff}}{\left(1+\left(\frac{z}{z_R}\right)^2\right)}}$$

In the case of Z-scan measurements, 2PA is measured by detecting transmitted beams power changes. To describe this analytically, we integrate equation (C5) over time and divide it with itself for the case when α_2=0 (no 2PA is present):

$$T = \frac{\int_{-\infty}^{+\infty}P_e dt}{\int_{-\infty}^{+\infty}I_0\cdot\frac{\pi\cdot{w_0}^2}{2}\cdot e^{-\alpha_0\cdot L}\cdot e^{-\frac{t^2}{\tau^2}}dt} = \frac{\left(1+\left(\frac{z}{z_R}\right)^2\right)}{\alpha_2\cdot I_0\cdot L_{eff}}\cdot\frac{\int_{-\infty}^{+\infty}\ln\left(\frac{\alpha_2\cdot I_0\cdot L_{eff}}{\left(1+\left(\frac{z}{z_R}\right)^2\right)}\cdot e^{-\frac{t^2}{\tau^2}}+1\right)dt}{\int_{-\infty}^{+\infty}e^{-\frac{t^2}{\tau^2}}dt} =$$

$$= \frac{\left(1+\left(\frac{z}{z_R}\right)^2\right)}{\alpha_2\cdot I_0\cdot L_{eff}}\cdot\frac{\int_{-\infty}^{+\infty}\ln\left(\frac{\alpha_2\cdot I_0\cdot L_{eff}}{\left(1+\left(\frac{z}{z_R}\right)^2\right)}\cdot e^{-\frac{t^2}{\tau^2}}+1\right)dt}{\sqrt{\pi}\cdot\tau} \quad (C6)$$

This is the general equation for transmittance changes due to the 2PA effect. In cases when $|\alpha_2\cdot I_0\cdot L_{eff}|$<1, a following logarithmic transformation can be used:

$$\ln(1+x) = \sum_{k=1}^{\infty}\frac{(-1)^{k+1}}{k}\cdot x^k \quad (C7)$$

By inserting equation (C7) into equation (C6) and integrating it the following equation is acquired:

$$T = \frac{\left(1+\left(\frac{z}{z_R}\right)^2\right)}{\alpha_2 \cdot I_0 \cdot L_{eff}} \cdot \frac{\int_{-\infty}^{+\infty} \sum_{k=1}^{\infty} \frac{(-1)^{k+1}}{k} \cdot \left(\frac{\alpha_2 \cdot I_0 \cdot L_{eff}}{\left(1+\left(\frac{z}{z_R}\right)^2\right)} \cdot e^{-\frac{t^2}{\tau^2}}\right)^k dt}{\sqrt{\pi} \cdot \tau} = \sum_{k=1}^{\infty} \frac{(-1)^{k+1}}{k^{\frac{3}{2}}} \cdot \left(\frac{\alpha_2 \cdot I_0 \cdot L_{eff}}{\left(1+\left(\frac{z}{z_R}\right)^2\right)}\right)^{k-1} =$$

$$= \sum_{k=0}^{\infty} \frac{1}{(k+1)^{\frac{3}{2}}} \cdot \left(-\frac{\alpha_2 \cdot I_0 \cdot L_{eff}}{\left(1+\left(\frac{z}{z_R}\right)^2\right)}\right)^k \quad \text{(C8)}$$

Appendix C: Derivation of closed-aperture expression

To derive an analytical expression for Z-scan closed-aperture measurements, first, let's look at the Gaussian decomposition method. Gaussian beams electrical field amplitude can be expressed as:

$$E(r,z,t) = E_0(t) \cdot \frac{w_0}{w(z)} \cdot e^{-\frac{r^2}{w(z)^2}} \cdot e^{-i\cdot\left(k\cdot z - atg\left(\frac{z}{z_R}\right) + \frac{k\cdot r^2}{2\cdot R(z)}\right)} \quad \text{(D1)}$$

In this case, the time-dependent component of the electrical field is not much of interest and will be put under the $E_0(t)$ component. If this beam is traveling through media with absorption and Kerr effect, equation (D1) needs to be supplemented with additional elements:

$$E_e(r,z,t) = E(r,z,t) \cdot A(z) \cdot e^{i\cdot\Delta\Phi(r,z,t)} \quad \text{(D2)}$$

where $\Delta\Phi(r,z,t)$ describes the Kerr effect induced phase changes and $A(z)$ is the absorption influence. To acquire analytical expression for this phase change, we need to solve the following differential equation:

$$\frac{d(\Delta\Phi)}{dz} = k \cdot (n_2 \cdot I_e) = k \cdot \left(n_2 \cdot \frac{I \cdot e^{-\alpha_0 \cdot L}}{1+\alpha_2 \cdot I \cdot \frac{(1-e^{-\alpha_0 \cdot z})}{\alpha_0}}\right) \quad \text{(D3)}$$

In this case, 2PA influence on laser beam intensity is also taken into account as both effects can be present in the same media. This differential equation can be solved in the following way:

$$\int_0^{\Delta\Phi_0} d(\Delta\Phi) = \int_0^L \frac{k\cdot n_2 \cdot I \cdot e^{-\alpha_0 \cdot L}}{1+\alpha_2 \cdot I \cdot \frac{(1-e^{-\alpha_0 \cdot z})}{\alpha_0}} dz$$

$$\Delta\Phi_0 = \int_0^L \frac{k\cdot n_2 \cdot I \cdot e^{-\alpha_0 \cdot L}}{\alpha_2 \cdot \left(1+\alpha_2 \cdot I \cdot \frac{(1-e^{-\alpha_0 \cdot z})}{\alpha_0}\right)} d\left(1 + \alpha_2 \cdot I \cdot \frac{(1-e^{-\alpha_0 \cdot z})}{\alpha_0}\right) = k \cdot n_2 \cdot \frac{\ln(1+\alpha_2 \cdot I \cdot L_{eff})}{\alpha_2} \quad \text{(D4)}$$

In case when α_2=0, this equation can be simplified as:

$$\Delta\Phi_0 = k \cdot n_2 \cdot I \cdot L_{eff} \quad \text{(D5)}$$

For general case $\Delta\Phi$ needs to be substituted with $\Delta\Phi(r,z)$ and I with $I(r,z)$. Influence of each parameter can be separated in the following way:

$$\Delta\Phi(z,r) = \Delta\Phi(z)\cdot e^{\left(\frac{-2\cdot r^2}{w^2(z)}\right)} = \frac{\Delta\Phi}{1+\frac{z^2}{{z_0}^2}}\cdot e^{\left(\frac{-2\cdot r^2}{w^2(z)}\right)} = \frac{k\cdot n_2\cdot I_0\cdot L_{eff}}{1+\frac{z^2}{{z_0}^2}}\cdot e^{\left(\frac{-2\cdot r^2}{w^2(z)}\right)} \quad \text{(D6)}$$

Here I_0 is the laser beams intensity at the focal point. It's difficult to acquire analytical expression of the Kerr effect influence on laser beams intensity if the phase change is written as a power of *e*. To solve this, we can use the Gaussian decomposition method that uses the following relation:

$$(1+x)^a = \sum_{n=0}^{\infty}\left(x^n\cdot\prod_{j=1}^{n}\frac{a-j+1}{j}\right) \quad \text{(D7)}$$

By inserting equation (D6) for Kerr effect and equation (C2) for absorption influence taking into account the 2PA effect into equation (D2) we acquire:

$$E_e(r,z,t) = E(r,z,t)\cdot e^{-\frac{\alpha\cdot z}{2}}\cdot(1+\alpha_2\cdot I\cdot L_{eff})^{i\cdot\frac{k\cdot n_2}{\alpha_2}-\frac{1}{2}} =$$

$$= E(r,z,t)\cdot e^{-\frac{\alpha\cdot z}{2}}\cdot\sum_{n=0}^{\infty}\left((1+\alpha_2\cdot I\cdot L_{eff})^n\cdot\prod_{j=1}^{n}\frac{i\cdot\frac{k\cdot n_2}{\alpha_2}+\frac{1}{2}-j}{j}\right) = \quad \text{(D8)}$$

$$= E(r,z,t)\cdot e^{-\frac{\alpha\cdot z}{2}}\cdot\sum_{n=0}^{\infty}\left(\frac{\left(i\cdot\Delta\Phi(r,z)\right)^n}{n!}\cdot\prod_{j=1}^{n}\left[1+i\frac{\alpha_2}{2\cdot k\cdot n_2}\cdot(1-2\cdot j)\right]\right)$$

It is widely accepted that the 2PA and Kerr contributions to transmittance can be separated into two different function multiplications. This means that we can assume that α_2=0 to acquire an expression for Kerr influence to transmittance. In this case, the electrical field can be expressed as:

$$E_e(r,z,t,\Delta\Phi) = E_0(t)\cdot e^{-\frac{\alpha\cdot L}{2}}\cdot\sum_{m=0}^{\infty}\frac{\left(i\cdot\Delta\Phi(z)\right)^m}{m!}\cdot\frac{w_{m0}}{w_m(z)}\cdot e^{\left(-\frac{r^2}{w_m(z)^2}+i\cdot\theta_m-i\cdot\frac{k\cdot r^2}{d\cdot R_m(z)}\right)} \quad \text{(D9)}$$

Where the following additional parameters are used:

$$\begin{cases} {w_{m0}}^2 = \frac{{w_0}^2\cdot\left(1+\left(\frac{z}{z_R}\right)^2\right)}{2\cdot m+1} \\ z_m = \frac{k\cdot {w_{m0}}^2}{2} \\ w_m(z)^2 = {w_{m0}}^2\cdot\left(g^2+\frac{z^2}{{z_m}^2}\right) \\ R_m(z) = \left(1-\frac{g}{g^2+\frac{z^2}{{z_m}^2}}\right)^{-1} \\ g = 1+\frac{z}{z\cdot\left(1+\left(\frac{z_R}{z}\right)^2\right)} \\ \theta_m = atg\left(\frac{z}{z_m\cdot g}\right) \end{cases} \quad \text{(D10)}$$

For further calculations we use far-field detection approximation ($z>>z_R$). Similarly as for the 2PA effect, the Kerr effect influence on transmittance is calculated by integrating over angle,

aperture size (r_a), and time modulus of electrical field squared and dividing this integral for the electrical field when the Kerr effect is present by the electrical field with no Kerr effect:

$$T(z) = \frac{\int_0^{\infty}\int_0^{2\pi}\int_0^{r_a}|E_e(r,z,t,\Delta\Phi)|^2\cdot r\,dr\,d\varphi\,dt}{\int_0^{\infty}\int_0^{2\pi}\int_0^{r_a}|E_e(r,z,t,\Delta\Phi=0)|^2\cdot r\,dr\,d\varphi\,dt} \tag{D11}$$

Integrations over time and angle do not give any significant influence to transmittance and will not be further studied. The main challenge is the integration over the radius. This can be expressed as:

$$T(z) = \frac{\int_0^{r_a}|E_e(r,z,\Delta\Phi)|^2\cdot r\,dr}{\int_0^{r_a}|E_e(r,z,\Delta\Phi=0)|^2\cdot r\,dr} = \frac{I_0\cdot e^{-\alpha\cdot L}\cdot\int_0^{r_a}\left|\sum_{m=0}^{\infty}\frac{(i\cdot\Delta\Phi_0(z))^m}{m!}\cdot\frac{w_{m0}}{w_m(z)}\cdot e^{\left(-\frac{r^2}{w_m(z)^2}+i\cdot\theta_m-i\frac{k\cdot r^2}{d\cdot R_m(z)}\right)}\right|^2\cdot r\,dr}{I_0\cdot\left(\frac{w_0}{w(z)}\right)^2\cdot e^{-\alpha\cdot L}\cdot\int_0^{r_a} e^{-\frac{2\cdot r^2}{w^2(z)}}\cdot r\,dr} =$$

$$= \frac{\int_0^{r_a}\left|\sum_{m=0}^{\infty}\frac{(i\cdot\Delta\Phi_0(z))^m}{m!}\cdot\frac{w_{m0}}{w_m(z)}\cdot e^{\left(-\frac{r^2}{w_m(z)^2}+i\cdot\theta_m-i\frac{k\cdot r^2}{d\cdot R_m(z)}\right)}\right|^2\cdot r\,dr}{{w_0}^2\cdot\left(1-e^{-\frac{2\cdot {r_a}^2}{w^2(z)}}\right)} \tag{D12}$$

Depending on how large phase changes are induced one or more sum elements have to be used. Although in most cases *m*=1 or *m*=2 is sufficient:

$$\begin{cases} m=1 \;\rightarrow T = 1-\dfrac{4\cdot\Delta\Phi\cdot\frac{z}{z_R}}{\left(\left(\frac{z}{z_R}\right)^2+9\right)\cdot\left(\left(\frac{z}{z_R}\right)^2+1\right)} \\ m=2 \;\rightarrow\; T = 1-\dfrac{4\cdot\Delta\Phi\cdot\frac{z}{z_R}}{\left(\left(\frac{z}{z_R}\right)^2+9\right)\cdot\left(\left(\frac{z}{z_R}\right)^2+1\right)}-\dfrac{4\cdot\Delta\Phi^2\cdot\left(3\cdot\left(\frac{z}{z_R}\right)^2-5\right)}{\left(\left(\frac{z}{z_R}\right)^2+9\right)\cdot\left(\left(\frac{z}{z_R}\right)^2+1\right)^2\cdot\left(\left(\frac{z}{z_R}\right)^2+25\right)} \end{cases} \tag{D13}$$

Appendix D: Mach-Zehnder interferometer analytical expressions

The general expression for two laser beam interference can be expressed as:

$$P_{out} = \frac{P_1+P_2+2\cdot\sqrt{P_1\cdot P_2}\cdot\cos(\Delta\Phi)}{2}, \tag{D14}$$

where P_1 and P_2 are the optical intensities of the first and the second beam and $\Delta\Phi$ is the phase difference between both beams. In the single-beam MZI setup presented in this work the following substitutions can be used:

$$\begin{cases} P_1 \rightarrow P_1 \\ P_2 \rightarrow C_{BS}\cdot P_1 \\ \Delta\Phi \rightarrow \Delta\Phi^*\cdot P_1+\Delta\Phi_0 \end{cases} \tag{D15}$$

where P_1 is the laser power in the sample arm, C_{BS} is the ratio of transmitted and reflected beam of Beam-splitter, $\Delta\Phi^*$is the phase change due to Kerr effect and $\Delta\Phi_0$ is the initial phase

difference between both arms of the MZI setup. Using these substitutions, equation (D14) can be rewritten in form:

$$P_{out} = \frac{P_1+P_2+2\cdot\sqrt{P_1\cdot P_2}\cdot\cos(\Delta\Phi)}{2} = \frac{P_1+C_{BS}\cdot P_1+2\cdot\sqrt{P_1\cdot C_{BS}\cdot P_1}\cdot\cos(\Delta\Phi^*\cdot P_1+\Delta\Phi_0)}{2} = \left(\frac{1+C_{BS}}{2}\right)\cdot P_1\cdot\left(1+\frac{\sqrt{C_{BS}}}{1+C_{BS}}\cdot\cos(\Delta\Phi^*\cdot P_1+\Delta\Phi_0)\right) = \mathrm{A}_1\cdot P_1\cdot(1+A_2\cdot\cos(\Delta\Phi^*\cdot P_1+\Delta\Phi_0)), \quad \text{(D16)}$$

If a 50/50 Beam-splitter is used C_{BS}=1 and A_1=1 while A_2=1/2.

In a two-beam setup a small alteration needs to be made in substitution (D15):

$$\begin{cases} P_1 \to P_1 \\ P_2 \to C_{BS}\cdot P_1 \\ \Delta\Phi \to \Delta\Phi^*\cdot P_2+\Delta\Phi_0 \end{cases} \quad \text{(D17)}$$

where P_1 is probing laser power and P_2 is inducing laser power. In this case, the main focus is on how the function depends on P_2 and all other parameters can be compiled in fitting constants. Inserting substitutions (D17) in equation (D14) we acquire:

$$P_{out} = \frac{P_1+P_2+2\cdot\sqrt{P_1\cdot P_2}\cdot\cos(\Delta\Phi)}{2} = \frac{P_1+C_{BS}\cdot P_1+2\cdot\sqrt{P_1\cdot C_{BS}\cdot P_1}\cdot\cos(\Delta\Phi^*\cdot P_2+\Delta\Phi_0)}{2} = \left(\frac{1+C_{BS}}{2}\right)\cdot P_1+\sqrt{C_{BS}}\cdot P_1\cdot\cos(\Delta\Phi^*\cdot P_2+\Delta\Phi_0) = B_1+B_2\cdot\cos(\Delta\Phi^*\cdot P_2+\Delta\Phi_0), \quad \text{(D18)}$$